Density Model for Harbor Porpoise (*Phocoena phocoena*) for the U.S. East Coast: Supplementary Report

Model Version 6.1

Duke University Marine Geospatial Ecology Laboratory[*]

2023-05-27

Citation

When citing our methodology or results generally, please cite Roberts et al. (2016, 2023). The complete references appear at the end of this document. We are preparing a new article for a peer-reviewed journal that will eventually replace those. Until that is published, those are the best general citations.

When citing this model specifically, please use this reference:

Roberts JJ, Yack TM, Cañadas A, Fujioka E, Halpin PN, Barco SG, Boisseau O, Chavez-Rosales S, Cole TVN, Cotter MP, Cummings EW, Davis GE, DiGiovanni Jr. RA, Garrison LP, Gowan TA, Jackson KA, Kenney RD, Khan CB, Lockhart GG, Lomac-MacNair KS, McAlarney RJ, McLellan WA, Mullin KD, Nowacek DP, O'Brien O, Pabst DA, Palka DL, Quintana-Rizzo E, Redfern JV, Rickard ME, White M, Whitt AD, Zoidis AM (2022) Density Model for Harbor Porpoise (*Phocoena phocoena*) for the U.S. East Coast, Version 6.1, 2023-05-27, and Supplementary Report. Marine Geospatial Ecology Laboratory, Duke University, Durham, North Carolina.

Copyright and License

Model Version History

Version	Date	Description
1	2014-11-05	Initial version.
2	2014-12-03	Fixed bug that prevented 144 observations from the NE_narwss_1999_widgeon_hapo dataset from being used in the winter model. Refitted the winter model and updated the documentation.
3	2015-01-21	Refitted the detection function and density models to segments where Beaufort sea state was less than or equal to 2, as suggested by A. Read, to see if the abundance estimates better match NOAA's.
3.1	2015-03-06	Updated the documentation. No changes to the model.
3.2	2015-05-14	Updated calculation of CVs. Switched density rasters to logarithmic breaks. No changes to the model.
3.3	2015-09-26	Updated the documentation. No changes to the model.

---

[*]For questions or to offer feedback please contact Jason Roberts (jason.roberts@duke.edu) and Tina Yack (tina.yack@duke.edu)

(continued)

Version	Date	Description
3.4	2016-04-21	Switched calculation of monthly 5% and 95% confidence interval rasters to the method used to produce the year-round rasters. (We intended this to happen in version 3.2 but I did not implement it properly.) Updated the monthly CV rasters to have value 0 where we assumed the species was absent, consistent with the year-round CV raster. No changes to the other (non-zero) CV values, the mean abundance rasters, or the model itself. Model files released as supplementary information to Roberts et al. (2016).
4	2017-06-01	Began update to Roberts et al. (2015) model. Introduced new surveys from AMAPPS, NARWSS, UNCW, and VAMSC. Updated modeling methodology. Refitted detection functions and spatial models from scratch using new and reprocessed covariates. Model released as part of a scheduled update to the U.S. Navy Marine Species Density Database (NMSDD).
5	2022-03-20	Experimental model, not released. This model was a major update over the prior version, with substantial additional data, improved statistical methods, and an increased spatial resolution. Several new collaborators joined and contributed survey data: New York State Department of Environmental Conservation, TetraTech, HDR, and Marine Conservation Research. We incorporated additional surveys from all continuing and new collaborators through the end of 2020. (Because some environmental covariates were only available through 2019, certain models only extend through 2019.) We increased the spatial resolution to 5 km and, at NOAA's request, we extended the model further inshore from New York through Maine. We reformulated and refitted all detection functions and spatial models. We updated all enviromental covariates to newer products, when available, and added several covariates to the set of candidates. We estimated model uncertainty using a new method that accounts for both model parameter error and temporal variability. After accruing more sightings from many survey programs at rougher sea states, we tested detection functions and a spatial model that incorporated data collected in sea states up to Beaufort 3 rather than Beaufort 2. The resulting model underestimated density and abundance, indicating that the new sightings did not yield detection functions with sufficient corrections to use Beaufort 3 as the cutoff. (We suspect stronger perception bias corrections would be needed, ideally that would scale with sea state.) We did not release this model, and reverted back to Beaufort 2 for the next one.
6	2022-06-20	This model was the same as version 5, but was limited to data collected in Beaufort 2 or less, after we found in version 5 that the use of Beaufort 3 as the cutoff led to an understimation of density and abundance. (Model versions 3-4 also used Beaufort 2 as the cutoff, because of the same problem.) This model was released as part of the final delivery of the U.S. Navy Marine Species Density Database (NMSDD) for the Atlantic Fleet Testing and Training (AFTT) Phase IV Environmental Impact Statement.
6.1	2023-05-27	Completed the supplementary report documenting the details of this model. Corrected the 5 and 95 percent rasters so that they contain the value 0 where the taxon was asssumed absent, rather than NoData. Nothing else was changed.

1 Survey Data

We built this model from data collected between 1998-2020 (Table 1, Figure 1). In keeping with our primary strategy for the 2022 modeling cycle, we excluded data prior to 1998 in order to utilize biological covariates derived from satellite ocean color observations, which were only available for a few months before 1998. Harbor porpoises are small, cryptic odontocetes that are difficult to detect from long distances or in poor conditions. Accordingly, we excluded all surveys that did not target harbor porpoises as well as aerial surveys flown at altitudes higher than 750 ft., which species experts within our collaboration determined was the maximum altitude they were likely to be reliably detected without a belly observer or belly camera. Although detections at higher altitudes are possible, we lacked the counts needed to fit detection functions unless we pooled surveys flown at lower altitudes, which species experts determined would be inappropriate. Consistent with our prior released model, version 4, we restricted this model, version 6, to survey transects collected in sea states of Beaufort 2 or less. We also excluded transects with poor weather or visibility for surveys that reported those conditions.

We also fitted but did not release an experimental model, version 5, that tested Beaufort 3 as the cutoff instead of Beaufort 2, which allowed more sightings to be retained, which was beneficial to fitting the spatial model. However, the total abundance predicted by the Beaufort 3 model was too low, suggesting that our detection functions or perception bias corrections were not sufficient for estimating the true detection probability in Beaufort 3 conditions, so we abandoned that approach for this modeling cycle.

Table 1: Survey effort and observations considered for this model. Effort is tallied as the cumulative length of on-effort transects. Observations are the number of groups and individuals encountered while on effort. Off effort observations and those lacking an estimate of group size or distance to the group were excluded.

Institution	Program	Period	Effort 1000s km	Observations Groups	Individuals	Mean Group Size
Aerial Surveys						
NEFSC	AMAPPS	2010-2019	23	519	1,321	2.5
NEFSC	NARWSS	2003-2016	123	1,107	2,055	1.9
NEFSC	Pre-AMAPPS	1999-2008	21	357	952	2.7
NJDEP	NJEBS	2008-2009	6	5	8	1.6
SEFSC	AMAPPS	2010-2020	38	4	5	1.2
SEFSC	MATS	2002-2005	24	0	0	
VAMSC	MD DNR WEA	2013-2015	4	0	0	
		Total	**238**	**1,992**	**4,341**	**2.2**
Shipboard Surveys						
MCR	SOTW Visual	2012-2019	4	12	19	1.6
NEFSC	AMAPPS	2011-2016	3	14	25	1.8
NEFSC	Pre-AMAPPS	1998-2007	3	606	1,862	3.1
NJDEP	NJEBS	2008-2009	4	32	58	1.8
SEFSC	AMAPPS	2011-2016	5	0	0	
SEFSC	Pre-AMAPPS	1998-2006	8	0	0	
SEFSC	SEFSC Caribbean	2000-2000	1	0	0	
		Total	**29**	**664**	**1,964**	**3.0**
		Grand Total	**267**	**2,656**	**6,305**	**2.4**

Table 2: Institutions that contributed surveys used in this model.

Institution	Full Name
MCR	Marine Conservation Research
NEFSC	NOAA Northeast Fisheries Science Center
NJDEP	New Jersey Department of Environmental Protection
SEFSC	NOAA Southeast Fisheries Science Center
VAMSC	Virginia Aquarium & Marine Science Center

Table 3: Descriptions and references for survey programs used in this model.

Program	Description	References
AMAPPS	Atlantic Marine Assessment Program for Protected Species	Palka et al. (2017), Palka et al. (2021)
MATS	Mid-Atlantic Tursiops Surveys	
MD DNR WEA	Aerial Surveys of the Maryland Wind Energy Area	Barco et al. (2015)
NARWSS	North Atlantic Right Whale Sighting Surveys	Cole et al. (2007)
NJEBS	New Jersey Ecological Baseline Study	Geo-Marine, Inc. (2010), Whitt et al. (2015)
Pre-AMAPPS	Pre-AMAPPS Marine Mammal Abundance Surveys	Mullin and Fulling (2003), Garrison et al. (2010), Palka (2006)
SEFSC Caribbean	SEFSC Surveys of the Caribbean Sea	Mullin (1995), Swartz and Burks (2000)
SOTW Visual	R/V Song of the Whale Visual Surveys	Ryan et al. (2013)
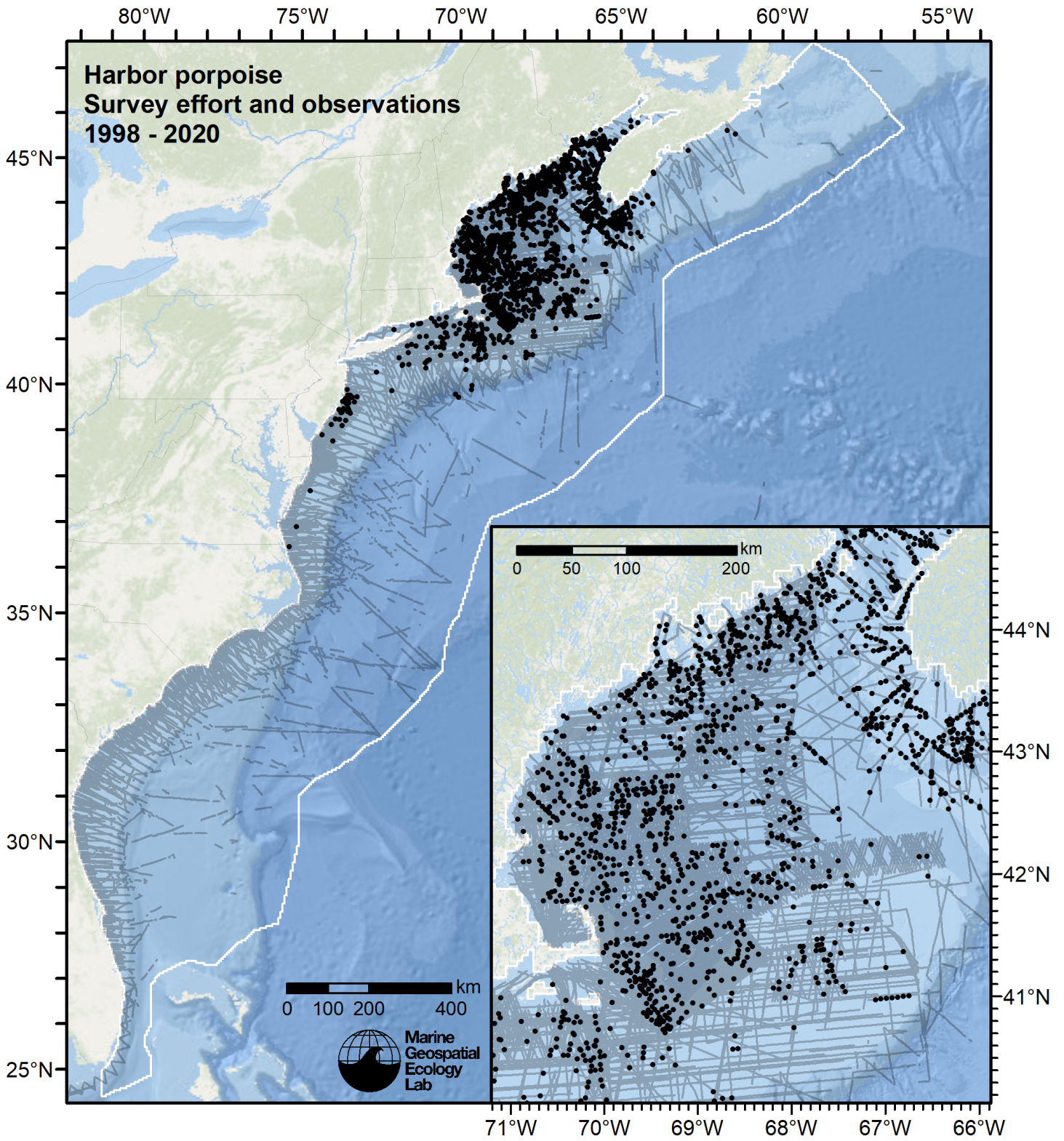
Figure 1: Survey effort and harbor porpoise observations available for density modeling, after detection functions were applied, and excluded segments and truncated observations were removed.

2 Detection Functions

2.1 Taxon Specific

We fitted the detection functions in this section to harbor porpoise observations exclusively, without pooling in other species. We usually adopted this approach when we had enough sightings of this taxon to fit a detection function without pooling and we judged that this taxon's detectability differed in important respects from others that pooling should be avoided if possible. We also occasionally used this approach for certain taxa that had similar detectability to others but for which we had so many sightings that pooling in other species provided little benefit.

2.1.1 Aerial Surveys
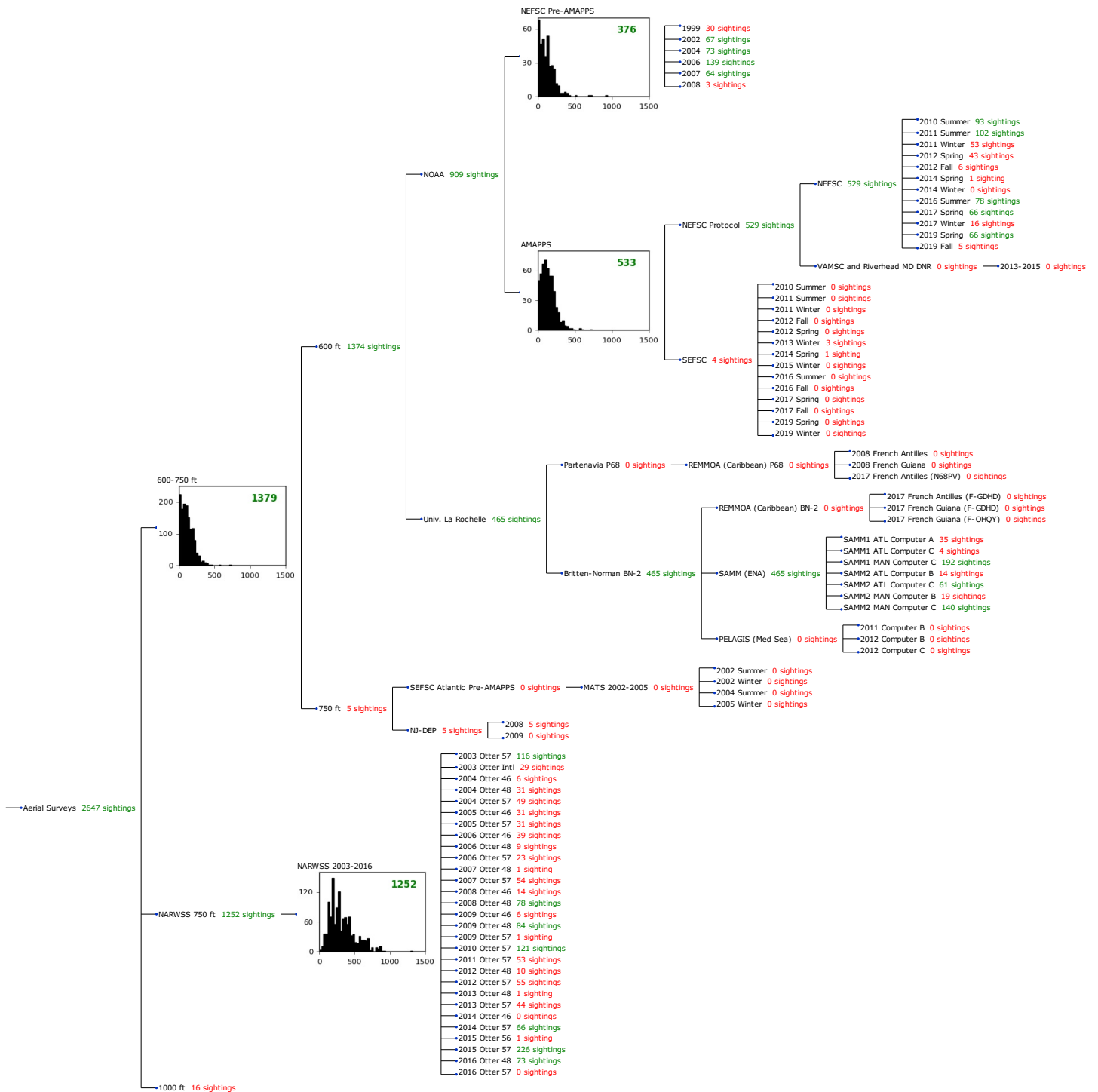
Figure 2: Detection hierarchy for aerial surveys, showing how they were pooled during detectability modeling, for taxon-specific detection functions. Each histogram represents a detection function and summarizes the perpendicular distances of observations that were pooled to fit it, prior to truncation. Observation counts, also prior to truncation, are shown in green when they met the recommendation of Buckland et al. (2001) that detection functions utilize at least 60 sightings, and red otherwise. For rare taxa, it was not always possible to meet this recommendation, yielding higher statistical uncertainty. During the spatial modeling stage of the analysis, effective strip widths were computed for each survey using the closest detection function above it in the hierarchy (i.e. moving from right to left in the figure). Surveys that do not have a detection function above them in this figure were either addressed by a detection function presented in a different section of this report, or were omitted from the analysis.

2.1.1.1 NEFSC Pre-AMAPPS

After right-truncating observations greater than 300 m, we fitted the detection function to the 358 observations that remained. The selected detection function (Figure 3) used a half normal key function with no covariates.
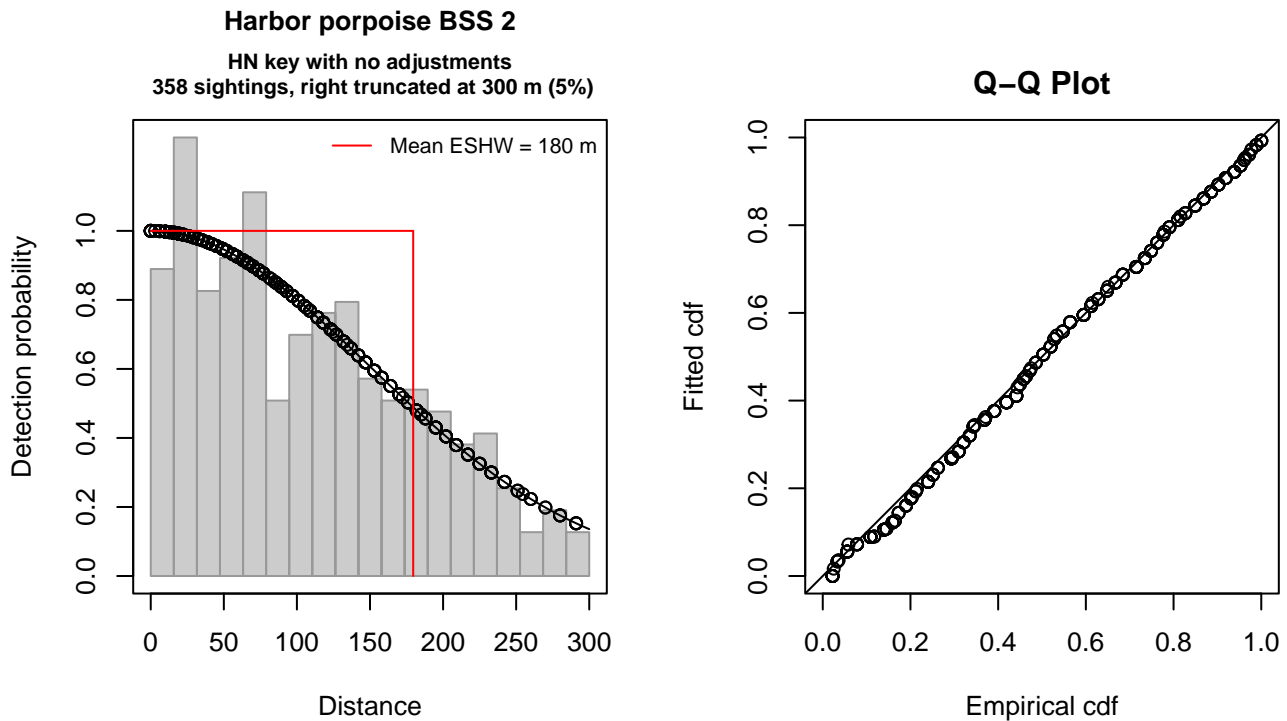

Figure 3: NEFSC Pre-AMAPPS detection function and Q-Q plot showing its goodness of fit.

Statistical output for this detection function:

```
Summary for ds object
Number of observations :  358
Distance range         :  0  -  300
AIC                    :  3995.163

Detection function:
 Half-normal key function

Detection function parameters
Scale coefficient(s):
            estimate          se
(Intercept) 5.011405 0.05947366

                     Estimate         SE          CV
Average p           0.5985002  0.02752153 0.04598416
N in covered region 598.1618758 34.02721497 0.05688630

Distance sampling Cramer-von Mises test (unweighted)
Test statistic = 0.065817  p = 0.777462
```

2.1.1.2 AMAPPS

After right-truncating observations greater than 400 m, we fitted the detection function to the 523 observations that remained. The selected detection function (Figure 4) used a hazard rate key function with Beaufort (Figure 5) and Season (Figure 6) as covariates.
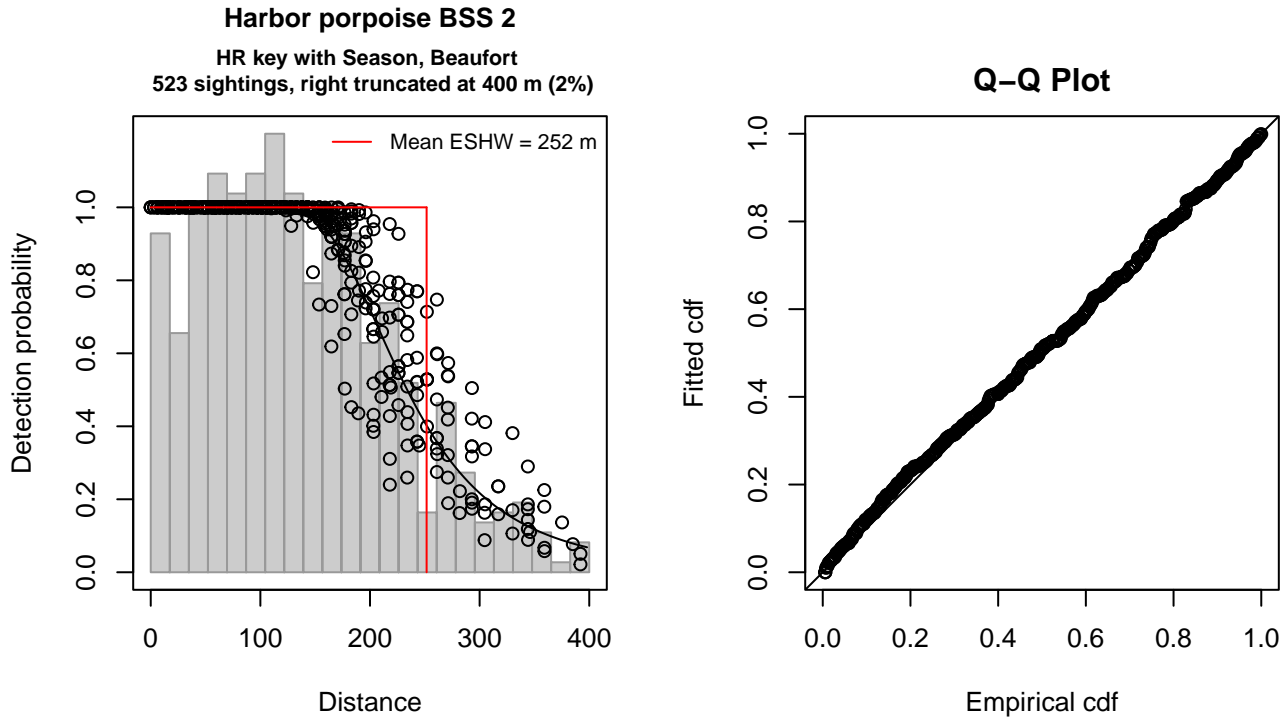
Figure 4: AMAPPS detection function and Q-Q plot showing its goodness of fit.

Statistical output for this detection function:

```
Summary for ds object
Number of observations :   523
Distance range         :   0  -  400
AIC                    :   6040.091

Detection function:
 Hazard-rate key function

Detection function parameters
Scale coefficient(s):
                        estimate          se
(Intercept)            5.3230990 0.11035439
SeasonSummer           0.2147934 0.08761022
SeasonWinter, Spring   0.3690854 0.09593585
Beaufort              -0.1133097 0.07024062

Shape coefficient(s):
            estimate         se
(Intercept) 1.500609 0.1315132


                    Estimate          SE          CV
Average p          0.6210409   0.01947048  0.03135137
N in covered region 842.1344844 34.95577341  0.04150854

Distance sampling Cramer-von Mises test (unweighted)
Test statistic = 0.102549  p = 0.572521
```
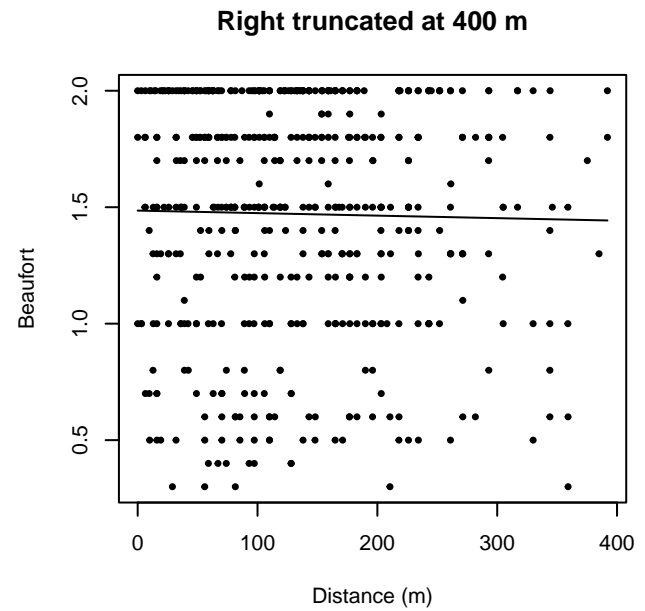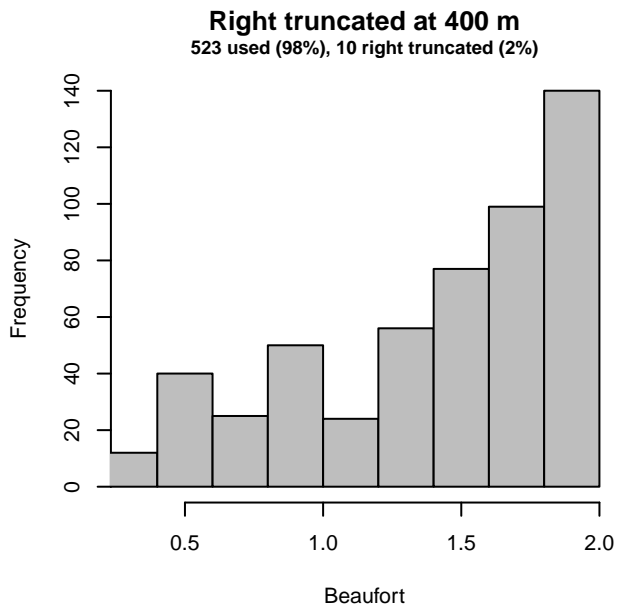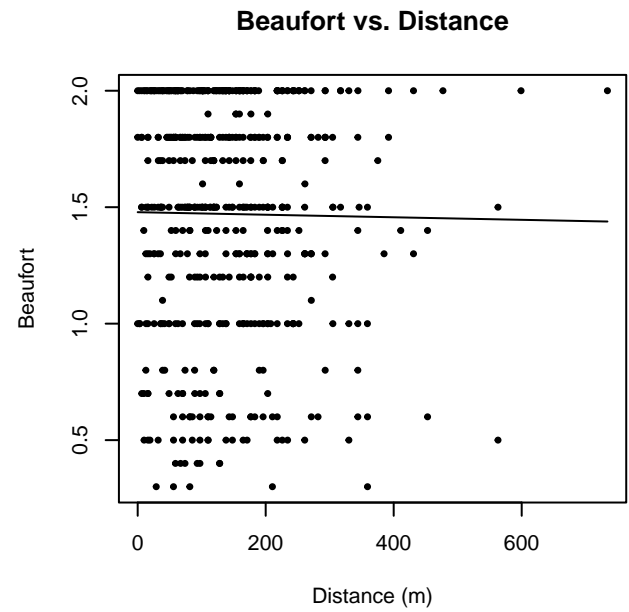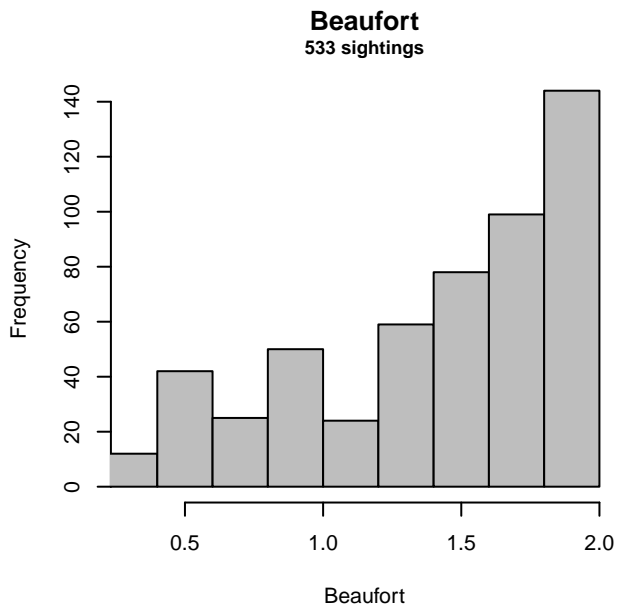
Figure 5: Distribution of the Beaufort covariate before (top row) and after (bottom row) observations were truncated to fit the AMAPPS detection function.
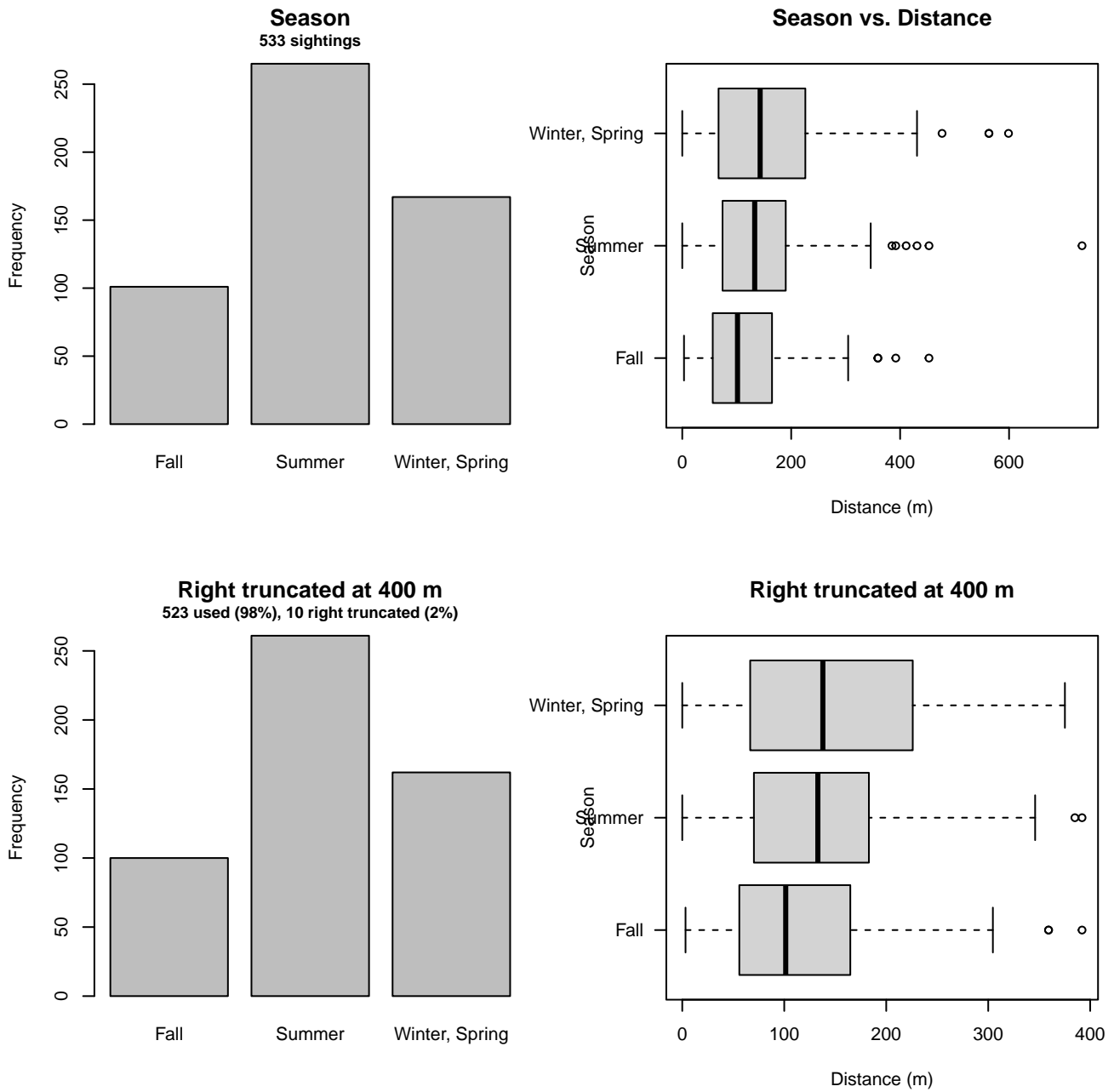
Figure 6: Distribution of the Season covariate before (top row) and after (bottom row) observations were truncated to fit the AMAPPS detection function.

2.1.1.3   600-750 ft

After right-truncating observations greater than 400 m, we fitted the detection function to the 1364 observations that remained. The selected detection function (Figure 7) used a half normal key function with no covariates.
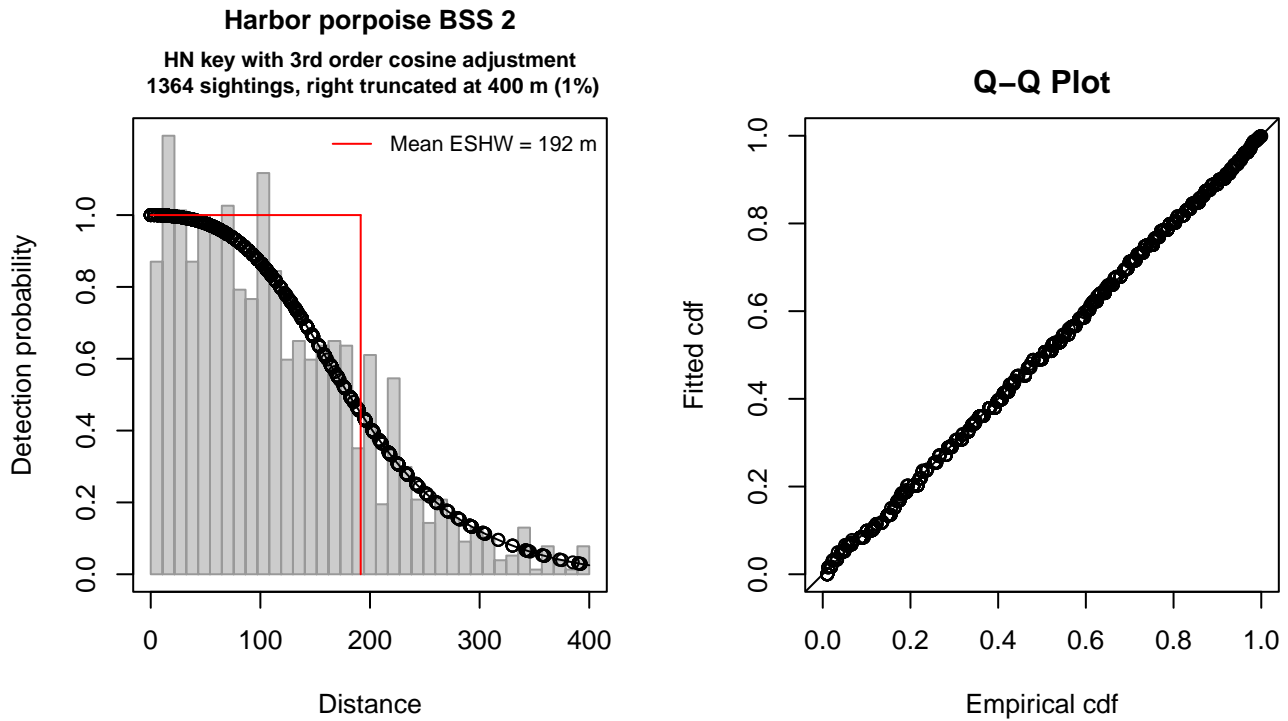
Figure 7: 600-750 ft detection function and Q-Q plot showing its goodness of fit.

Statistical output for this detection function:

```
Summary for ds object
Number of observations :   1364
Distance range          :   0  -   400
AIC                     :   15479.8

Detection function:
 Half-normal key function with cosine adjustment term of order 3

Detection function parameters
Scale coefficient(s):
            estimate          se
(Intercept) 4.978261 0.02175286

Adjustment term coefficient(s):
              estimate          se
cos, order 3 -0.05554482 0.03862351


Monotonicity constraints were enforced.
                   Estimate           SE          CV
Average p          0.4787984    0.02137815 0.04464959
N in covered region 2848.7984019 138.85368229 0.04874114

Monotonicity constraints were enforced.

Distance sampling Cramer-von Mises test (unweighted)
Test statistic = 0.064519  p = 0.785576
```

2.1.1.4 NARWSS 2003-2016

After right-truncating observations greater than 725 m and left-truncating observations less than 122 m (Figure 9), we fitted the detection function to the 1107 observations that remained. The selected detection function (Figure 8) used a hazard rate key function with Glare (Figure 10) as a covariate.
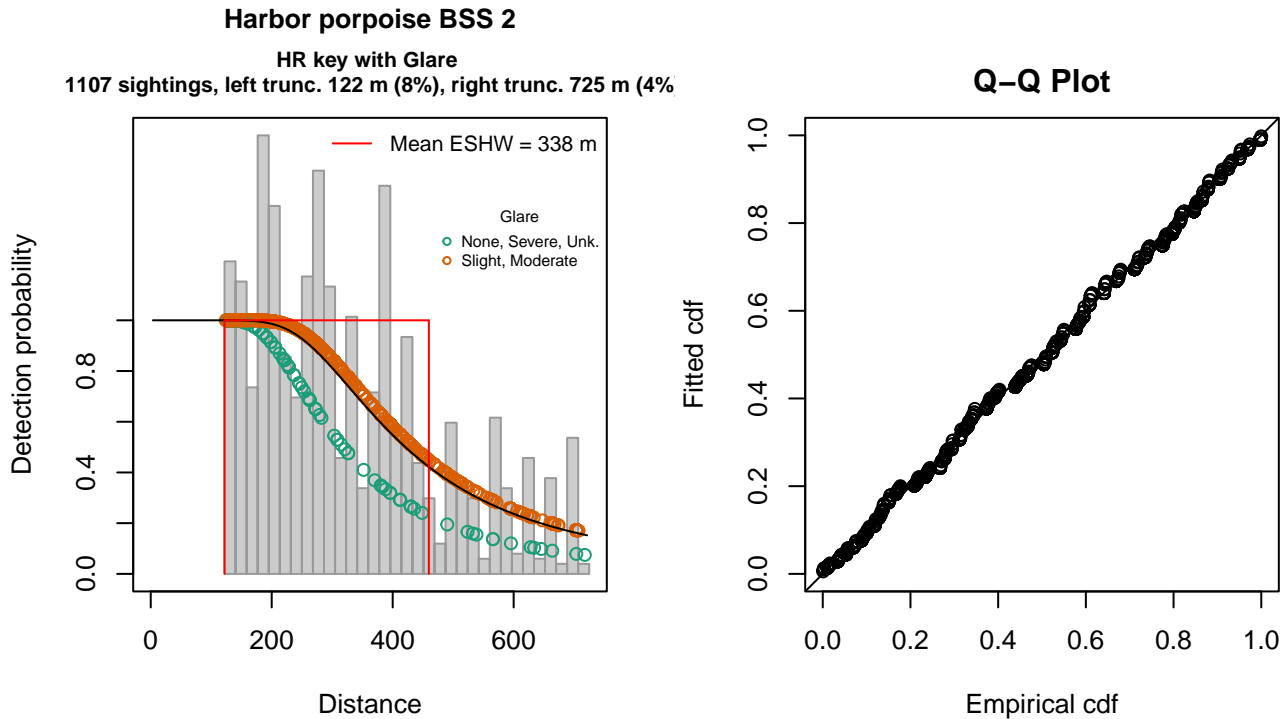

Figure 8: NARWSS 2003-2016 detection function and Q-Q plot showing its goodness of fit.

Statistical output for this detection function:

```
Summary for ds object
Number of observations :  1107
Distance range         :  122  -  725
AIC                    :  13826.97

Detection function:
 Hazard-rate key function

Detection function parameters
Scale coefficient(s):
                       estimate        se
(Intercept)           5.6259399 0.1307435
GlareSlight, Moderate 0.3114994 0.1242634

Shape coefficient(s):
            estimate         se
(Intercept) 0.9886834 0.09358979

                        Estimate         SE         CV
Average p              0.5546046 0.02482989 0.04477044
N in covered region 1996.0164523 98.02397977 0.04910981

Distance sampling Cramer-von Mises test (unweighted)
Test statistic = 0.140947  p = 0.418379
```

Left trucated sightings (in red)

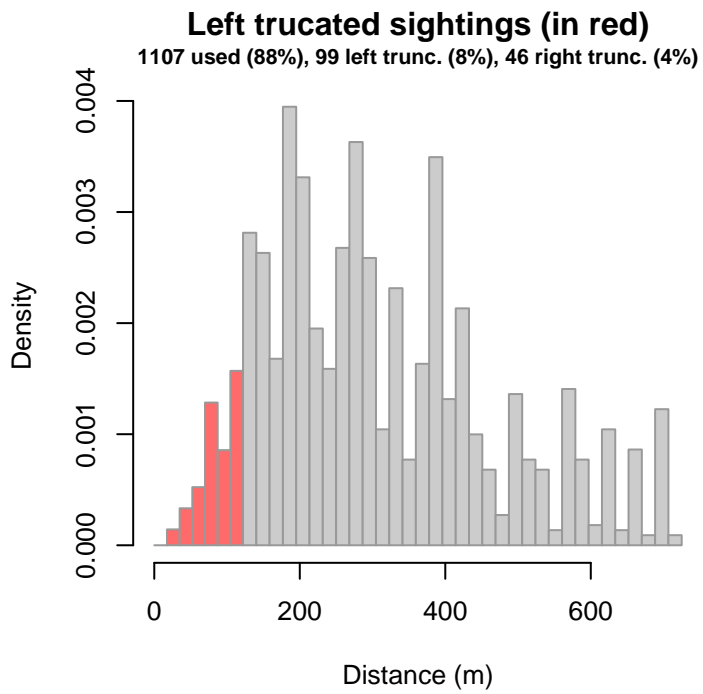**1107 used (88%), 99 left trunc. (8%), 46 right trunc. (4%)**

Figure 9: Density histogram of observations used to fit the NARWSS 2003-2016 detection function, with the left-most bar showing observations at distances less than 122 m, which were left-truncated and excluded from the analysis [Buckland et al. (2001)]. (This bar may be very short if there were very few left-truncated sightings, or very narrow if the left truncation distance was very small; in either case it may not appear red.)
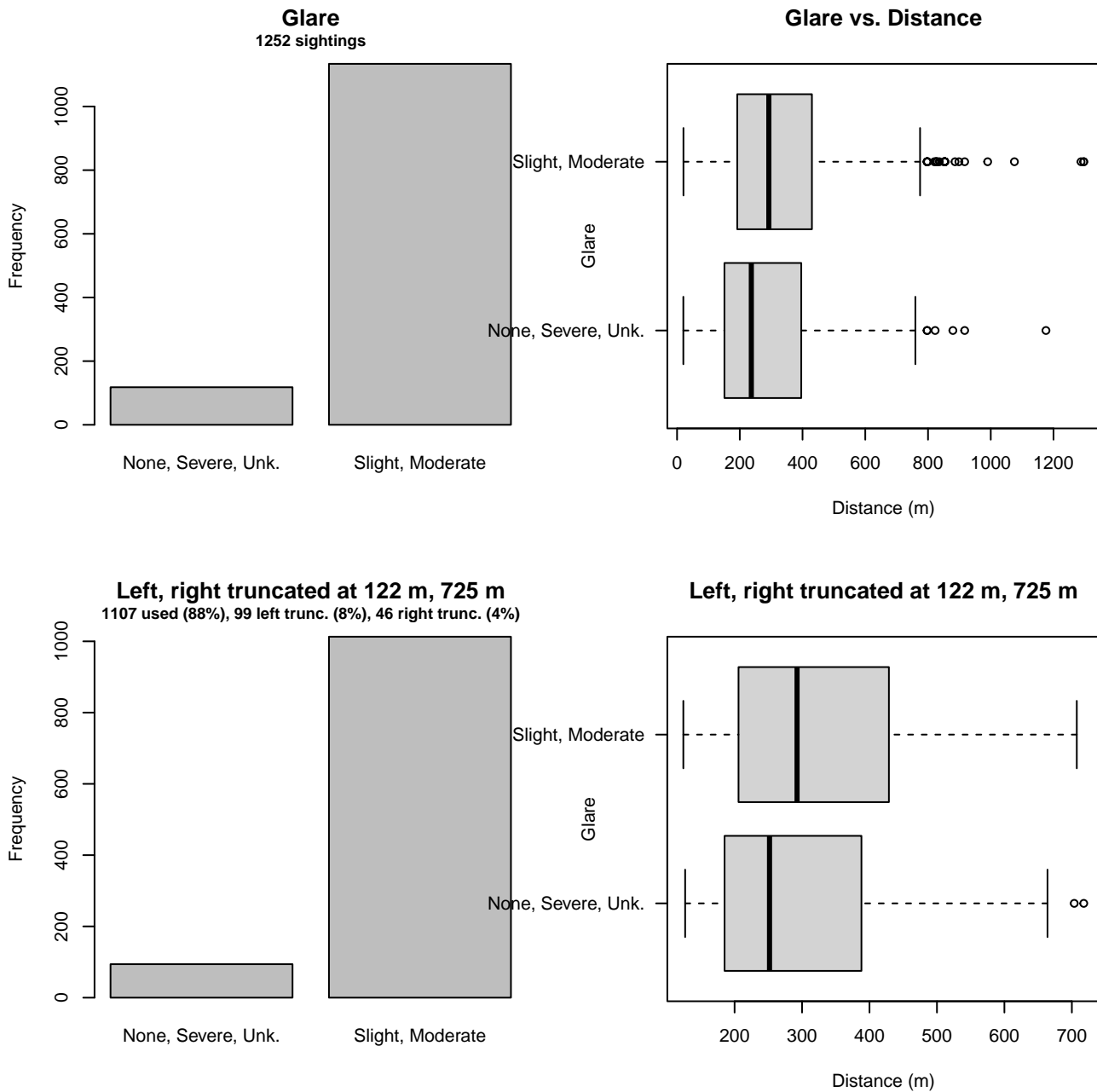
Figure 10: Distribution of the Glare covariate before (top row) and after (bottom row) observations were truncated to fit the NARWSS 2003-2016 detection function.
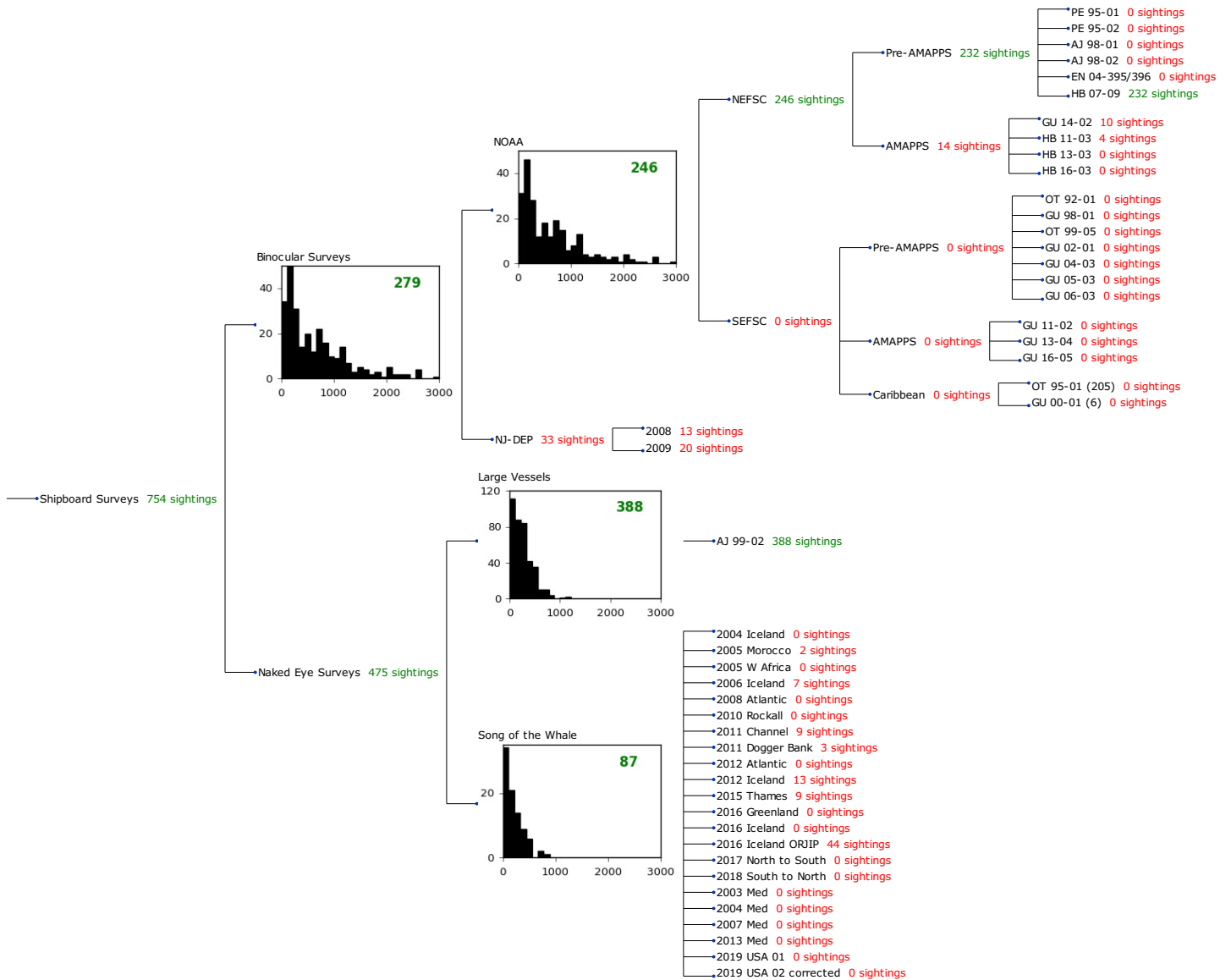
2.1.2 Shipboard Surveys

Binocular Surveys **279**

NOAA **246**

Large Vessels **388**

Song of the Whale **87**

Shipboard Surveys 754 sightings

Naked Eye Surveys 475 sightings

NEFSC 246 sightings

SEFSC 0 sightings

NJ-DEP 33 sightings
- 2008 13 sightings
- 2009 20 sightings

Pre-AMAPPS 232 sightings
- PE 95-01 0 sightings
- PE 95-02 0 sightings
- AJ 98-01 0 sightings
- AJ 98-02 0 sightings
- EN 04-395/396 0 sightings
- HB 07-09 232 sightings

AMAPPS 14 sightings
- GU 14-02 10 sightings
- HB 11-03 4 sightings
- HB 13-03 0 sightings
- HB 16-03 0 sightings

Pre-AMAPPS 0 sightings
- OT 92-01 0 sightings
- GU 98-01 0 sightings
- OT 99-05 0 sightings
- GU 02-01 0 sightings
- GU 04-03 0 sightings
- GU 05-03 0 sightings
- GU 06-03 0 sightings

AMAPPS 0 sightings
- GU 11-02 0 sightings
- GU 13-04 0 sightings
- GU 16-05 0 sightings

Caribbean 0 sightings
- OT 95-01 (205) 0 sightings
- GU 00-01 (6) 0 sightings

AJ 99-02 388 sightings

- 2004 Iceland 0 sightings
- 2005 Morocco 2 sightings
- 2005 W Africa 0 sightings
- 2006 Iceland 7 sightings
- 2008 Atlantic 0 sightings
- 2010 Rockall 0 sightings
- 2011 Channel 9 sightings
- 2011 Dogger Bank 3 sightings
- 2012 Atlantic 0 sightings
- 2012 Iceland 13 sightings
- 2015 Thames 9 sightings
- 2016 Greenland 0 sightings
- 2016 Iceland 0 sightings
- 2016 Iceland ORJIP 44 sightings
- 2017 North to South 0 sightings
- 2018 South to North 0 sightings
- 2003 Med 0 sightings
- 2004 Med 0 sightings
- 2007 Med 0 sightings
- 2013 Med 0 sightings
- 2019 USA 01 0 sightings
- 2019 USA 02 corrected 0 sightings

Figure 11: Detection hierarchy for shipboard surveys, showing how they were pooled during detectability modeling, for taxon-specific detection functions. Each histogram represents a detection function and summarizes the perpendicular distances of observations that were pooled to fit it, prior to truncation. Observation counts, also prior to truncation, are shown in green when they met the recommendation of Buckland et al. (2001) that detection functions utilize at least 60 sightings, and red otherwise. For rare taxa, it was not always possible to meet this recommendation, yielding higher statistical uncertainty. During the spatial modeling stage of the analysis, effective strip widths were computed for each survey using the closest detection function above it in the hierarchy (i.e. moving from right to left in the figure). Surveys that do not have a detection function above them in this figure were either addressed by a detection function presented in a different section of this report, or were omitted from the analysis.

2.1.2.1 NOAA

After right-truncating observations greater than 2400 m, we fitted the detection function to the 236 observations that remained. The selected detection function (Figure 12) used a hazard rate key function with Beaufort (Figure 13) as a covariate.
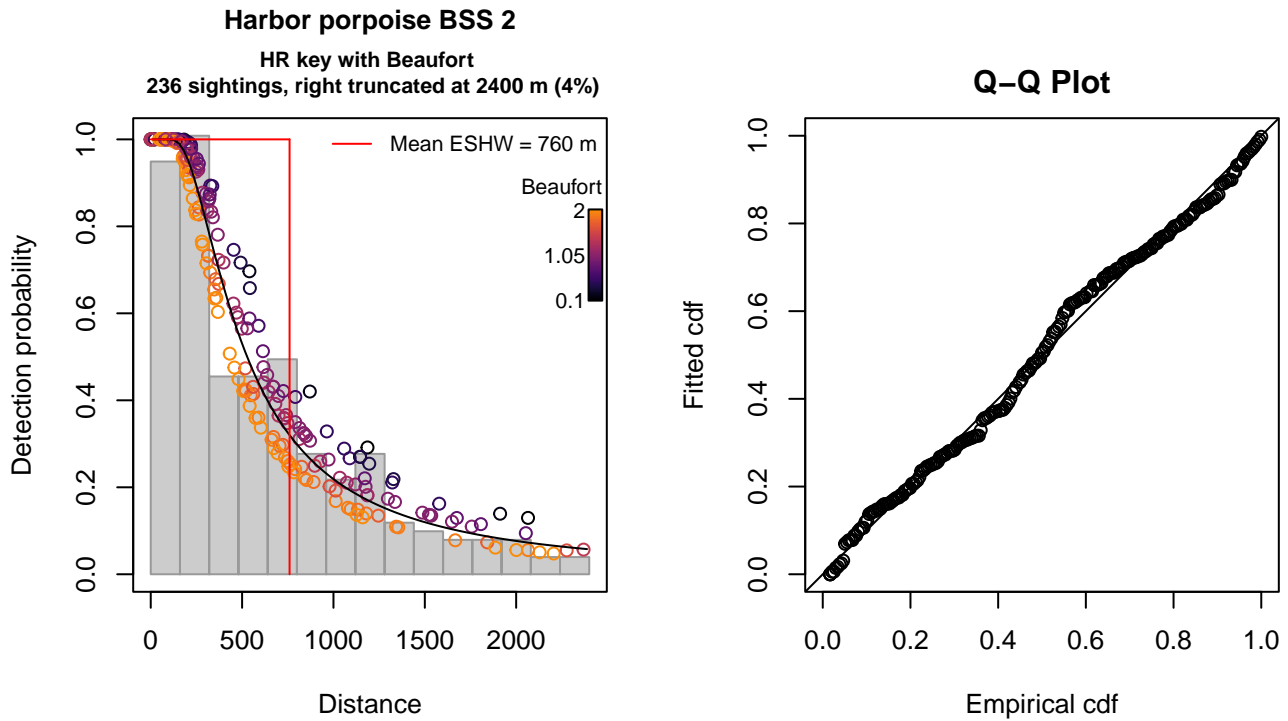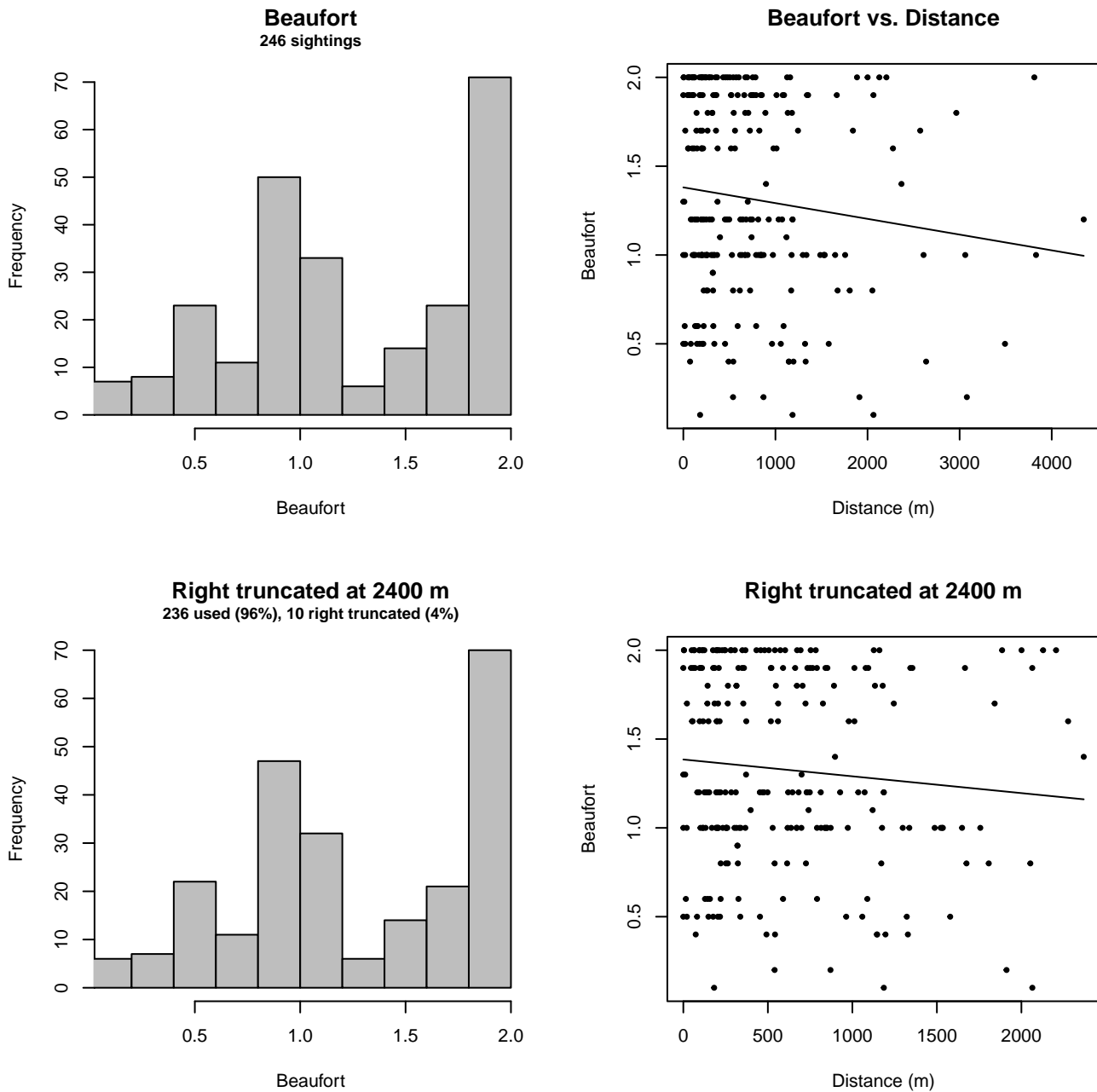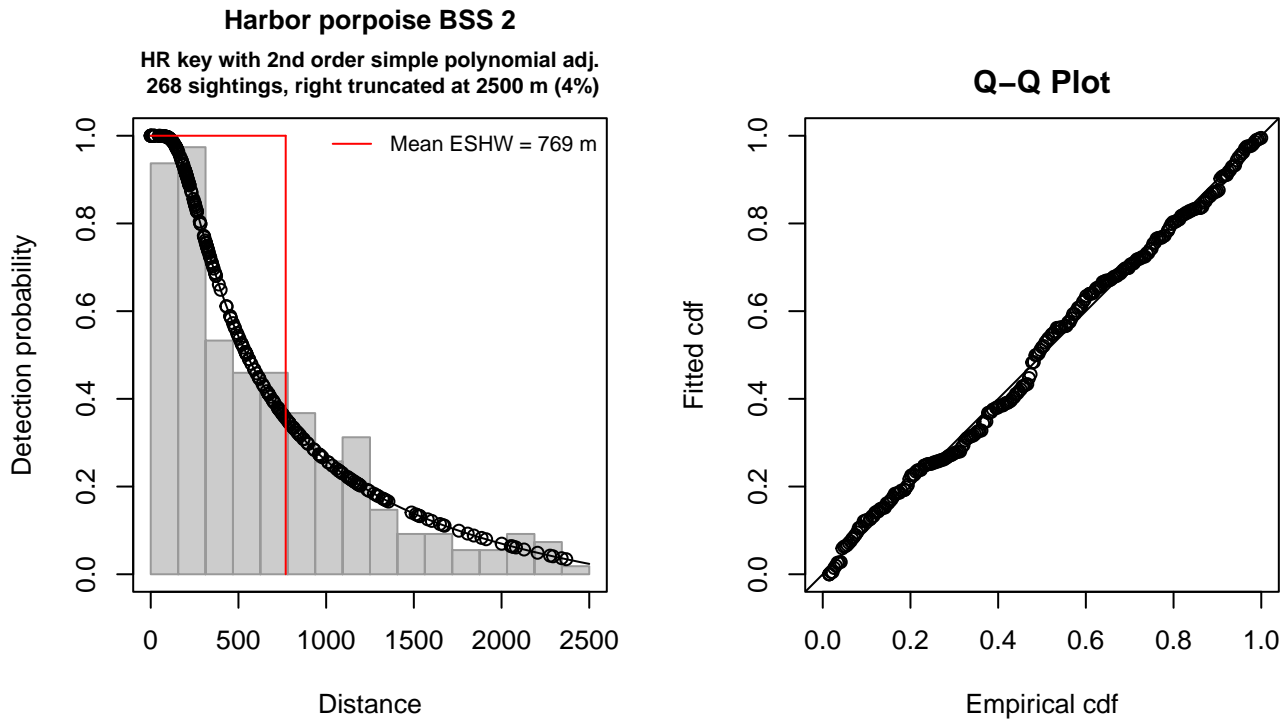
Figure 12: NOAA detection function and Q-Q plot showing its goodness of fit.

Statistical output for this detection function:

```
Summary for ds object
Number of observations :   236
Distance range         :   0  -  2400
AIC                    :   3486.175

Detection function:
 Hazard-rate key function

Detection function parameters
Scale coefficient(s):
              estimate          se
(Intercept)  6.4593524  0.3016068
Beaufort    -0.3002036  0.1973819

Shape coefficient(s):
             estimate         se
(Intercept) 0.4950994  0.1374732


                        Estimate          SE         CV
Average p              0.3110705   0.0315895  0.1015509
N in covered region  758.6704059  87.3463615  0.1151308


Distance sampling Cramer-von Mises test (unweighted)
Test statistic = 0.109104  p = 0.542059
```

Figure 13: Distribution of the Beaufort covariate before (top row) and after (bottom row) observations were truncated to fit the NOAA detection function.

2.1.2.2 Binocular Surveys

After right-truncating observations greater than 2500 m, we fitted the detection function to the 268 observations that remained. The selected detection function (Figure 14) used a hazard rate key function with no covariates.
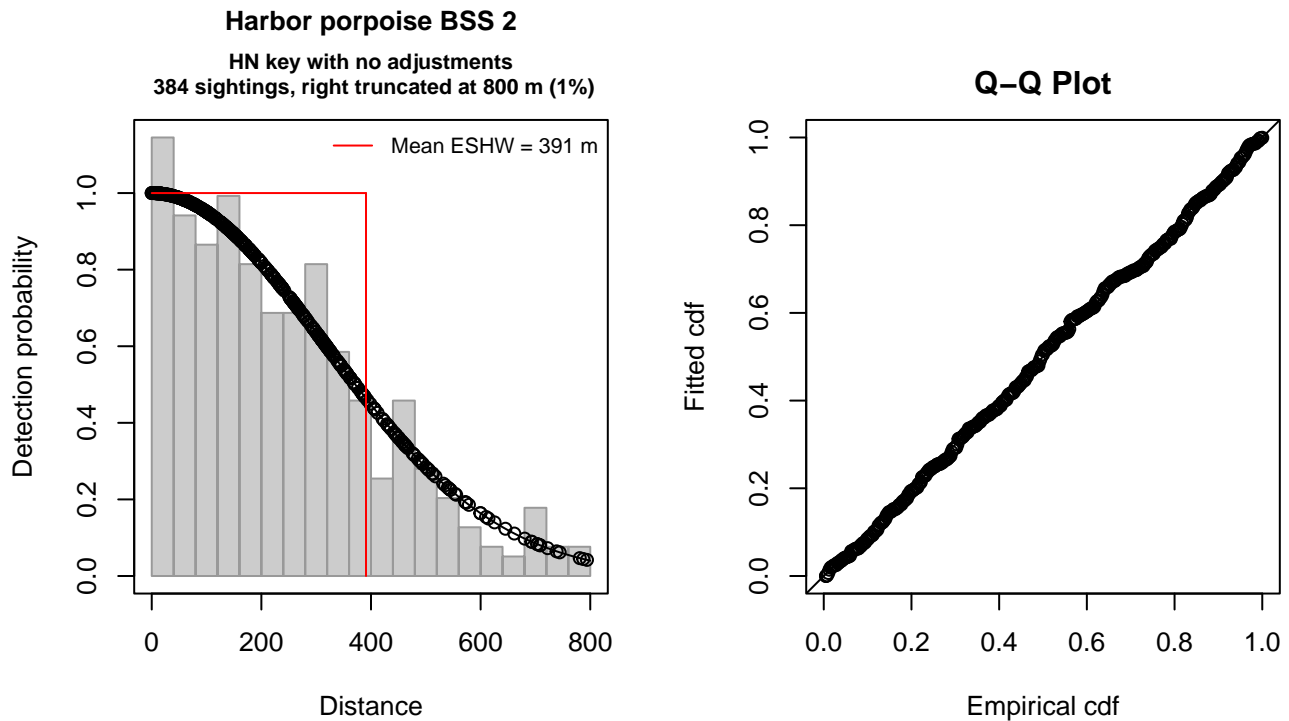
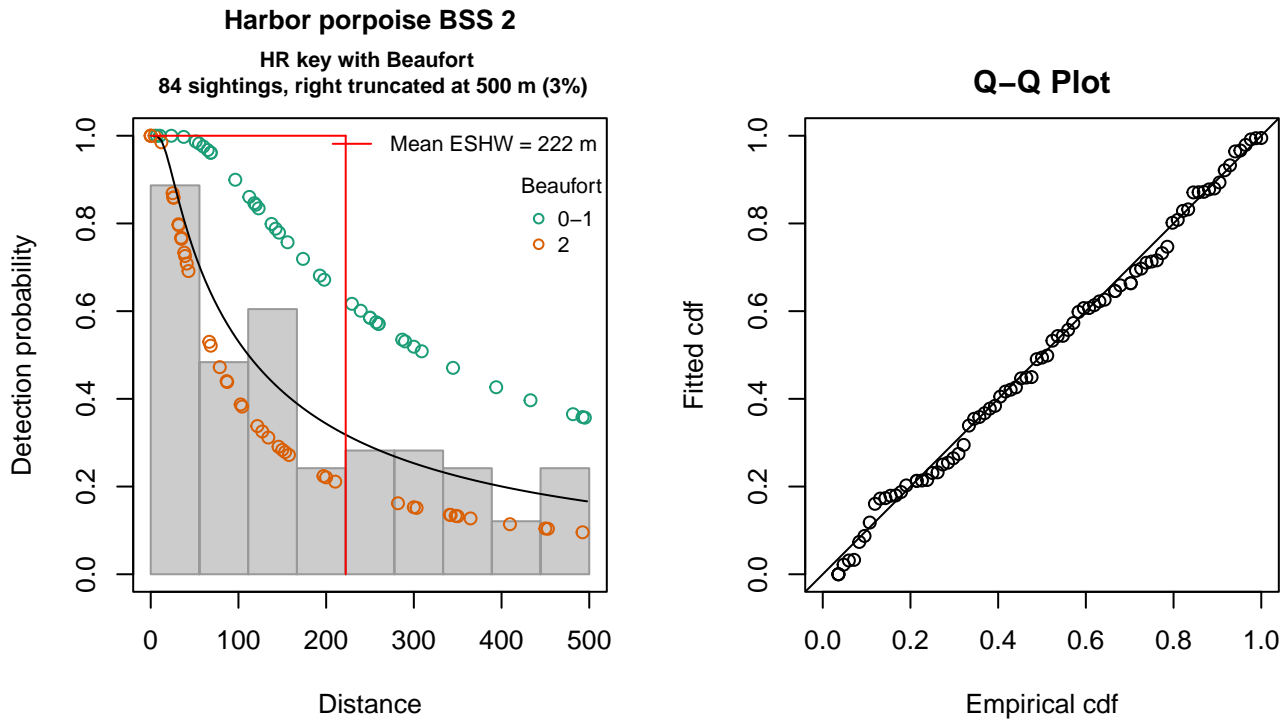Figure 14: Binocular Surveys detection function and Q-Q plot showing its goodness of fit.

Statistical output for this detection function:

```
Summary for ds object
Number of observations :  268
Distance range         :  0  -  2500
AIC                    :  3982.066


Detection function:
 Hazard-rate key function with simple polynomial adjustment term of order 2

Detection function parameters
Scale coefficient(s):
            estimate        se
(Intercept) 6.053603 0.2711461


Shape coefficient(s):
            estimate        se
(Intercept) 0.2019974 0.2432124


Adjustment term coefficient(s):
              estimate        se
poly, order 2 -0.7813994 0.2378876



Monotonicity constraints were enforced.
                     Estimate          SE         CV
Average p            0.3077835   0.03840985 0.1247950
N in covered region 870.7420286 117.32969852 0.1347468

Monotonicity constraints were enforced.

Distance sampling Cramer-von Mises test (unweighted)
Test statistic = 0.087087  p = 0.651922
```

2.1.2.3 Large Vessels

After right-truncating observations greater than 800 m, we fitted the detection function to the 384 observations that remained. The selected detection function (Figure 15) used a half normal key function with no covariates.

Figure 15: Large Vessels detection function and Q-Q plot showing its goodness of fit.

Statistical output for this detection function:

```
Summary for ds object
Number of observations :  384
Distance range         :  0  -  800
AIC                    :  4938.234

Detection function:
 Half-normal key function

Detection function parameters
Scale coefficient(s):
          estimate         se
(Intercept) 5.753891 0.04205698

                  Estimate        SE         CV
Average p          0.488608  0.01886316 0.03860592
N in covered region 785.906100 41.75053376 0.05312407

Distance sampling Cramer-von Mises test (unweighted)
Test statistic = 0.034812  p = 0.957820
```

2.1.2.4 Song of the Whale

After right-truncating observations greater than 500 m, we fitted the detection function to the 84 observations that remained. The selected detection function (Figure 16) used a hazard rate key function with Beaufort (Figure 17) as a covariate.

Figure 16: Song of the Whale detection function and Q-Q plot showing its goodness of fit.

Statistical output for this detection function:

```
Summary for ds object
Number of observations :   84
Distance range         :   0  -  500
AIC                    :   1021.761

Detection function:
 Hazard-rate key function

Detection function parameters
Scale coefficient(s):
            estimate         se
(Intercept)  5.394070  0.6376508
Beaufort2   -1.471877  0.9031148

Shape coefficient(s):
             estimate          se
(Intercept) 0.008373544  0.2989196


                     Estimate         SE         CV
Average p            0.3762195  0.1142156  0.3035877
N in covered region 223.2738969 70.7484253 0.3168683

Distance sampling Cramer-von Mises test (unweighted)
Test statistic = 0.031639  p = 0.970477
```
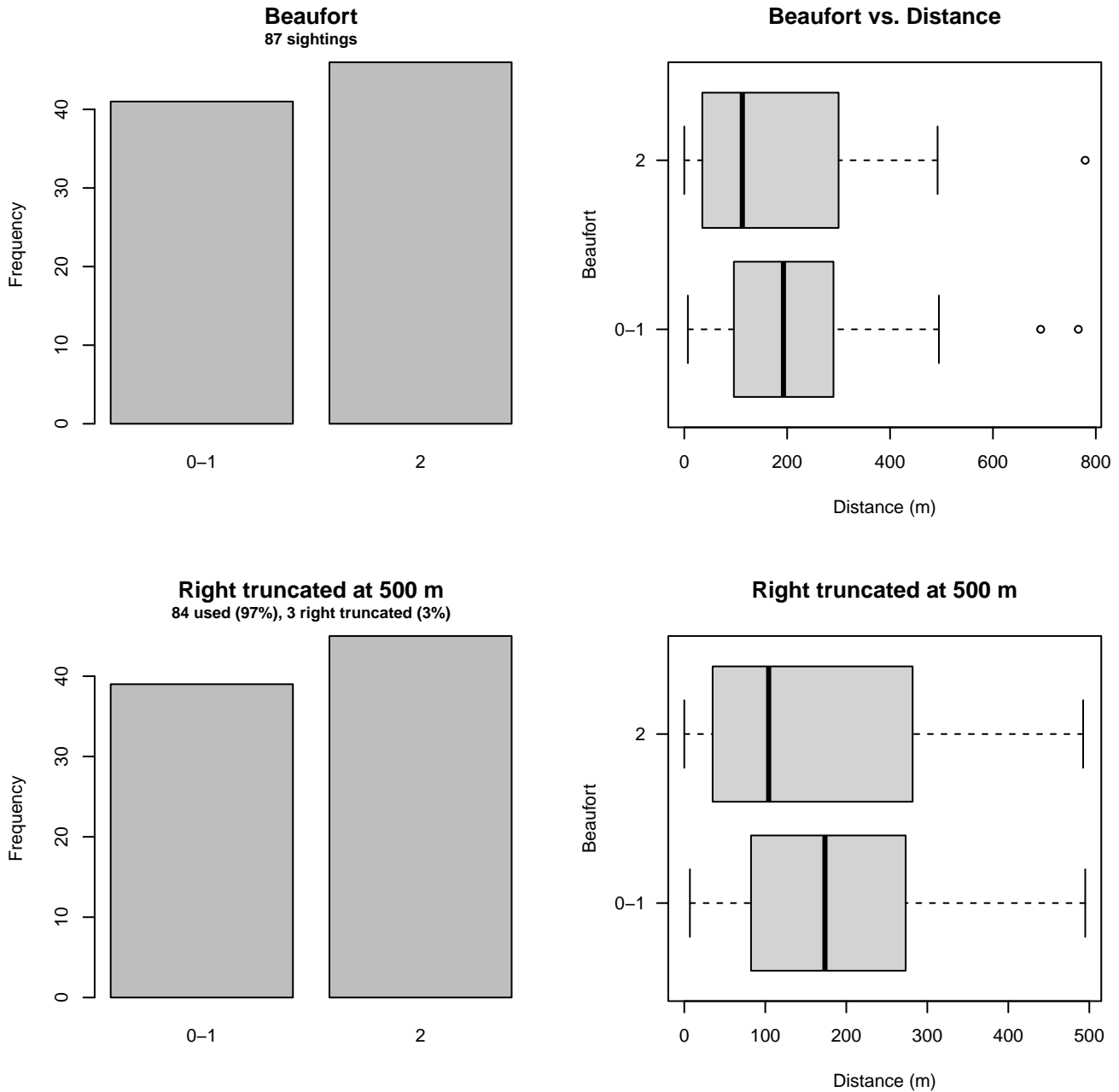
Figure 17: Distribution of the Beaufort covariate before (top row) and after (bottom row) observations were truncated to fit the Song of the Whale detection function.

3 Bias Corrections

Density surface modeling methodology uses *distance sampling* (Buckland et al. 2001) to model the probability that an observer on a line transect survey will detect an animal given the perpendicular distance to it from the transect line. Distance sampling assumes that detection probability is 1 when perpendicular distance is 0. When this assumption is not met, detection probability is biased high, leading to an underestimation of density and abundance. This is known as the $g_0 < 1$ problem, where g_0 refers to the detection probability at distance 0. Modelers often try to address this problem by estimating g_0 empirically and dividing it into estimated density or abundance, thereby correcting those estimates to account for the animals that were presumed missed.

Two important sources of bias for visual surveys are known as *availability bias*, in which an animal was present on the transect line but impossible to detect, e.g. because it was under water, and *perception bias*, in which an animal was present and available but not noticed, e.g. because of its small size or cryptic coloration or behavior (Marsh and Sinclair 1989). Modelers often

22

estimate the influence of these two sources of bias on detection probability independently, yielding two estimates of g_0, hereafter referred to as g_{0A} and g_{0P}, and multiply them together to obtain a final, combined estimate: $g_0 = g_{0A}.g_{0P}$.

Our overall approach was to perform this correction on a per-observation basis, to have the flexibility to account for many factors such as platform type, surveyor institution, group size, group composition (e.g. singleton, mother-calf pair, or surface active group), and geographic location (e.g. feeding grounds vs. calving grounds). The level of complexity of the corrections varied by species according to the amount of information available, with North Atlantic right whale having the most elaborate corrections, derived from a substantial set of publications documenting its behavior, and various lesser known odontocetes having corrections based only on platform type (aerial or shipboard), derived from comparatively sparse information. Here we document the corrections used for harbor porpoise.

3.1 Aerial Surveys

Reflecting the northerly distribution of the species, all but 9 of the nearly 2000 aerial sightings of harbor porpoise were reported by NEFSC (Table 1). Palka et al. (2021) developed perception bias corrections using two team, mark recapture distance sampling (MRDS) methodology (Burt et al. 2014) for aerial surveys conducted in 2010-2017 by NEFSC during the AMAPPS program. This was the only extant perception bias estimate developed from aerial surveys used in our analysis, aside from estimates developed earlier by Palka and colleagues (Palka 2006; Palka et al. 2017). Those earlier efforts utilized older methods and less data than their 2021 analysis, so we applied the Palka et al. (2021) estimate to all aerial survey programs (Table 4).

For all aerial surveys, to account for the influence of large group sizes on perception bias, we followed Carretta et al. (2000) and set the perception bias correction factor for sightings of more than 25 animals to $g_{0P} = 0.994$. Due to the typically small group sizes of harbor porpoise, only 3 out of the nearly 2000 aerial sightings received this correction.

We caution that it is possible that perception bias was different on the other aerial programs, as they often used different aircraft, flew at different altitudes, and were staffed by different personnel. Of particular concern are that many programs flew Cessna 337 Skymasters, which had flat windows, while NOAA flew de Havilland Twin Otters, which had bubble windows, which likely afforded a better view of the transect line and therefore might have required less of a correction than the Skymasters. Correcting the other programs using NOAA's estimate as we have done is likely to yield less bias than leaving them uncorrected, but we urge all programs to undertake their own efforts to estimate perception bias, as resources allow.

We estimated availability bias corrections using the Laake et al. (1997) estimator and dive intervals reported by Palka et al. (2017) (Table 5). To estimate time in view, needed by the Laake estimator, we used results reported by Robertson et al. (2015), rescaled linearly for each survey program according to its target altitude and speed. We caution that Robertson's analysis was done for a de Havilland Twin Otter, which may have a different field of view than that of the other aircraft used here, which mainly comprised Cessna 337 Skymasters with flat windows. However, we note that McLellan et al. (2018) conducted a sensitivity analysis on the influence of the length of the "window of opportunity" to view beaked whales from a Cessna Skymaster on their final density estimates and found that they varied by only a few thousandths of an animal per kilometer when the window of opportunity more than doubled. Still, we urge additional program-specific research into estimation of availability bias.

To address the influence of group size on availability bias, we applied the group availability estimator of McLellan et al. (2018) on a per-observation basis. Following Palka et al. (2021), who also used that method, we assumed that individuals in the group dived asynchronously. The resulting g_{0A} corrections ranged from about 0.6 to 1.0 (Figure 18). We caution that the assumption of asynchronous diving can lead to an underestimation of density and abundance if diving is actually synchronous; see McLellan et al. (2018) for an exploration of this effect. However, if future research finds that this species conducts synchronous dives and characterizes the degree of synchronicity, the model can be updated to account for this knowledge.

Table 4: Perception bias corrections for harbor porpoise applied to aerial surveys.

Surveys	Group Size	g_{0P}	g_{0P} Source
All	≤ 25	0.52	Palka et al. (2021): NEFSC
All	> 25	0.99	Carretta et al. (2000)

Table 5: Surface and dive intervals for harbor porpoise used to estimate availability bias corrections.

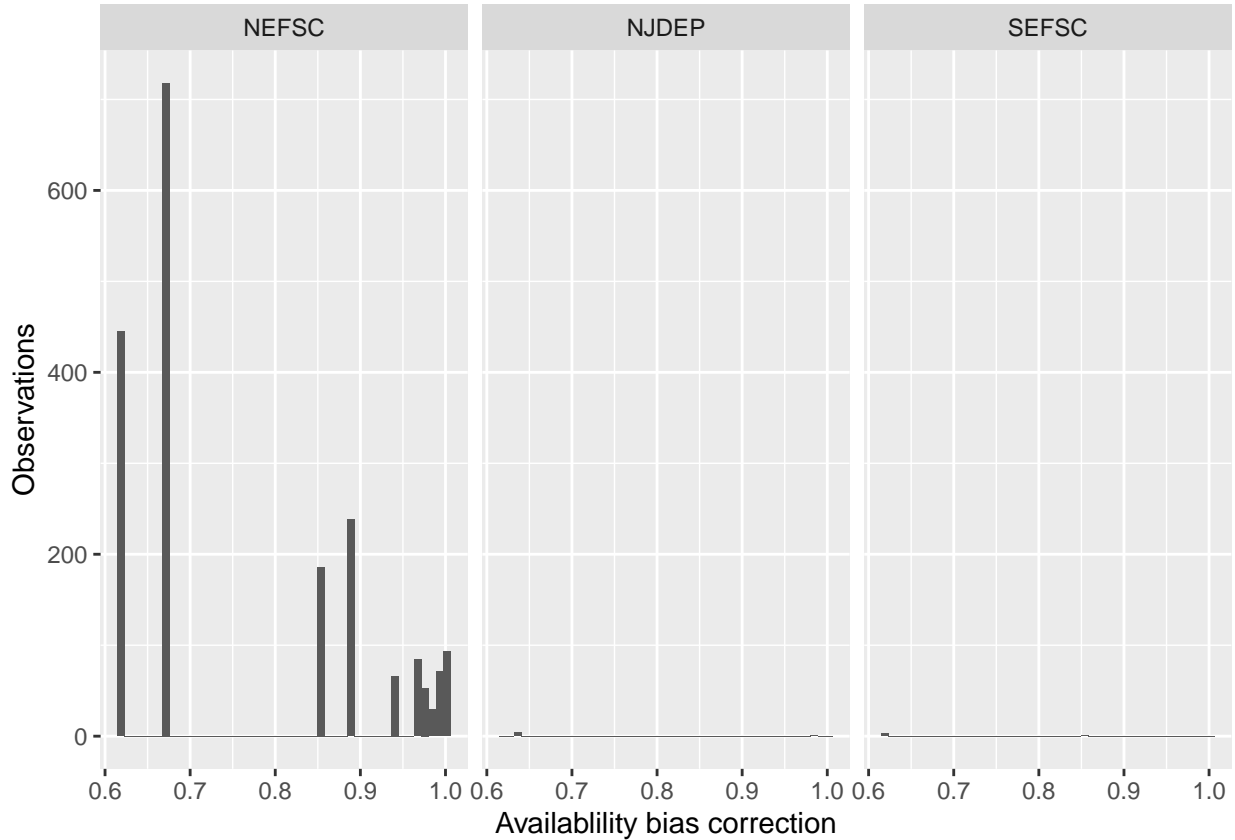| Surface Interval (s)	Dive Interval (s)	Source
49	64	Palka et al. (2017)

Figure 18: Availability bias corrections for harbor porpoise for aerial surveys, by institution.

3.2 Shipboard Surveys

Most of the shipboard surveys in our analysis used high-power (25x150), pedestal-mounted binoculars. The only institutions that reported sightings of harbor porpoises during high-power binocular surveys were NOAA NEFSC[1] and NJDEP. Palka et al. (2021) developed perception bias corrections using two team, MRDS methodology (Burt et al. 2014) for high-power binocular surveys conducted in 2010-2017 by NEFSC during the AMAPPS program (Table 6). We also considered Palka and colleagues' earlier estimates (Palka 2006; Palka et al. 2017), but they utilized older methods and less data than the 2021 analysis, so we applied the Palka et al. (2021) estimates to all shipboard surveys that searched with high-power binoculars.

Palka (2006) also developed a correction for an NEFSC shipboard survey (AJ 99-02) in which the primary team observers searched by naked eye. We applied this estimate to that survey as well as to the MCR Song of the Whale surveys, which also searched by naked eye but did not have a program-specific estimate. We caution that the platform height for the MCR surveys was substantially lower than the NEFSC survey, and the target survey speed was slower (6 knots for MCR vs. 10 knots for NEFSC).

Given that the dive interval of this species (Table 5) was short relative to the amount of time a given patch of water remained in view to shipboard observers, we assumed that no availability bias correction was needed ($g_{0A} = 1$), following Palka et al. (2021).

---

[1]Table 6-6 of Palka et al. (2021) lists harbor porpoise sightings for SEFSC during spring, but this refers to sightings made during the 2014 R/V Gordon Gunter cruise (GU 14-02) conducted by NEFSC personnel in a region traditionally covered by NEFSC, as documented by Palka et al. (2014). Accordingly, we tallied these sightings as being from NEFSC rather than SEFSC. We suspect Palka et al. (2021) tallied them as being from SEFSC because the survey was conducted on R/V Gordon Gunter, a vessel traditionally used by SEFSC but not NEFSC.

Table 6: Perception and availability bias corrections for harbor porpoise applied to shipboard surveys.

Surveys	Searching Method	Group Size	g_{0P}	g_{0P} Source	g_{0A}	g_{0A} Source
NEFSC, NJDEP	Binoculars	Any	0.52	Palka et al. (2021): NEFSC	1	Assumed
NEFSC, MCR	Naked eye	Any	0.35	Palka et al. (2006)	1	Assumed

4 Density Model

Harbor porpoises inhabit temperate and subarctic waters, often close to shore or at shallow depths. Analyses of genetic, chemical tracer, and life history data suggest there are four stocks in the North Atlantic: the Gulf of Maine/Bay of Fundy, Gulf of St. Lawrence, Newfoundland, and Greenland populations (Hayes et al. 2022). Our study area encompasses much of the reported spatial extent of the the Gulf of Maine/Bay of Fundy stock. The northern part of the study area, along the Scotian Shelf, also partially overlaps with the southernmost extent of the Gulf of St. Lawrence stock. Although genetic data suggest there may be some mixing between these two stocks, they are fairly spatially distinct. Our objective was to model the Gulf of Maine/Bay of Fundy stock; the remainder of this document pertains to that stock, unless explicitly stated otherwise.

Palka (1996) summarized the seasonal distribution of the Gulf of Maine/Bay of Fundy stock as follows. In July, the population migrates into the northern Gulf of Maine and lower Bay of Fundy region and remains there during summer. In September, it begins migrating out to the lower Gulf of Maine, the northern mid-Atlantic states, and coastal waters off Nova Scotia to Halifax. In winter, defined in Palka's report as December to March, harbor porpoises occur as far south as North Carolina, typically no farther south than Cape Hatteras. In April to June, the population returns north.

Consistent with this, Byrd et al. (2014) reported that during 1997-2008, harbor porpoises stranded in North Carolina from January through May, with a peak in March. Most occurred north of Cape Hatteras, substantially fewer occurred between Cape Lookout and Cape Hatteras, and almost none occurred south of Cape Lookout. Wingfield et al. (2017) reported a similar temporal pattern in acoustic detections from a line of four C-POD hydrophones deployed at the latitude of Maryland's wind energy lease area. A few acoustic detections were reported in October through December, and substantial counts during January through May, with two sites peaking in March, one in February, and one in January.

Sightings available as of April 2022 in the OBIS-SEAMAP archive (Halpin et al. 2009), which included both sightings from systematic surveys utilized in the model presented here and sightings from other sources not usable by this model, showed a similar pattern. Sightings in fall (September-November) strongly resembled those from summer (June-August), with highest concentrations ranging from New Hampshire to the lower Bay of Fundy, and few occurring south of Nantucket. Similarly, sightings in spring (March-May) strongly resembled those from winter (December-February), mostly occurring from New Hampshire and south, with substantial numbers seen south of Nantucket, unlike the summer and fall months.

Although NOAA's 2021 Stock Assessment Report stated that "there does not appear to be a temporally coordinated migration or a specific migratory route to and from the Bay of Fundy region", we believe a reasonably clear temporal pattern is evident in the available sightings, strandings, and acoustics data. Based on that, and the species' clear preference for the southern Bay of Fundy in summer and fall, we split the model into two seasons, Winter (December-May) and Summer (June-November), and modeled them independently.

4.1 Winter Model

The Winter model, spanning the months of December-May, suffered from a severe lack of offshore segments collected in sea states of Beaufort 2 or less. Given this, and that harbor porpoises are known to occur in deep waters far offshore (Palka et al. 1996; Westgate et al. 1998; Bjorge 2003), we constrained the model to a maximum depth of 1500 m, leaving depths beyond this unmodeled. Also lacking survey transects north during these months along the Scotian Shelf and in the upper Bay of Fundy, we excluded these areas as well. For the focal time period, December 1997 through May 2019, the available surveys reported nearly 1000 sightings, ranging from the lower Bay of Fundy to just south of the Virginia-North Carolina border (Figure 19).

When ranked by REML score (Wood 2011), the highest ranked candidate models with contemporaneous covariates slightly outranked those with climatological covariates, and explained 0.1% more deviance. We selected the top-ranked contemporaneous-covariate model, which included six covariates (Table 7). Relationships with static covariates indicated an avoidance of very shallow or nearshore waters, with a bimodal effect indicating highest marginal boosts to density at about 50 and 200 m depth, and about 90 and 200 km from shore (Figure 22). The relationship with sea surface temperature (SST), and salinity (SSS) indicated a preference for waters cooler than 10 °C and fresher than 33.5 PSU, consistent with on-shelf habitat north of Cape Hatteras. Similarly, the relationship with primary productivity (EVGPM) was positive, indicating a preference for more productive waters, which are found on the shelf north of Cape Hatteras. Finally, a positive effect on

density was fitted for waters closer than 35 km to SST fronts, consistent with the findings of Johnston et al. (2005), who tracked harbor porpoises in close proximity to prey-aggregating fronts in the lower Bay of Fundy.
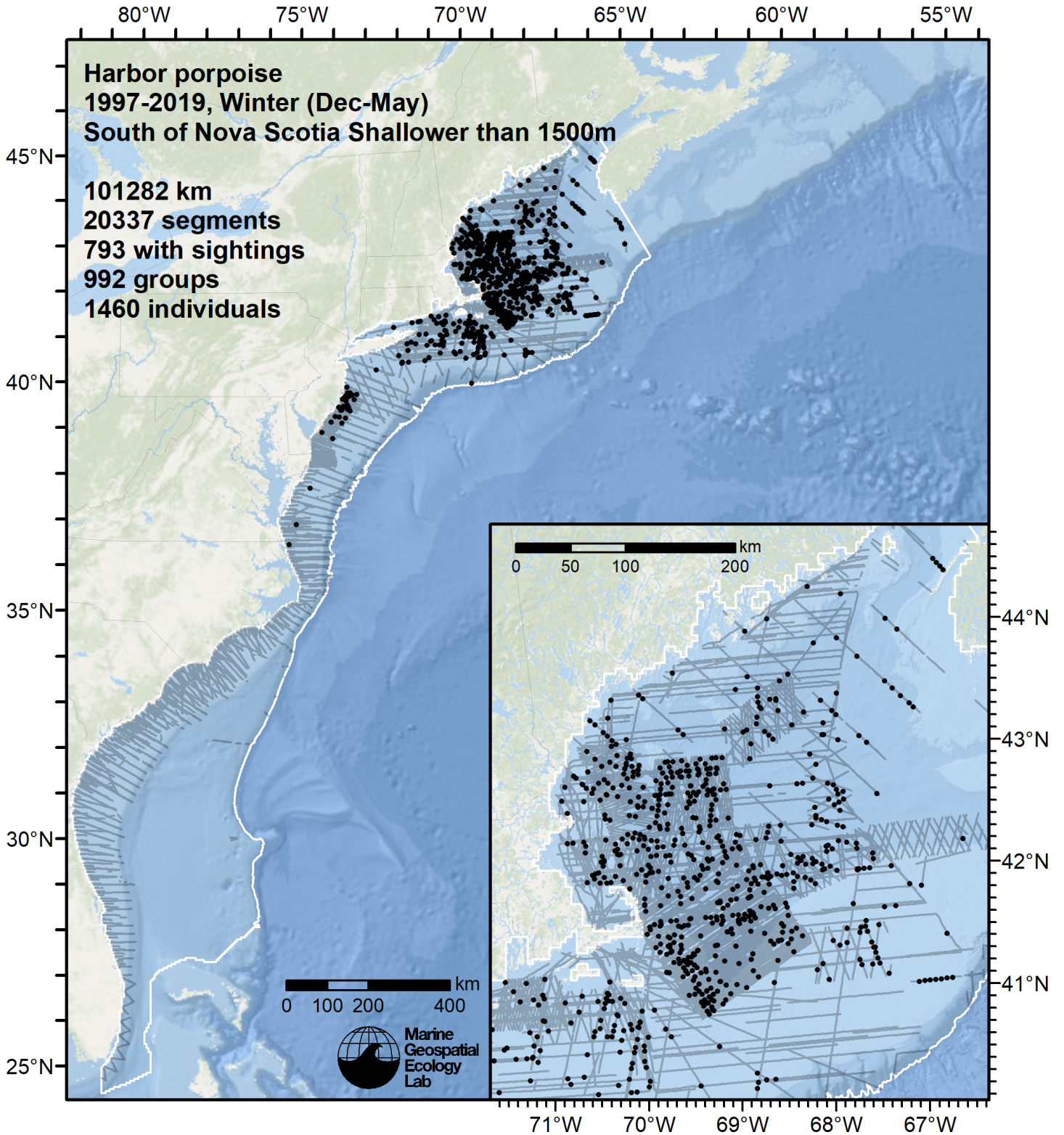
4.1.1 Final Model

Figure 19: Survey segments used to fit the model for the region South of Nova Scotia Shallower than 1500m for Winter. Black points indicate segments with observations.
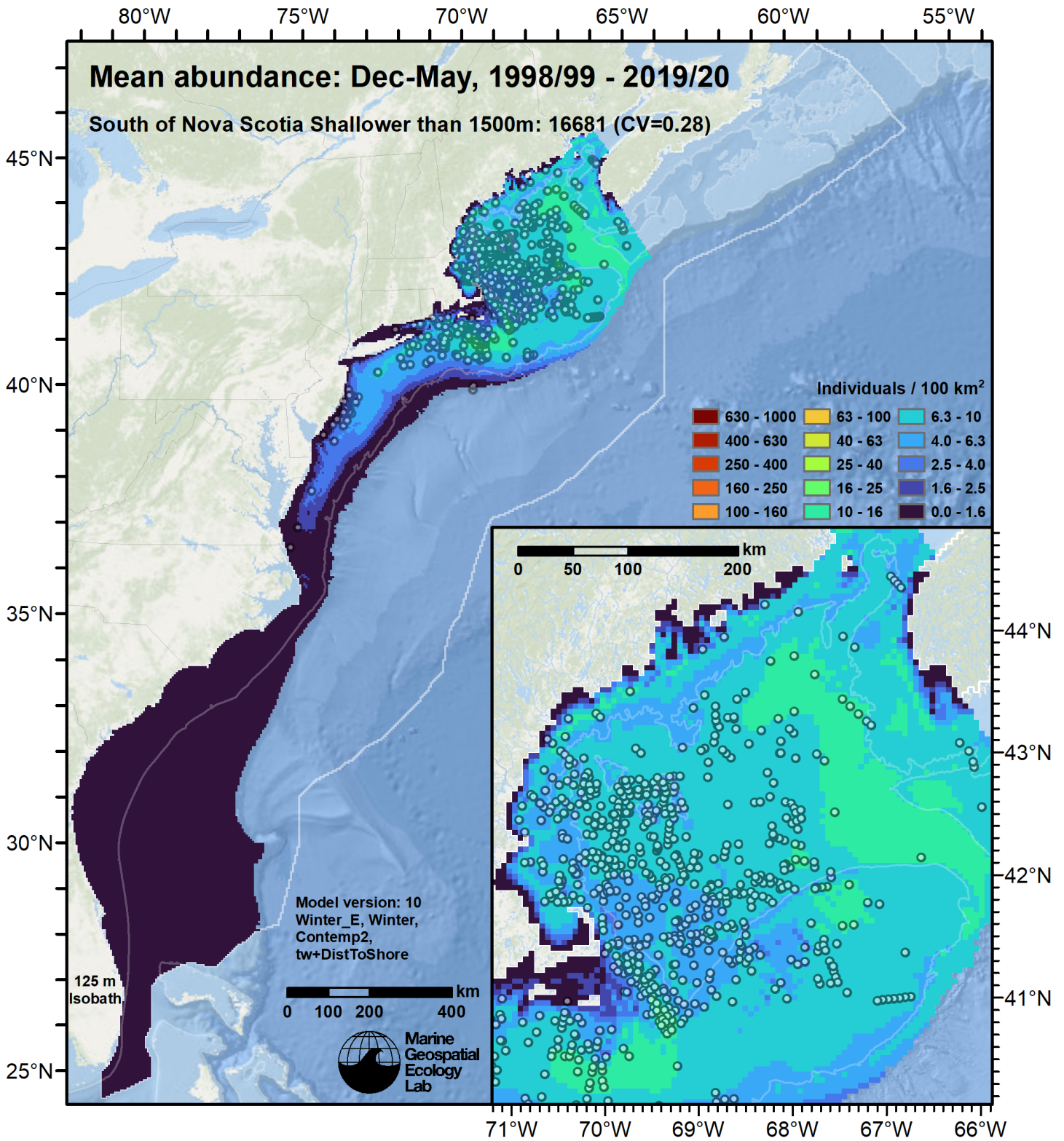
Figure 20: Harbor porpoise mean density for the indicated period, as predicted by the model for the region South of Nova Scotia Shallower than 1500m for Winter. Open circles indicate segments with observations. Mean total abundance and its coefficient of variation (CV) are given in the subtitle. Variance was estimated with the analytic approach given by Miller et al. (2022), Appendix S1, and accounts both for uncertainty in model parameter estimates and for seasonal and interannual variability in dynamic covariates.
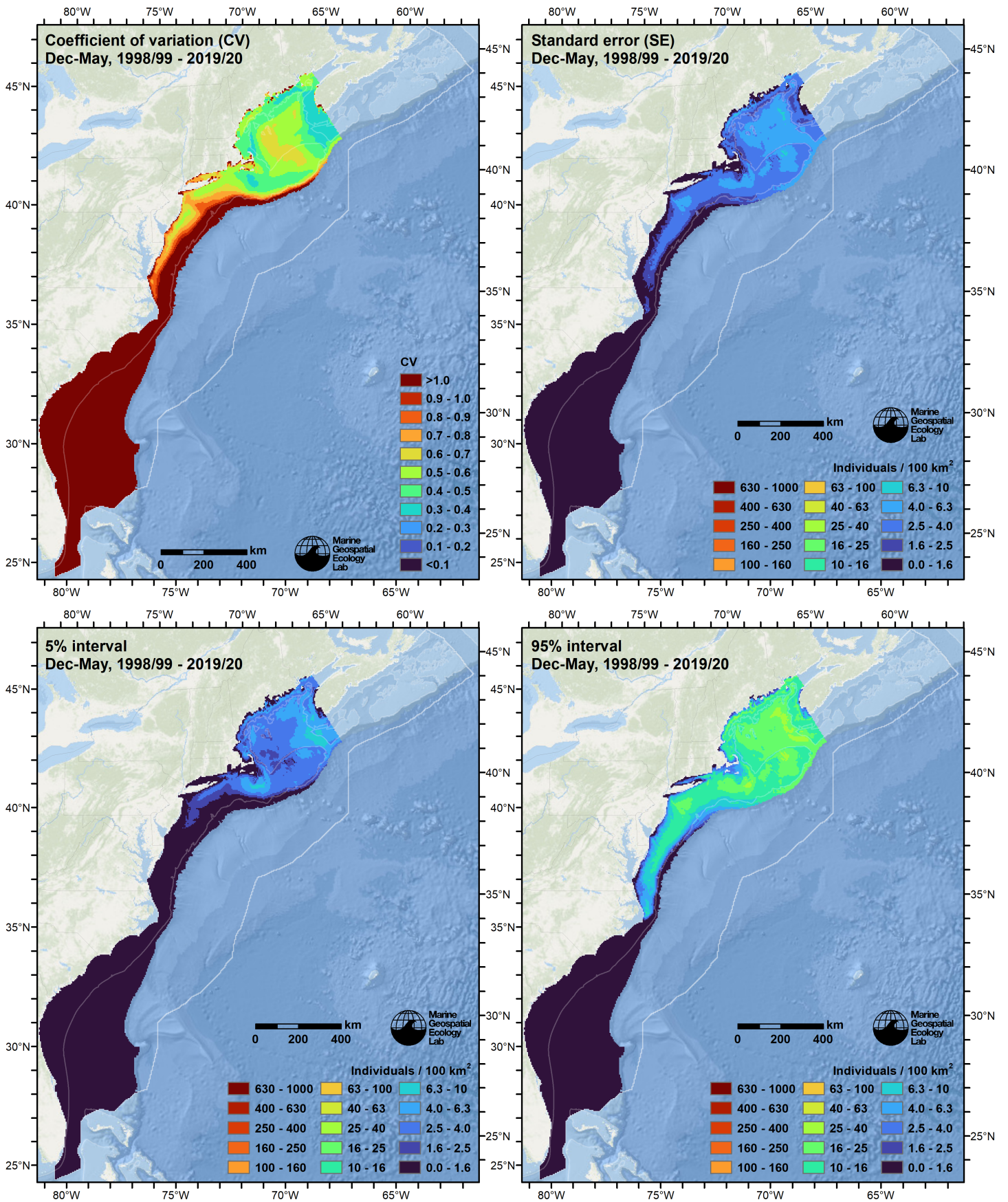
Figure 21: Uncertainty statistics for the harbor porpoise mean density surface (Figure 20) predicted by the model for the region South of Nova Scotia Shallower than 1500m for Winter. Variance was estimated with the analytic approach given by Miller et al. (2022), Appendix S1, and accounts both for uncertainty in model parameter estimates and for seasonal and interannual variability in dynamic covariates.

Statistical output for this model:

```
Family: Tweedie(p=1.14)
Link function: log

Formula:
IndividualsCorrected ~ offset(log(SegmentArea)) + s(log10(pmax(3,
    pmin(Depth, 300))), bs = "ts") + s(pmax(2, pmin(SST_CMC,
    18)), bs = "ts") + s(pmax(30.5, pmin(SSS_HYCOM, 36.5)), bs = "ts") +
    s(pmin(I(DistToFront063/1000), 75), bs = "ts") + s(pmax(200,
    pmin(PP_EVGPM, 2500)), bs = "ts") + s(pmin(I(DistToShore/1000),
    200), bs = "ts")

Parametric coefficients:
            Estimate Std. Error t value Pr(>|t|)
(Intercept) -18.8439     0.5738  -32.84   <2e-16 ***
---
Signif. codes:  0 '***' 0.001 '**' 0.01 '*' 0.05 '.' 0.1 ' ' 1

Approximate significance of smooth terms:
                                      edf Ref.df      F  p-value
s(log10(pmax(3, pmin(Depth, 300))))   5.868      9  6.344  < 2e-16 ***
s(pmax(2, pmin(SST_CMC, 18)))         5.393      9  9.588  < 2e-16 ***
s(pmax(30.5, pmin(SSS_HYCOM, 36.5)))  3.644      9  5.029  < 2e-16 ***
s(pmin(I(DistToFront063/1000), 75))   3.036      9  4.751  < 2e-16 ***
s(pmax(200, pmin(PP_EVGPM, 2500)))    1.018      9  1.844 2.49e-05 ***
s(pmin(I(DistToShore/1000), 200))     3.446      9  1.843 0.000519 ***
---
Signif. codes:  0 '***' 0.001 '**' 0.01 '*' 0.05 '.' 0.1 ' ' 1

R-sq.(adj) =  0.0256   Deviance explained = 15.3%
-REML = 4688.1  Scale est. = 5.7913    n = 20337

Method: REML   Optimizer: outer newton
full convergence after 10 iterations.
Gradient range [-0.002572193,0.0007545939]
(score 4688.066 & scale 5.791295).
Hessian positive definite, eigenvalue range [0.2883761,5280.952].
Model rank =  55 / 55

Basis dimension (k) checking results. Low p-value (k-index<1) may
indicate that k is too low, especially if edf is close to k'.

                                       k'  edf k-index p-value
s(log10(pmax(3, pmin(Depth, 300))))   9.00 5.87    0.79   0.005 **
s(pmax(2, pmin(SST_CMC, 18)))         9.00 5.39    0.78   <2e-16 ***
s(pmax(30.5, pmin(SSS_HYCOM, 36.5)))  9.00 3.64    0.75   <2e-16 ***
s(pmin(I(DistToFront063/1000), 75))   9.00 3.04    0.82   0.525
s(pmax(200, pmin(PP_EVGPM, 2500)))    9.00 1.02    0.80   0.080 .
s(pmin(I(DistToShore/1000), 200))     9.00 3.45    0.81   0.350
---
Signif. codes:  0 '***' 0.001 '**' 0.01 '*' 0.05 '.' 0.1 ' ' 1
```

(a) Seafloor depth (m) (b) Distance to SST front (km) (c) Distance to shore (km)

(d) Net primary productivity (mg C m^{-2} day^{-1}) (EVGPM) (e) Sea surface salinity (PSU) (f) Sea surface temperature (°C)
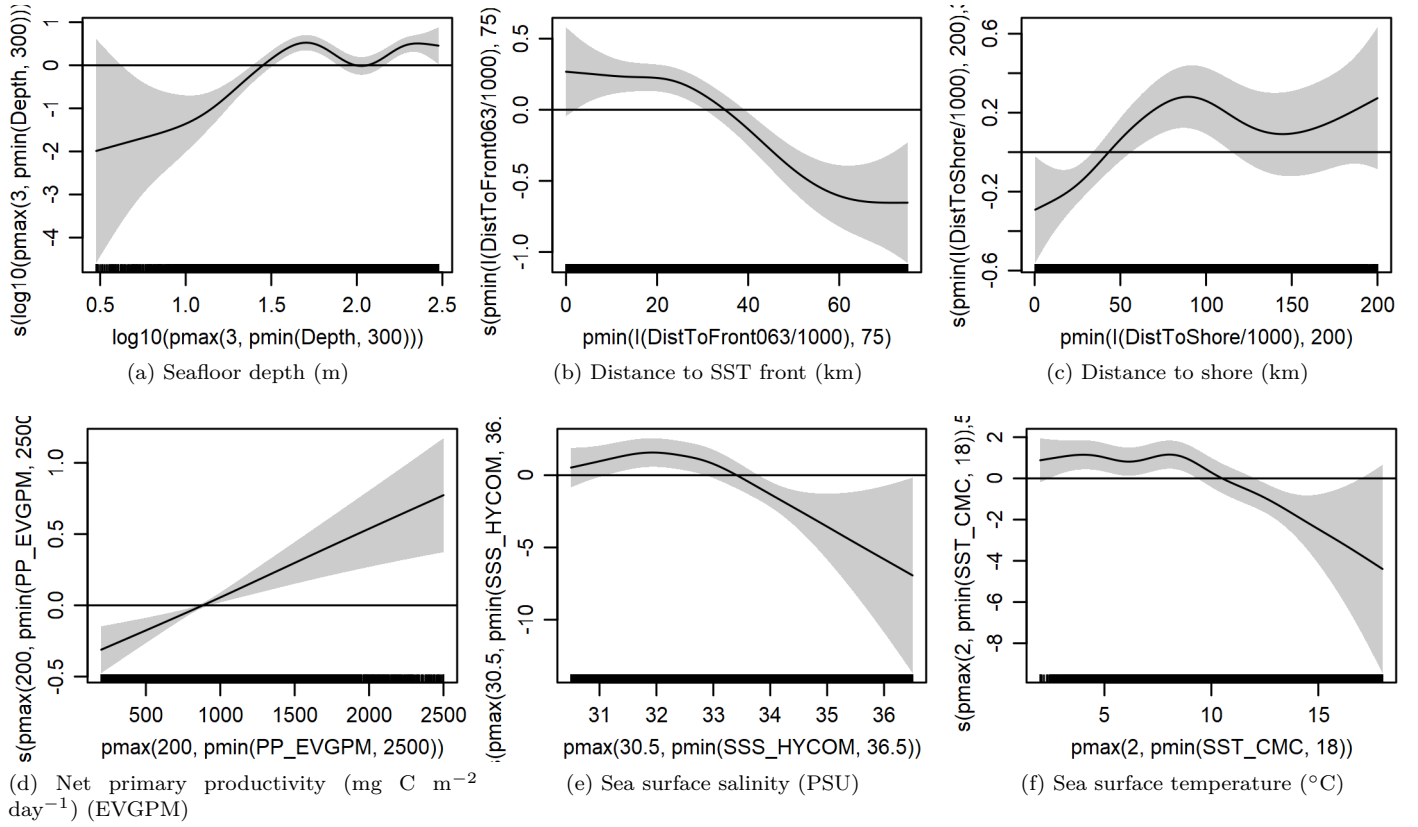
Figure 22: Functional plots for the final model for the region South of Nova Scotia Shallower than 1500m for Winter. Transforms and other treatments are indicated in axis labels. *log10* indicates the covariate was $\log_{10}$ transformed. *pmax* and *pmin* indicate the covariate's minimum and maximum values, respectively, were Winsorized to the values shown. Winsorization was used to prevent runaway extrapolations during prediction when covariates exceeded sampled ranges, or for ecological reasons, depending on the covariate. */1000* indicates meters were transformed to kilometers for interpretation convenience.
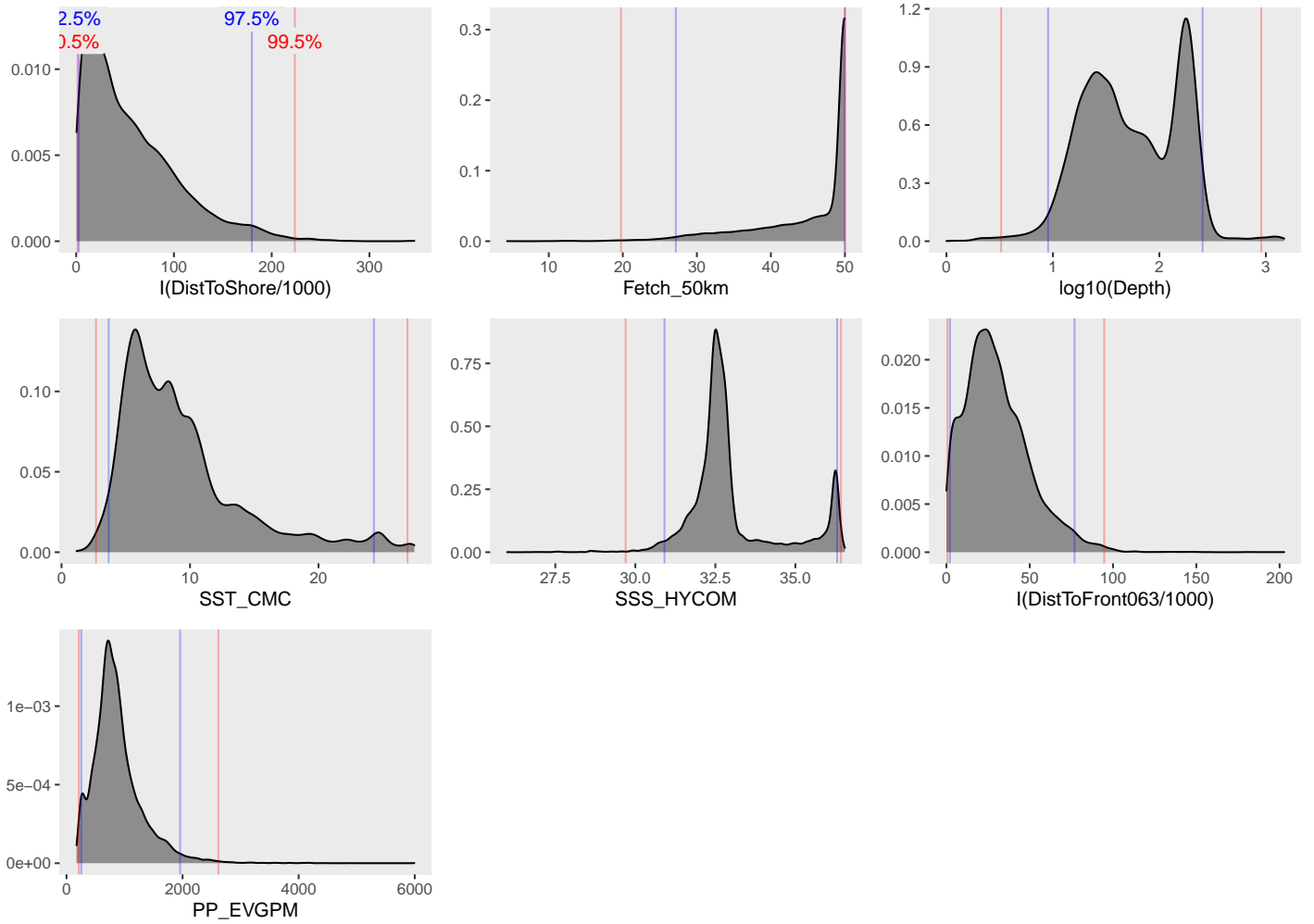
Table 7: Covariates used in the final model for the region South of Nova Scotia Shallower than 1500m for Winter.

Covariate	Description
Depth	Depth (m) of the seafloor, from SRTM30_PLUS (Becker et al. (2009))
DistToFront063	Monthly mean distance (km) to the closest sea surface temperature front detected in daily GHRSST Level 4 CMC0.2deg and CMC0.1deg images (Brasnett (2008); Canada Meteorological Center (2012); Meissner et al. (2016); Canada Meteorological Center (2016)) with MGET's implementation of the Canny edge detector (Roberts et al. (2010); Canny (1986))
DistToShore	Distance (km) to shore excluding Bermuda and Sable Island, derived from SRTM30_PLUS (Becker et al. (2009))
PP_EVGPM	Monthly mean net primary productivity (mg C m^{-2} day^{-1}) from the "Eppley" Vertically Generalized Production Model (EVGPM) (Behrenfeld and Falkowski (1997); Eppley (1972); Morel (1991))
SSS_HYCOM	Monthly mean sea surface salinity (PSU) from the HYCOM GOFS 3.1 1/12° ocean model (Chassignet et al. (2009))
SST_CMC	Monthly mean sea surface temperature (°C) from GHRSST Level 4 CMC0.2deg and CMC0.1deg (Brasnett (2008); Canada Meteorological Center (2012); Meissner et al. (2016); Canada Meteorological Center (2016))

4.1.2 Diagnostic Plots
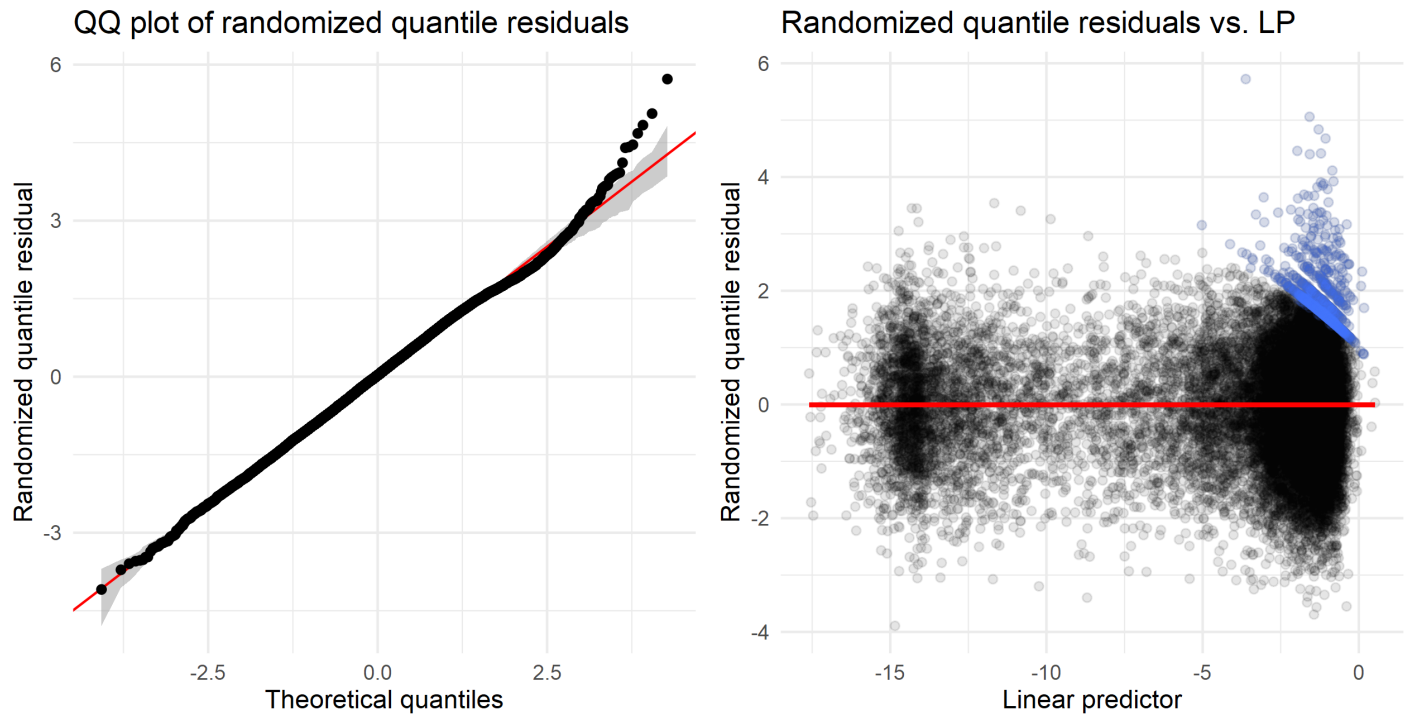
Figure 23: Residual plots for the final model for the region South of Nova Scotia Shallower than 1500m for Winter.
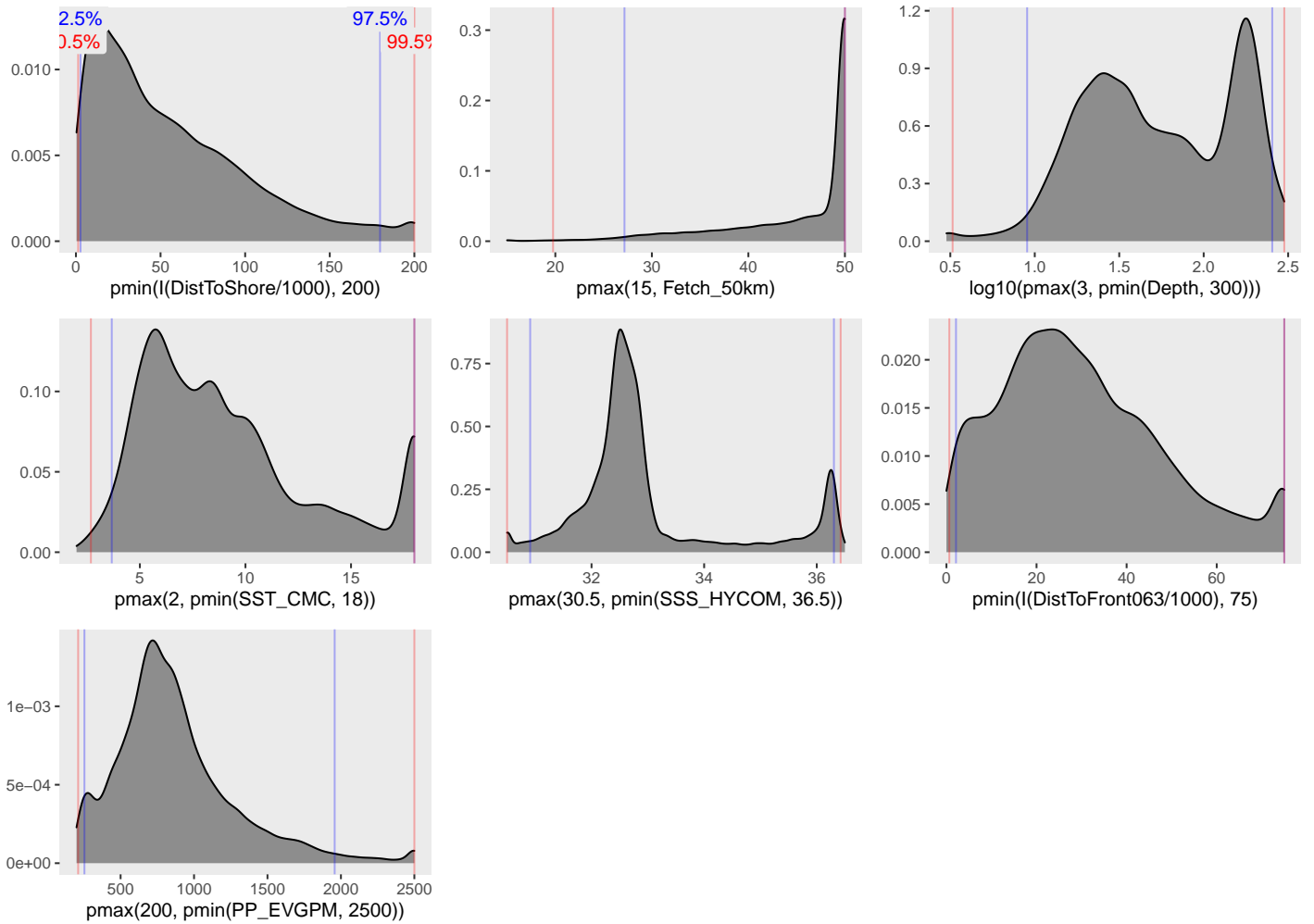
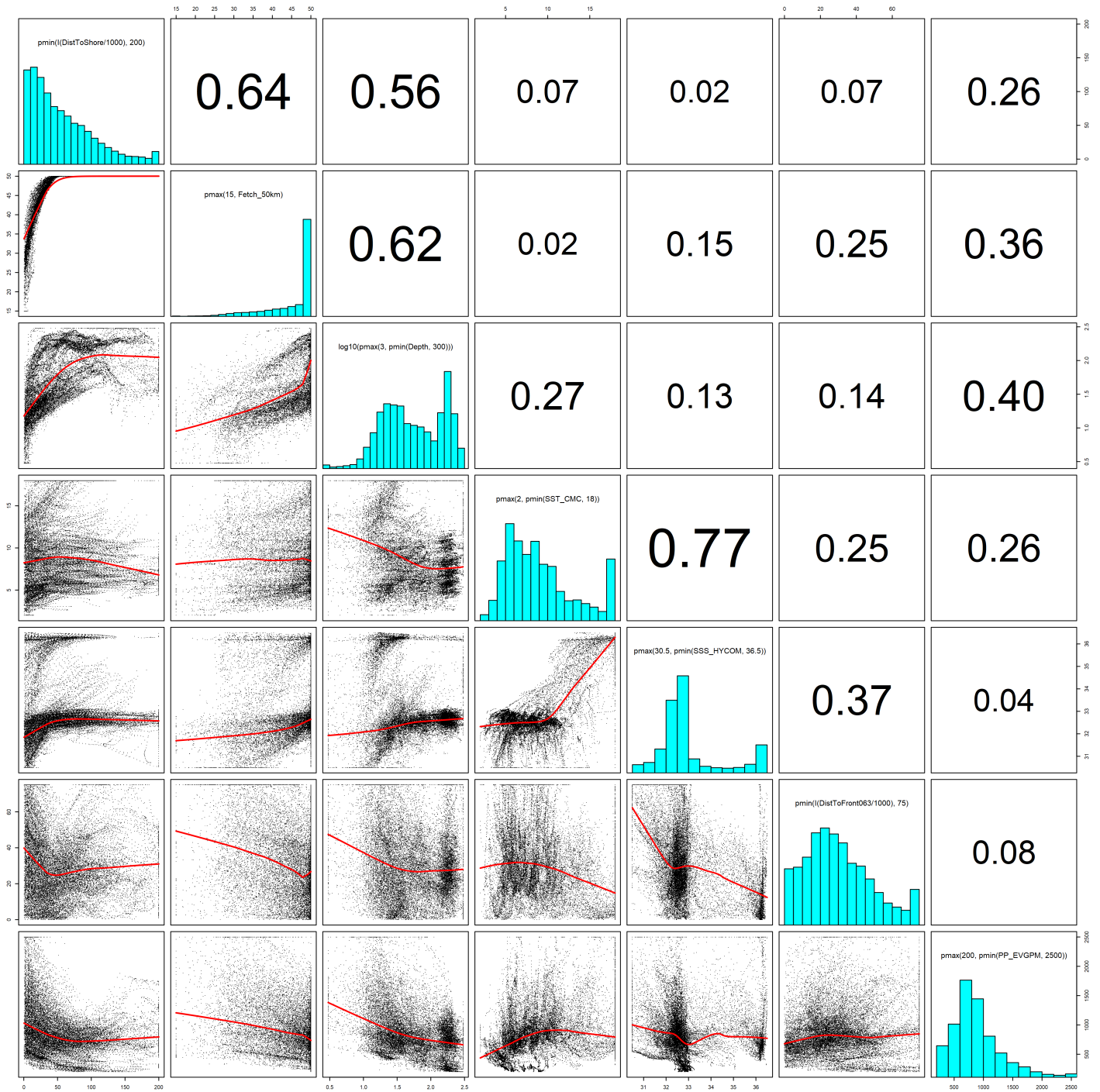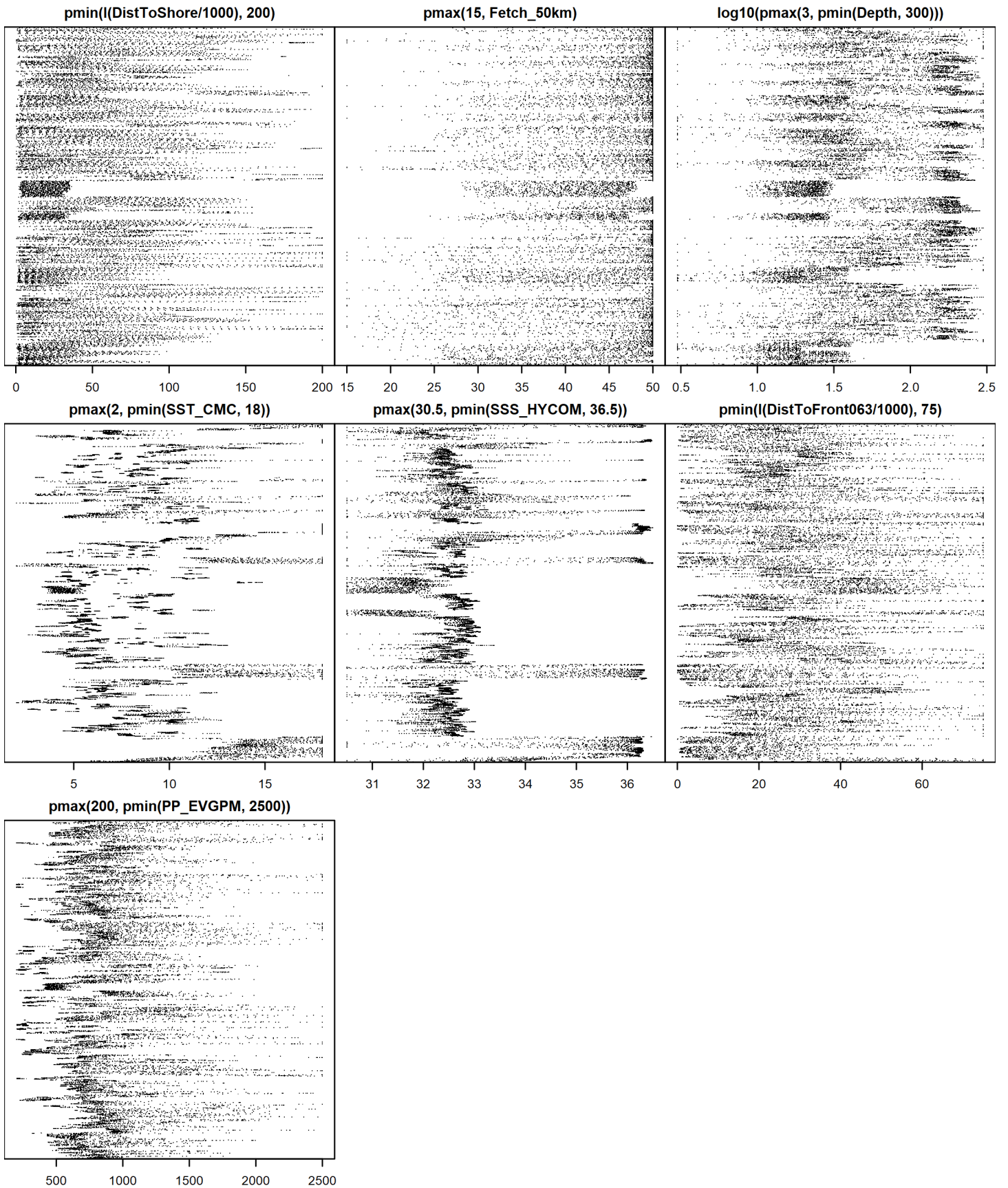Figure 24: Density histograms showing the distributions of the covariates considered during the final model selection step. The final model may have included only a subset of the covariates shown here (see Figure 22), and additional covariates may have been considered in preceding selection steps. Red and blue lines enclose 99% and 95% of the distributions, respectively. Transforms and other treatments are indicated in axis labels. *log10* indicates the covariate was $\log_{10}$ transformed. *pmax* and *pmin* indicate the covariate's minimum and maximum values, respectively, were Winsorized to the values shown. Winsorization was used to prevent runaway extrapolations during prediction when covariates exceeded sampled ranges, or for ecological reasons, depending on the covariate. */1000* indicates meters were transformed to kilometers for interpretation convenience.

Figure 25: Density histograms shown in Figure 24 replotted without Winsorization, to show the full range of sampling represented by survey segments.

Figure 26: Scatterplot matrix of the covariates considered during the final model selection step. The final model may have included only a subset of the covariates shown here (see Figure 22), and additional covariates may have been considered in preceding selection steps. Covariates are transformed and Winsorized as shown in Figure 24. This plot is used to check simple correlations between covariates (via pairwise Pearson coefficients above the diagonal) and visually inspect for concurvity (via scatterplots and red lowess curves below the diagonal).

Figure 27: Dotplot of the covariates considered during the final model selection step. The final model may have included only a subset of the covariates shown here (see Figure 22), and additional covariates may have been considered in preceding selection steps. Covariates are transformed and Winsorized as shown in Figure 24. This plot is used to check for suspicious patterns and outliers in the data. Points are ordered vertically by segment ID, sequentially in time.

4.1.3 Extrapolation Diagnostics

4.1.3.1 Univariate Extrapolation

(a) Depth covariate
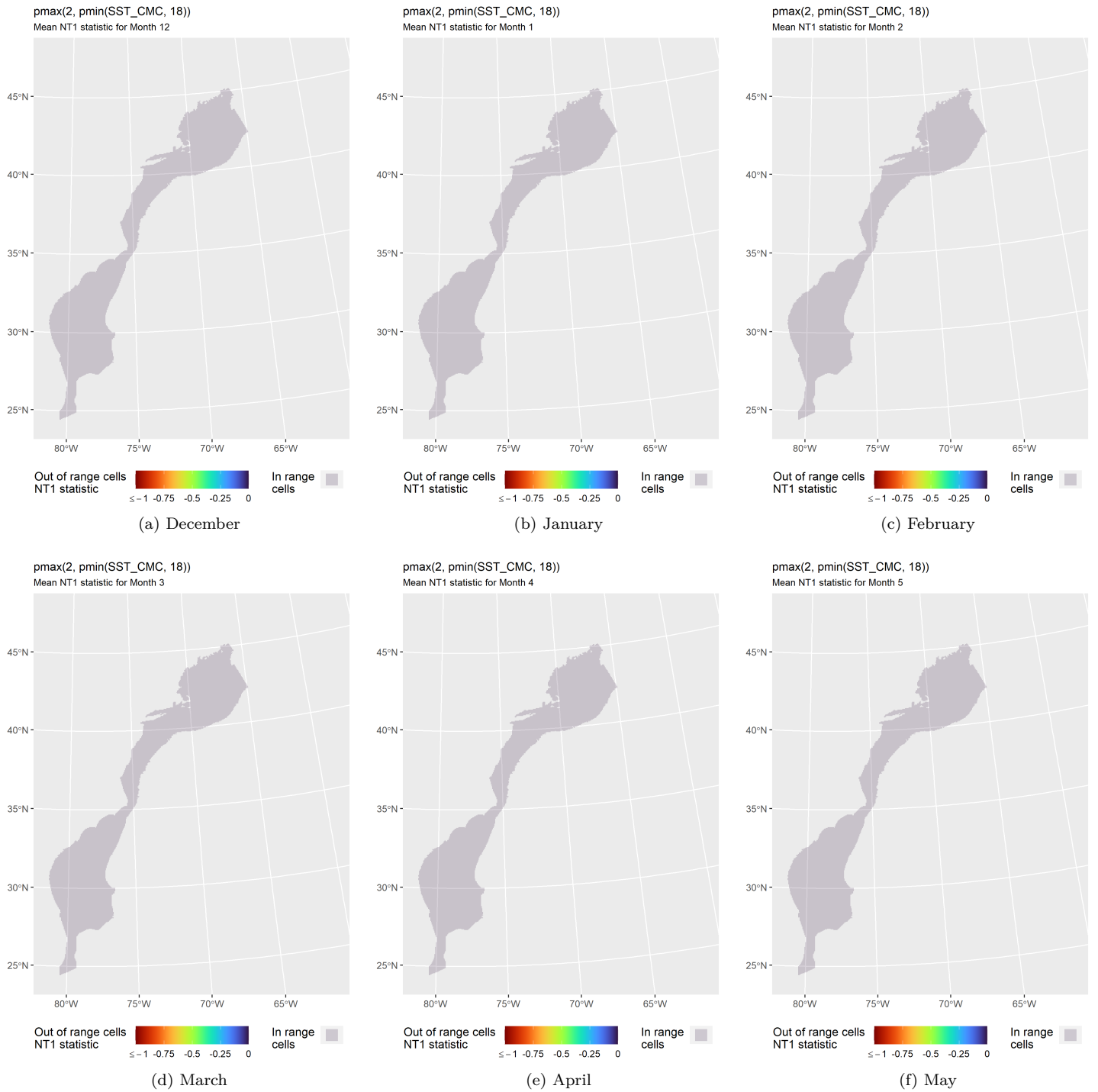
(b) DistToShore covariate
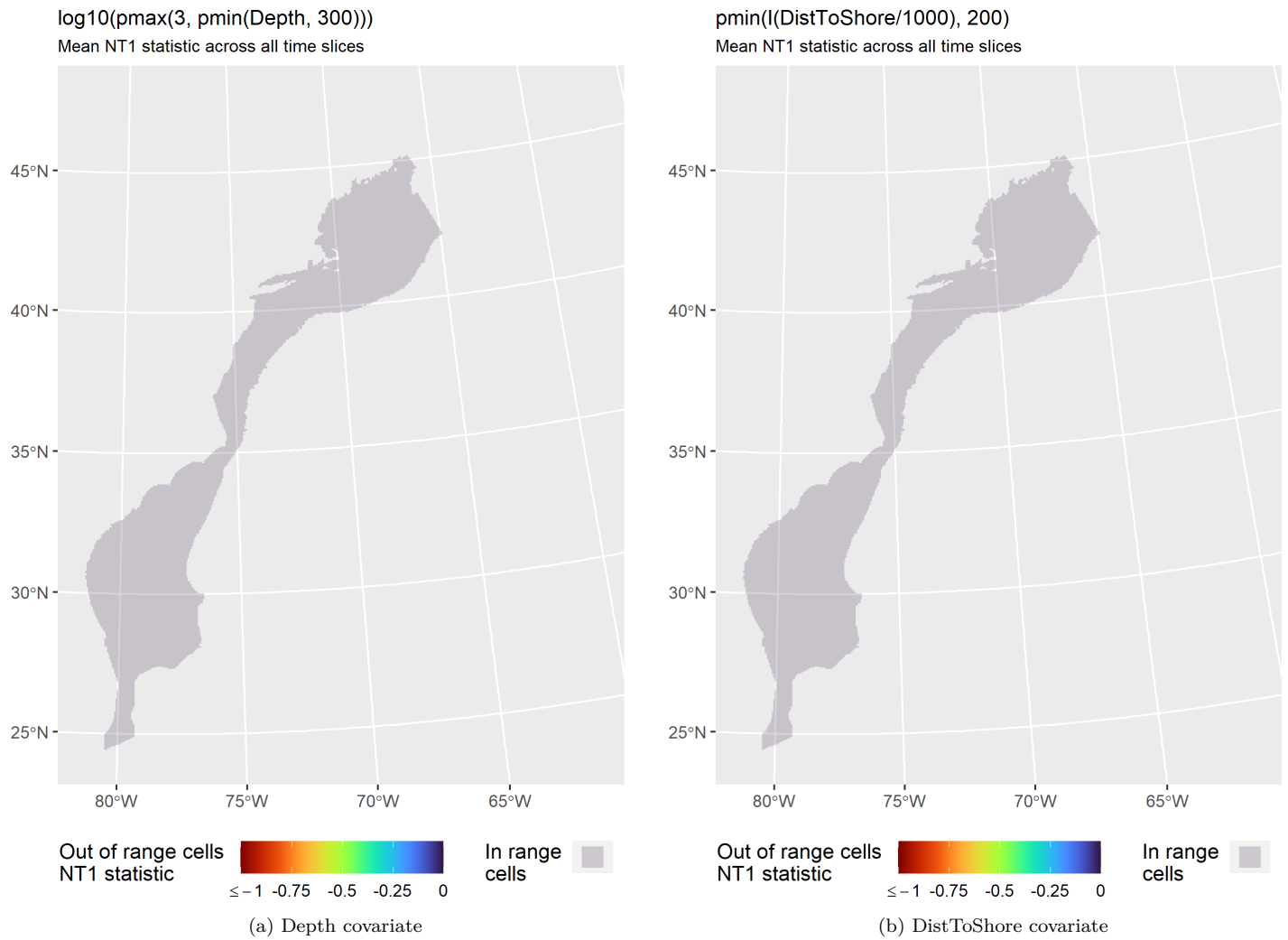
Figure 28: NT1 statistic (Mesgaran et al. (2014)) for static covariates used in the model for the region South of Nova Scotia Shallower than 1500m for Winter. Areas outside the sampled range of a covariate appear in color, indicating univariate extrapolation of that covariate occurred there. Areas within the sampled range appear in gray, indicating it did not occur.
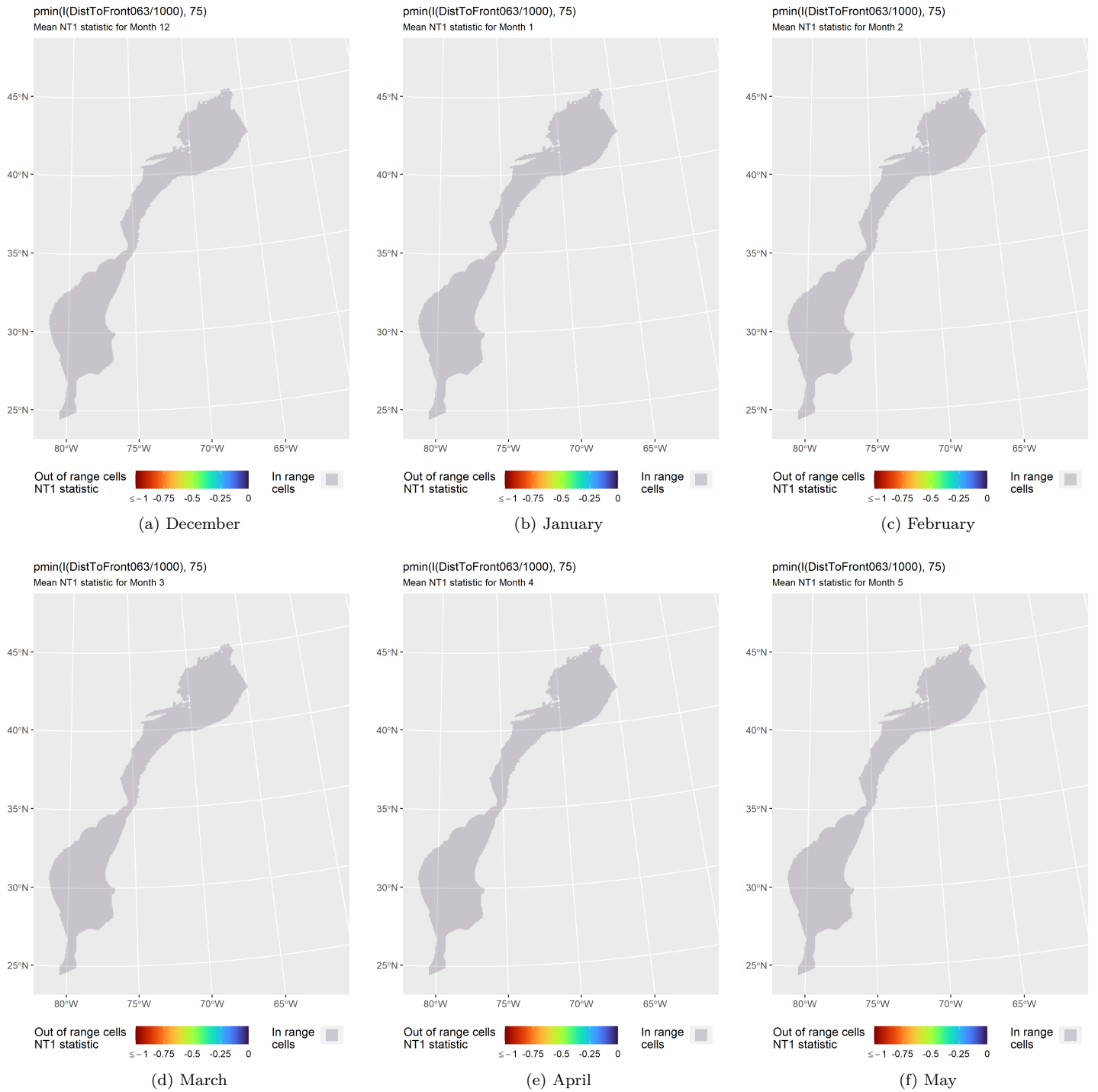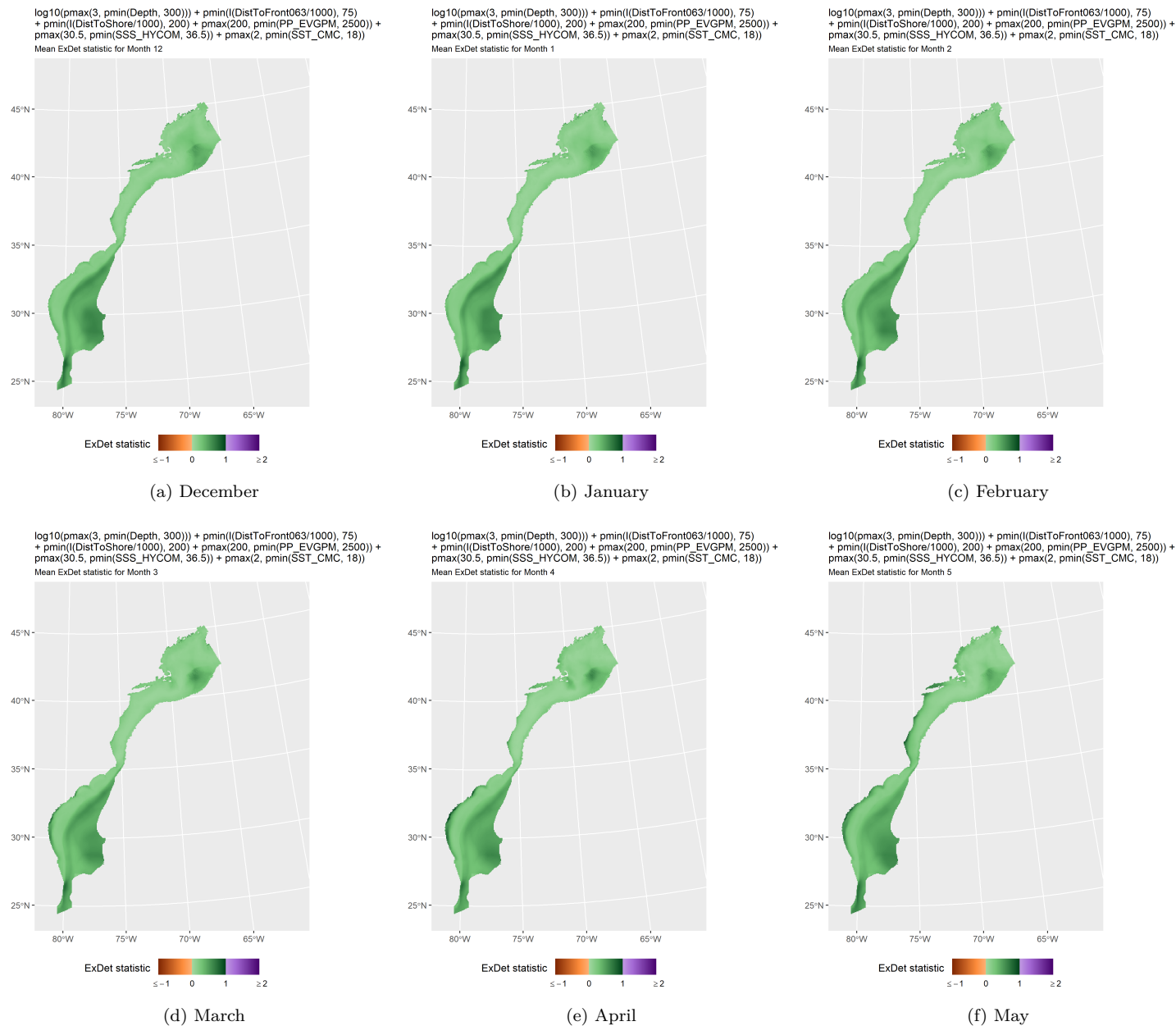
Figure 29: NT1 statistic (Mesgaran et al. (2014)) for the DistToFront063 covariate in the model for the region South of Nova Scotia Shallower than 1500m for Winter. Areas outside the sampled range of a covariate appear in color, indicating univariate extrapolation of that covariate occurred there during the month. Areas within the sampled range appear in gray, indicating it did not occur.
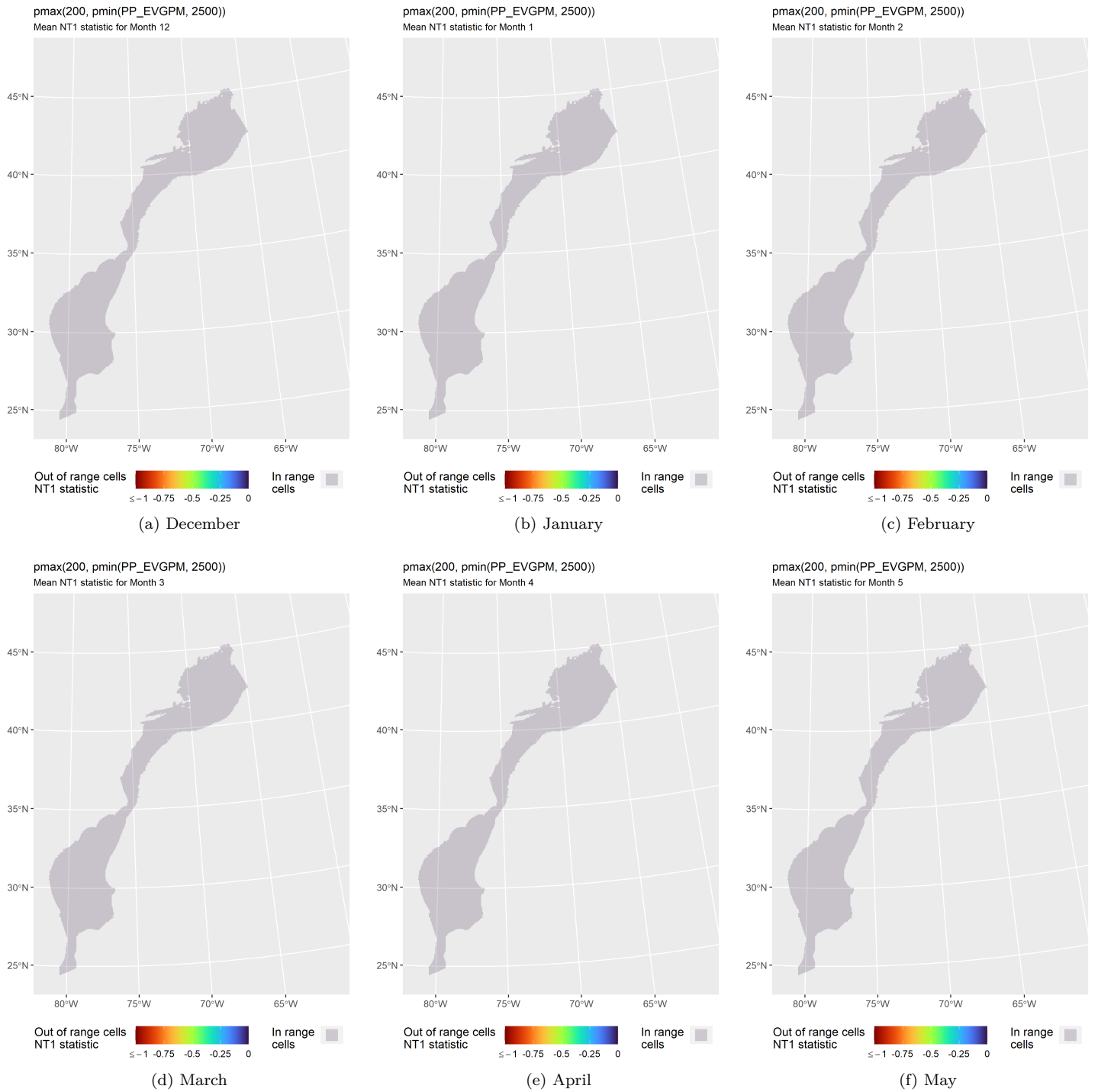
Figure 30: NT1 statistic (Mesgaran et al. (2014)) for the PP_EVGPM covariate in the model for the region South of Nova Scotia Shallower than 1500m for Winter. Areas outside the sampled range of a covariate appear in color, indicating univariate extrapolation of that covariate occurred there during the month. Areas within the sampled range appear in gray, indicating it did not occur.
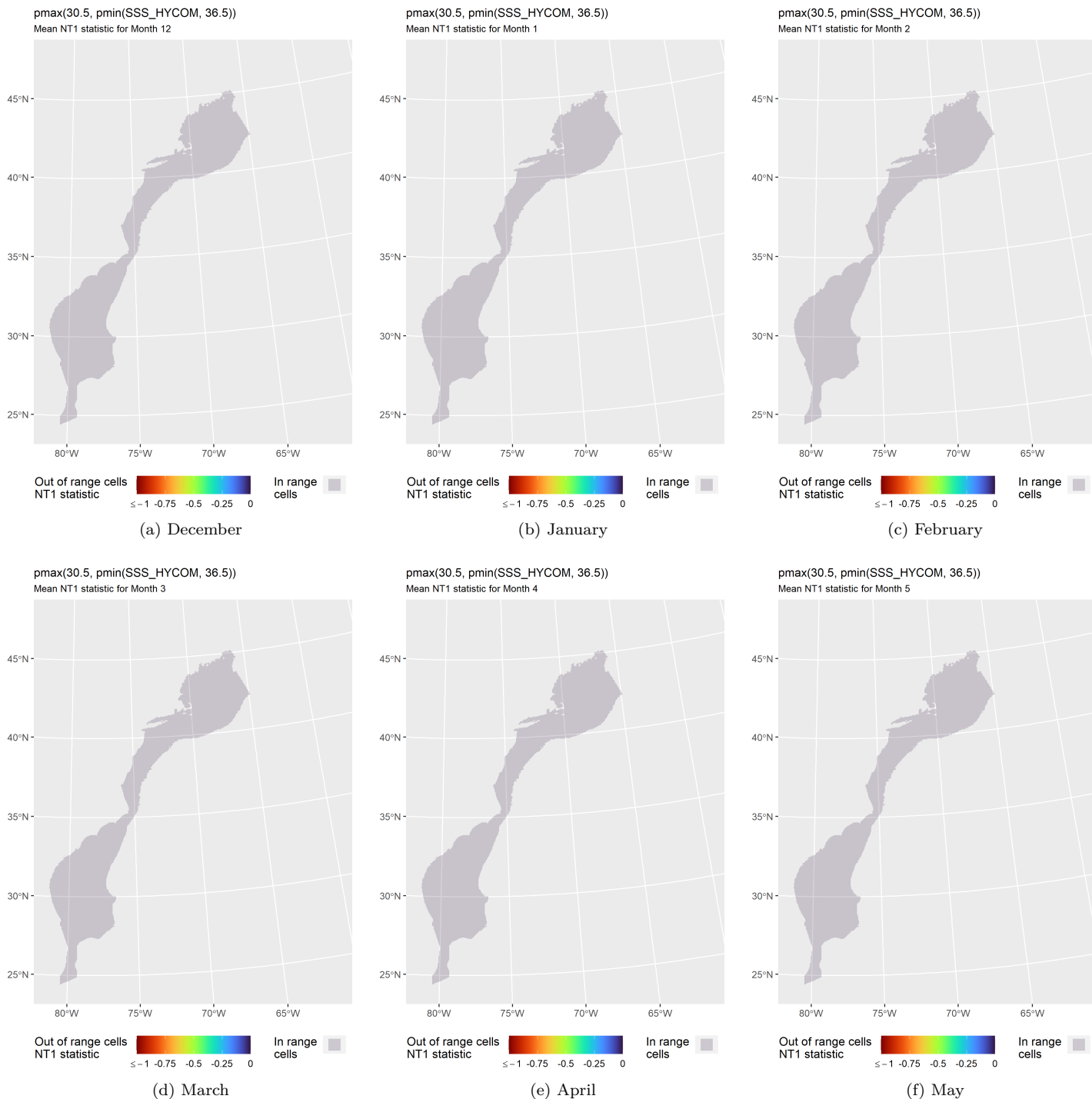
Figure 31: NT1 statistic (Mesgaran et al. (2014)) for the SSS_HYCOM covariate in the model for the region South of Nova Scotia Shallower than 1500m for Winter. Areas outside the sampled range of a covariate appear in color, indicating univariate extrapolation of that covariate occurred there during the month. Areas within the sampled range appear in gray, indicating it did not occur.

Figure 32: NT1 statistic (Mesgaran et al. (2014)) for the SST_CMC covariate in the model for the region South of Nova Scotia Shallower than 1500m for Winter. Areas outside the sampled range of a covariate appear in color, indicating univariate extrapolation of that covariate occurred there during the month. Areas within the sampled range appear in gray, indicating it did not occur.

4.1.3.2 Multivariate Extrapolation

(a) December

(b) January

(c) February

(d) March

(e) April

(f) May

Figure 33: ExDet statistic (Mesgaran et al. (2014)) for all of the covariates used in the model for the region South of Nova Scotia Shallower than 1500m for Winter. Areas in orange (ExDet < 0) required univariate extrapolation of one or more covariates (see previous section). Areas in purple (ExDet > 1), did not require univariate extrapolation but did require multivariate extrapolation, by virtue of having novel combinations of covariates not represented in the survey data, according to the NT2 statistic (Mesgaran et al. (2014)). Areas in green (0 ≥ ExDet ≤ 1) did not require either type of extrapolation.

4.2 Summer Model

The Summer model, spanning the months of June-November, had sufficient effort in sea states of Beaufort 2 or less to include offshore waters out to the edge of our study area. The southernmost sighting was reported off New Jersey. To avoid confounding model relationships with data collected in locations of clear absence that are believed to be incompatible with the species' known habitat, we excluded the portion of the study area south of Cape Hatteras and the north wall of the Gulf Stream. South of here we assumed that density was zero. Given that our objective was to model the Gulf of Maine/Bay of Fundy stock, and that neither substantial effort nor sightings were available for the northern half of the Scotian Shelf, we limited the northern extent of the model to Halifax.

The final model retained more than 900 sightings, concentrated mainly around northern Maine, the lower Bay of Fundy, and

southern Nova Scotia (Figure 34). Given the extreme density of sightings in this area, the lack of environmental covariates that specifically highlighted it, and the reasonably dense spatial coverage in surveying except in offshore waters where the species was absent, we included a bivariate interaction of projected spatial coordinates (x and y) to account for the spatial pattern in density that could not be explained by the environmental covariates.

When ranked by REML score (Wood 2011), the highest ranked candidate models with contemporaneous covariates slightly outranked those with climatological covariates. We selected the top-ranked contemporaneous-covariate model, which included six covariates (Table 8). Relationships with static covariates indicated a positive influence on density in waters between 50-200 m deep and within 70 km of shore (Figure 37). A negative relationship with SST indicated a preference for waters colder than 17 °C. The relationship with bottom temperature was more complex, indicating an envelope of positive influence on density between 7-17 °C, and also below 4 °C. The relationship with primary productivity as estimated by the CAFE model was positive, indicating a preference for more productive waters, which peak during these months in the Maine-Bay of Fundy-Nova Scotia region where porpoises congregate, but also east of Nantucket and the shallow center of Georges Bank, where more moderate counts of sightings were recorded. Finally, the bivariate interaction of spatial coordinates showed a clear peak in the vicinity of the lower Bay of Fundy.
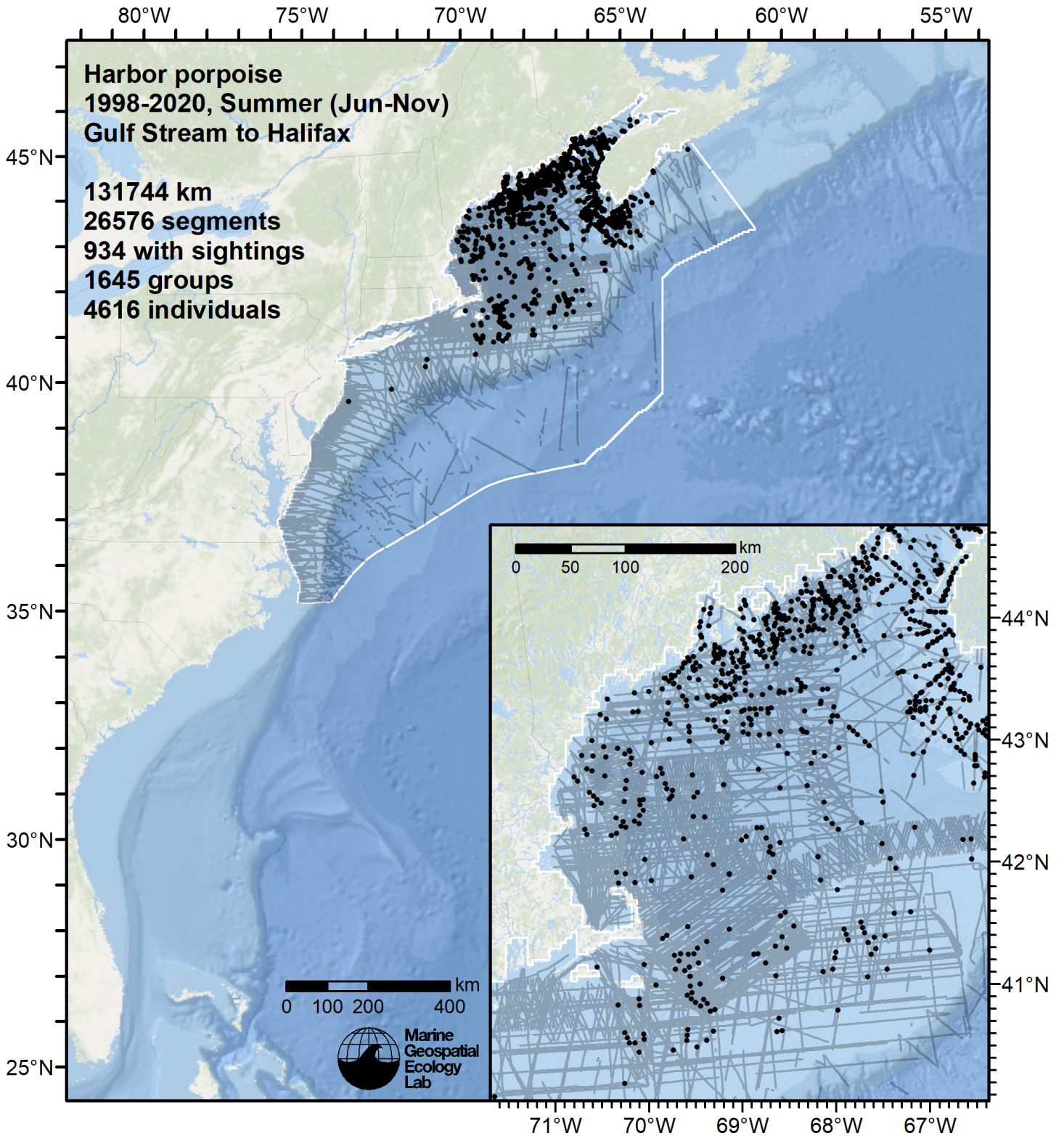
Figure 34: Survey segments used to fit the model for the region Gulf Stream to Halifax for Summer. Black points indicate segments with observations.
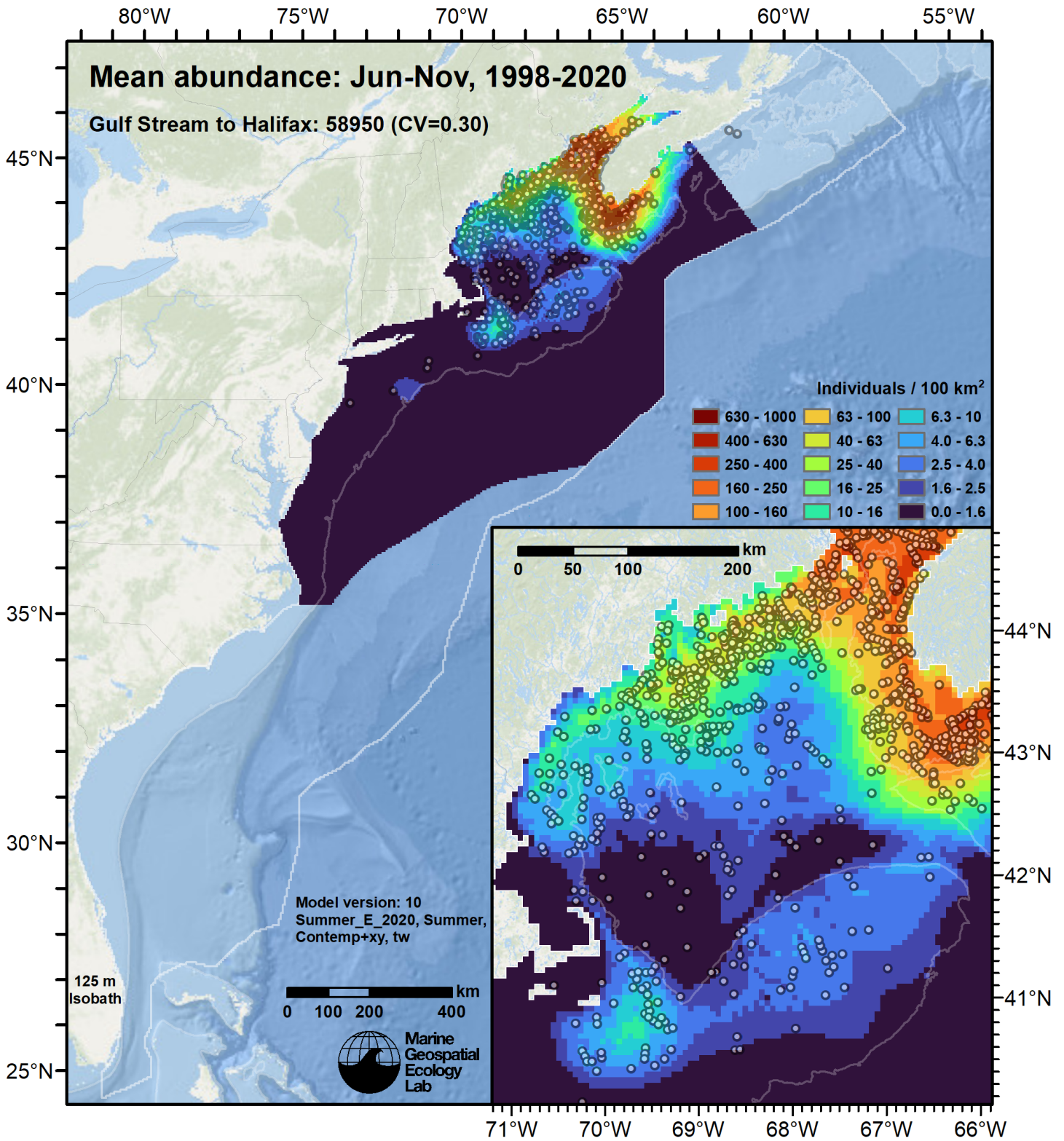
Figure 35: Harbor porpoise mean density for the indicated period, as predicted by the model for the region Gulf Stream to Halifax for Summer. Open circles indicate segments with observations. Mean total abundance and its coefficient of variation (CV) are given in the subtitle. Variance was estimated with the analytic approach given by Miller et al. (2022), Appendix S1, and accounts both for uncertainty in model parameter estimates and for seasonal and interannual variability in dynamic covariates.
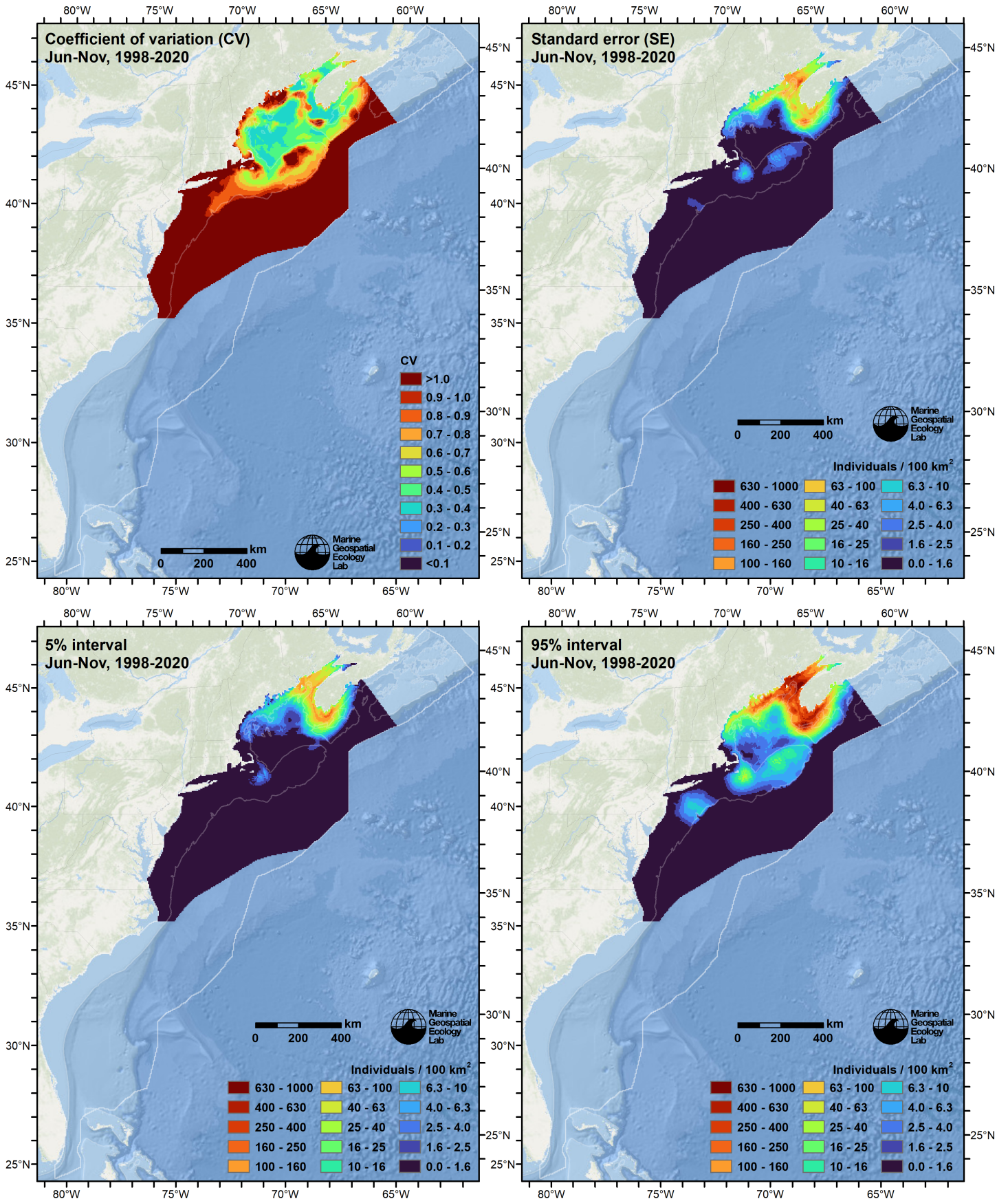
Figure 36: Uncertainty statistics for the harbor porpoise mean density surface (Figure 35) predicted by the model for the region Gulf Stream to Halifax for Summer. Variance was estimated with the analytic approach given by Miller et al. (2022), Appendix S1, and accounts both for uncertainty in model parameter estimates and for seasonal and interannual variability in dynamic covariates.

Statistical output for this model:

```
Family: Tweedie(p=1.287)
Link function: log

Formula:
IndividualsCorrected ~ offset(log(SegmentArea)) + s(I(x/1000),
    I(y/1000), bs = "ts", k = 50) + s(pmin(I(DistToShore/1000),
    300), bs = "ts") + s(log10(pmax(3, pmin(Depth, 1000)))), bs = "ts") +
    s(pmax(10, pmin(SST_CMC, 27)), bs = "ts") + s(pmax(2, pmin(BotT_HYCOM,
    24)), bs = "ts") + s(pmax(400, pmin(PP_CAFE, 1400)), bs = "ts")

Parametric coefficients:
            Estimate Std. Error t value Pr(>|t|)
(Intercept) -19.3608     0.4796  -40.37   <2e-16 ***
---
Signif. codes:  0 '***' 0.001 '**' 0.01 '*' 0.05 '.' 0.1 ' ' 1

Approximate significance of smooth terms:
                                    edf Ref.df      F  p-value
s(I(x/1000),I(y/1000))          30.3265     49 21.090  < 2e-16 ***
s(pmin(I(DistToShore/1000), 300))  0.9775      9  0.815 0.000364 ***
s(log10(pmax(3, pmin(Depth, 1000))))  5.2510   9  5.743  < 2e-16 ***
s(pmax(10, pmin(SST_CMC, 27)))    0.9077      9  0.765 0.004680 **
s(pmax(2, pmin(BotT_HYCOM, 24)))  5.1317      9  4.964  < 2e-16 ***
s(pmax(400, pmin(PP_CAFE, 1400)))  3.7879     9 16.203  < 2e-16 ***
---
Signif. codes:  0 '***' 0.001 '**' 0.01 '*' 0.05 '.' 0.1 ' ' 1

R-sq.(adj) =    0.2   Deviance explained = 55.7%
-REML = 5924.1  Scale est. = 11.39      n = 26576

Method: REML   Optimizer: outer newton
full convergence after 10 iterations.
Gradient range [-0.0004199744,0.0001214645]
(score 5924.053 & scale 11.38975).
Hessian positive definite, eigenvalue range [0.3783753,3287.857].
Model rank =  95 / 95

Basis dimension (k) checking results. Low p-value (k-index<1) may
indicate that k is too low, especially if edf is close to k'.


                                      k'     edf k-index p-value
s(I(x/1000),I(y/1000))            49.000 30.326    0.72  <2e-16 ***
s(pmin(I(DistToShore/1000), 300))  9.000  0.978    0.81   0.030 *
s(log10(pmax(3, pmin(Depth, 1000))))  9.000 5.251  0.79   0.005 **
s(pmax(10, pmin(SST_CMC, 27)))     9.000  0.908    0.78  <2e-16 ***
s(pmax(2, pmin(BotT_HYCOM, 24)))   9.000  5.132    0.78  <2e-16 ***
s(pmax(400, pmin(PP_CAFE, 1400)))  9.000  3.788    0.83   0.630
---
Signif. codes:  0 '***' 0.001 '**' 0.01 '*' 0.05 '.' 0.1 ' ' 1
```

(a) Bottom temperature (°C)

(b) Seafloor depth (m)

(c) Distance to shore (km)

(d) Net primary productivity (mg C m^{-2} day^{-1}) (CAFE model)

(e) Sea surface temperature (°C)

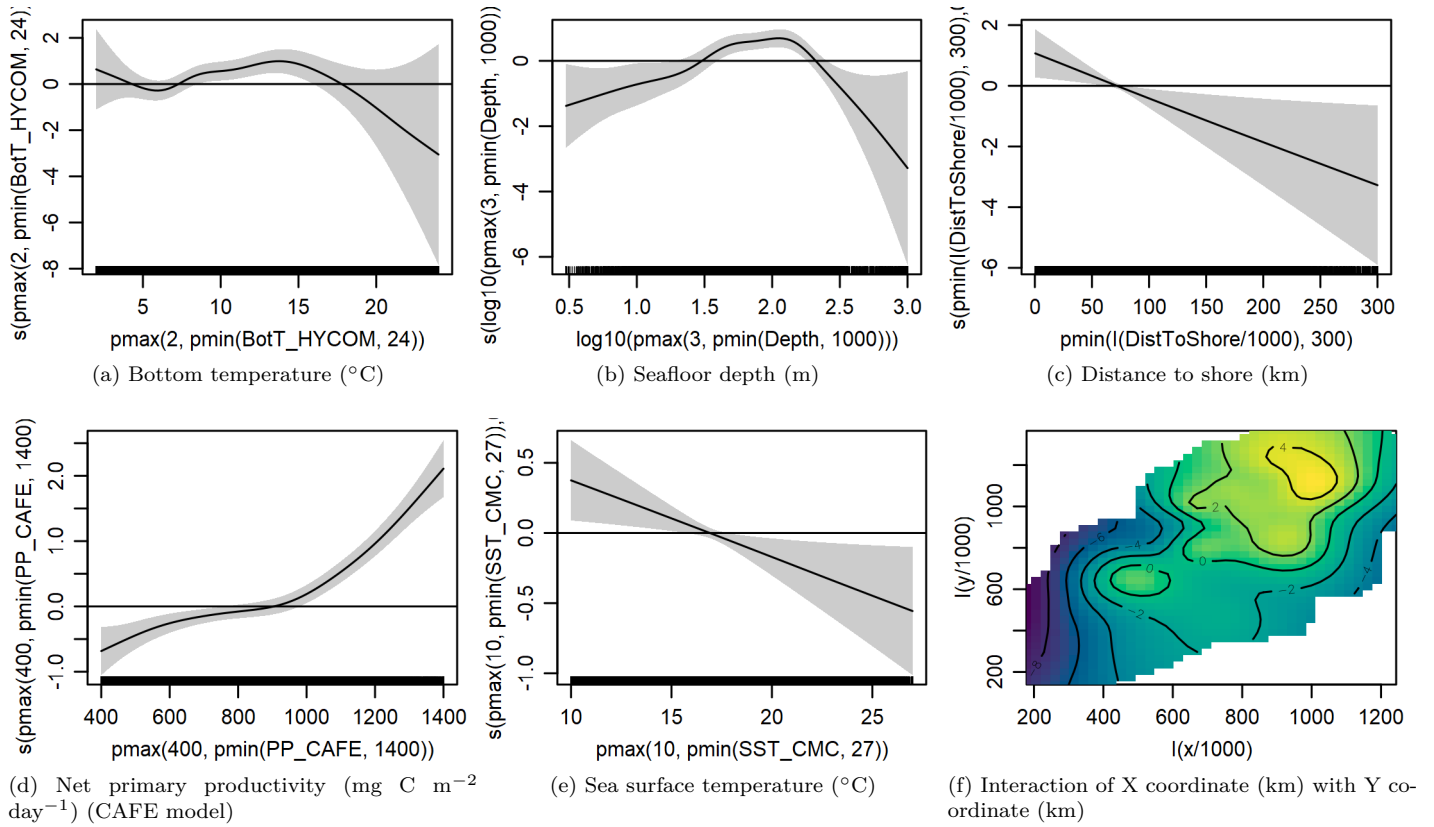(f) Interaction of X coordinate (km) with Y coordinate (km)

Figure 37: Functional plots for the final model for the region Gulf Stream to Halifax for Summer. Transforms and other treatments are indicated in axis labels. *log10* indicates the covariate was $\log_{10}$ transformed. *pmax* and *pmin* indicate the covariate's minimum and maximum values, respectively, were Winsorized to the values shown. Winsorization was used to prevent runaway extrapolations during prediction when covariates exceeded sampled ranges, or for ecological reasons, depending on the covariate. */1000* indicates meters were transformed to kilometers for interpretation convenience.

Table 8: Covariates used in the final model for the region Gulf Stream to Halifax for Summer.

Covariate	Description
BotT_HYCOM	Monthly mean bottom temperature (°C) from the HYCOM GOFS 3.1 1/12° ocean model (Chassignet et al. (2009))
Depth	Depth (m) of the seafloor, from SRTM30_PLUS (Becker et al. (2009))
DistToShore	Distance (km) to shore excluding Bermuda and Sable Island, derived from SRTM30_PLUS (Becker et al. (2009))
PP_CAFE	Monthly mean net primary productivity (mg C m^{-2} day^{-1}) from the Carbon, Absorption, and Fluorescence Euphotic-resolving (CAFE) model (Silsbe et al. (2016))
SST_CMC	Monthly mean sea surface temperature (°C) from GHRSST Level 4 CMC0.2deg and CMC0.1deg (Brasnett (2008); Canada Meteorological Center (2012); Meissner et al. (2016); Canada Meteorological Center (2016))
x	X coordinate (km) in the Albers equal area map projection of the analysis
y	Y coordinate (km) in the Albers equal area map projection of the analysis

4.2.2 Diagnostic Plots
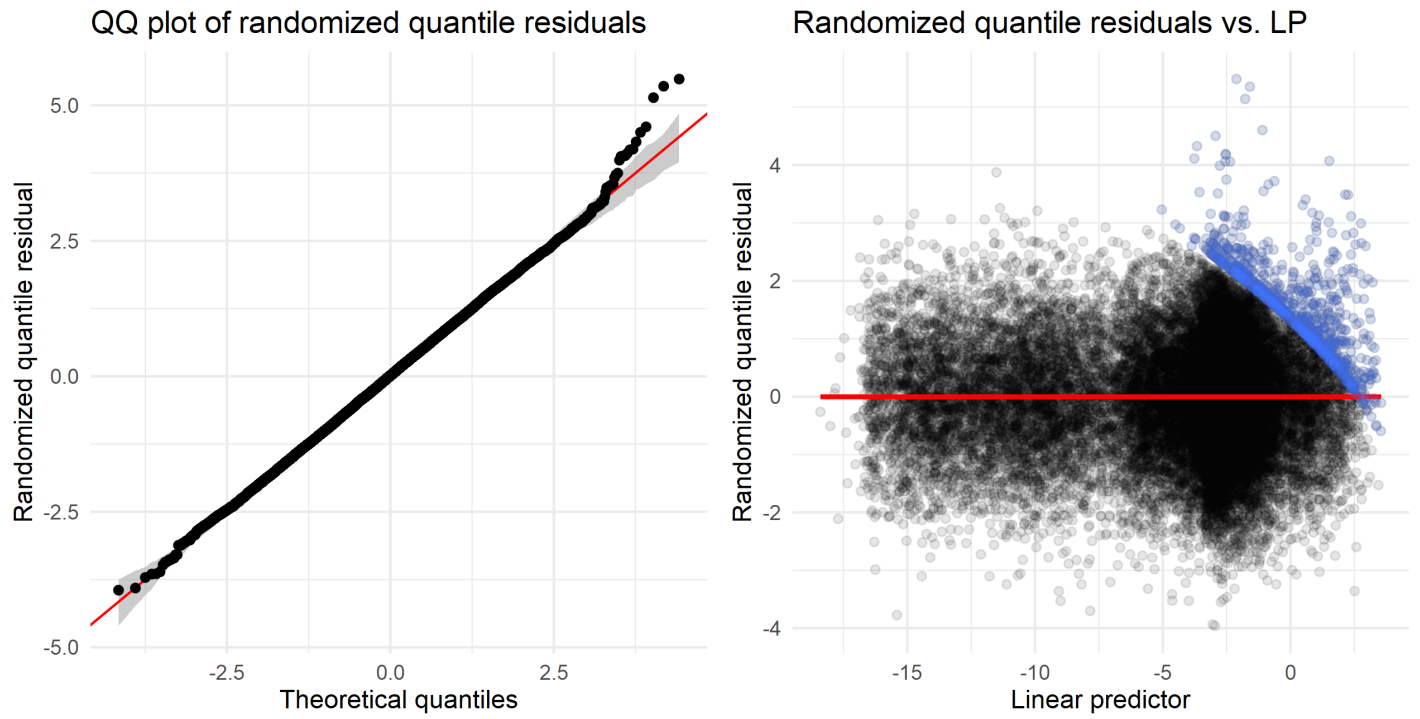
Figure 38: Residual plots for the final model for the region Gulf Stream to Halifax for Summer.
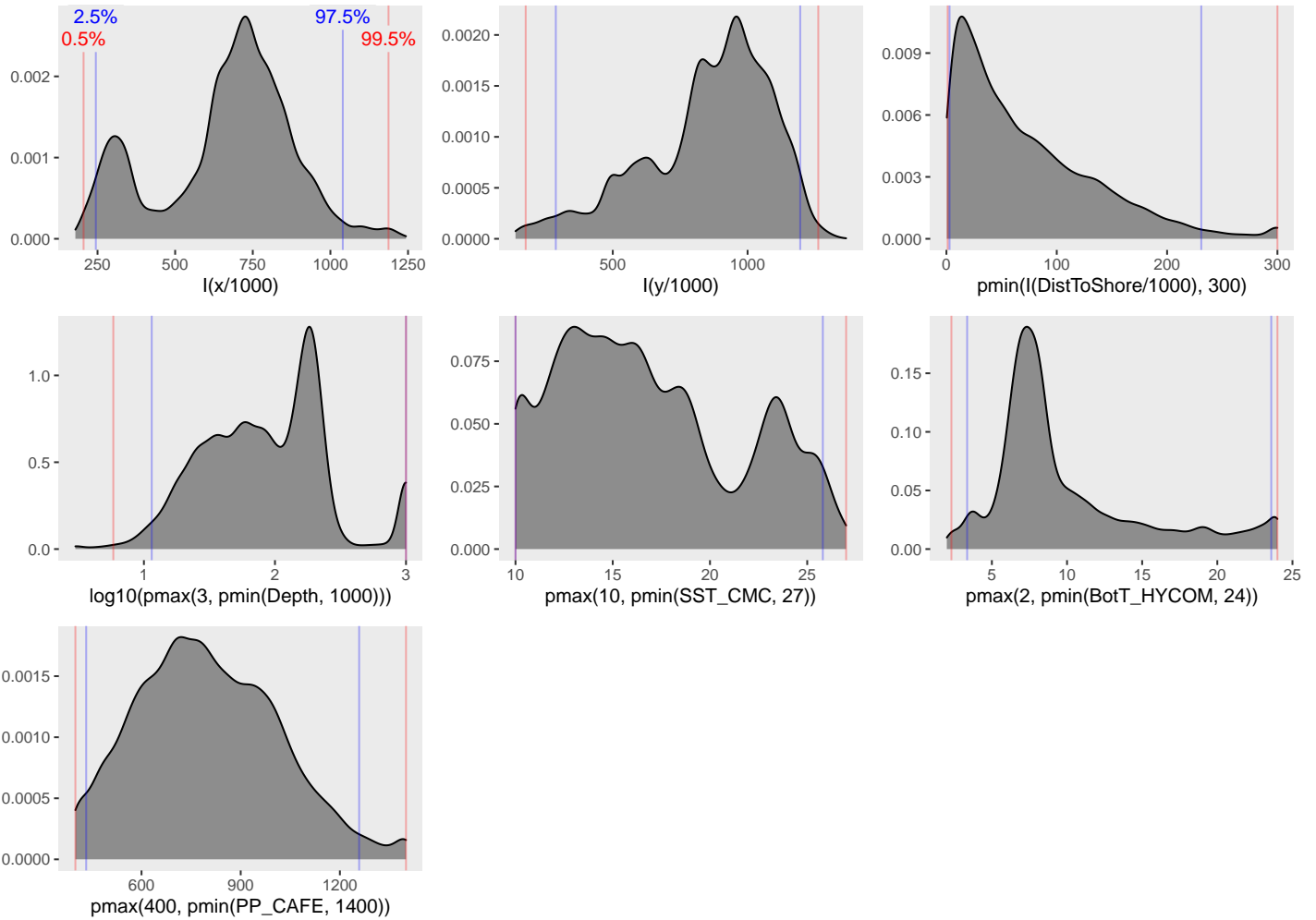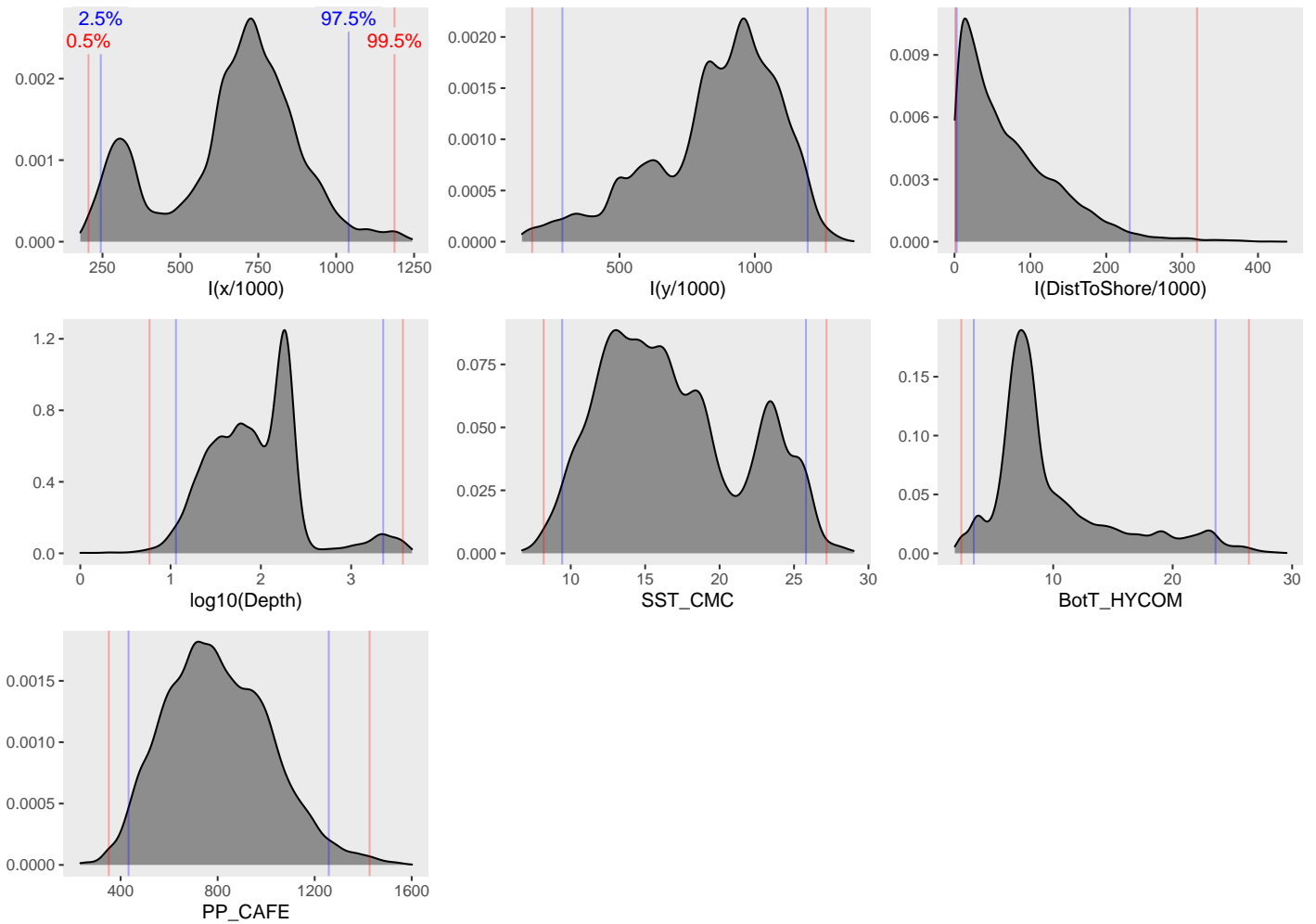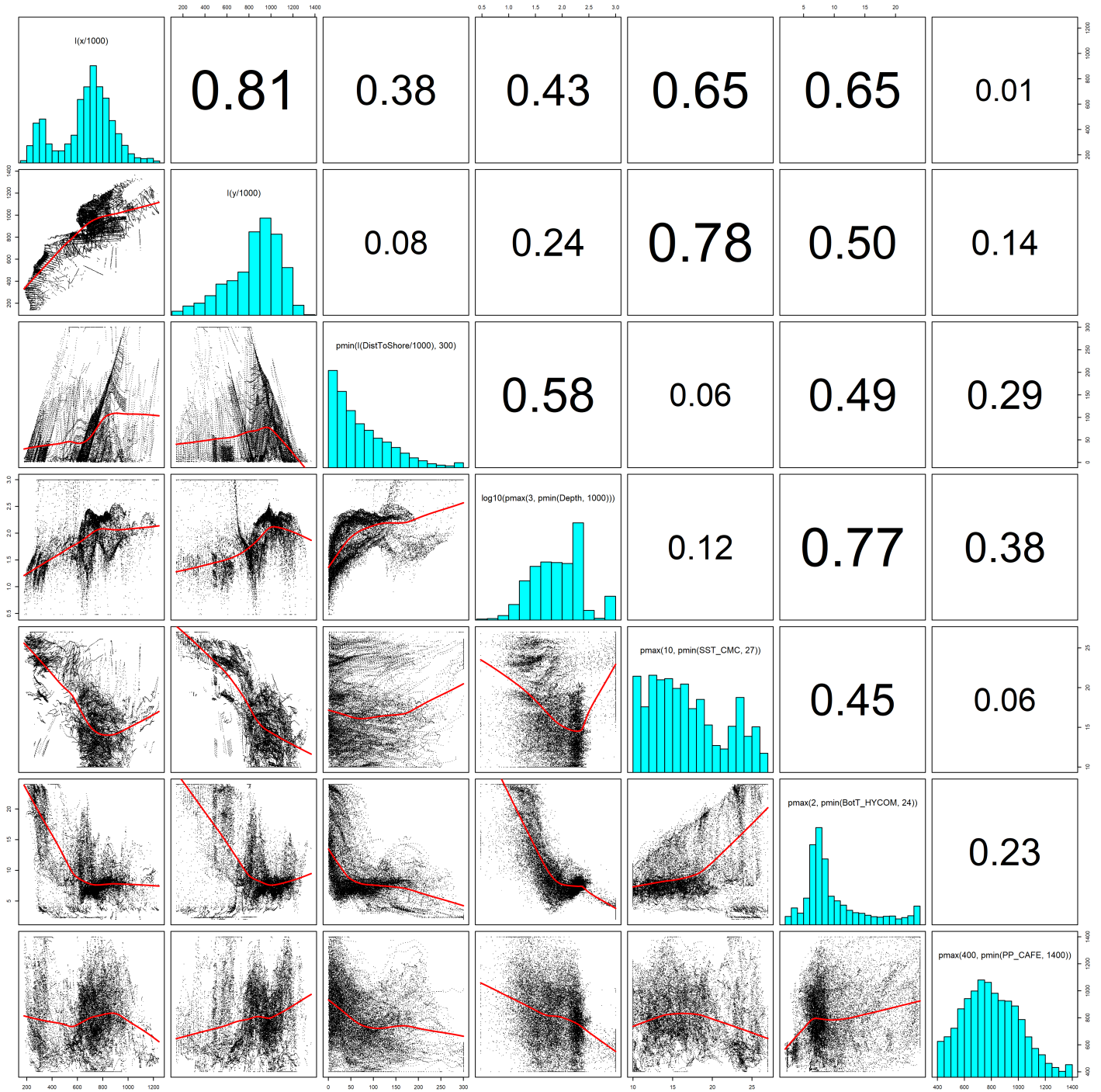
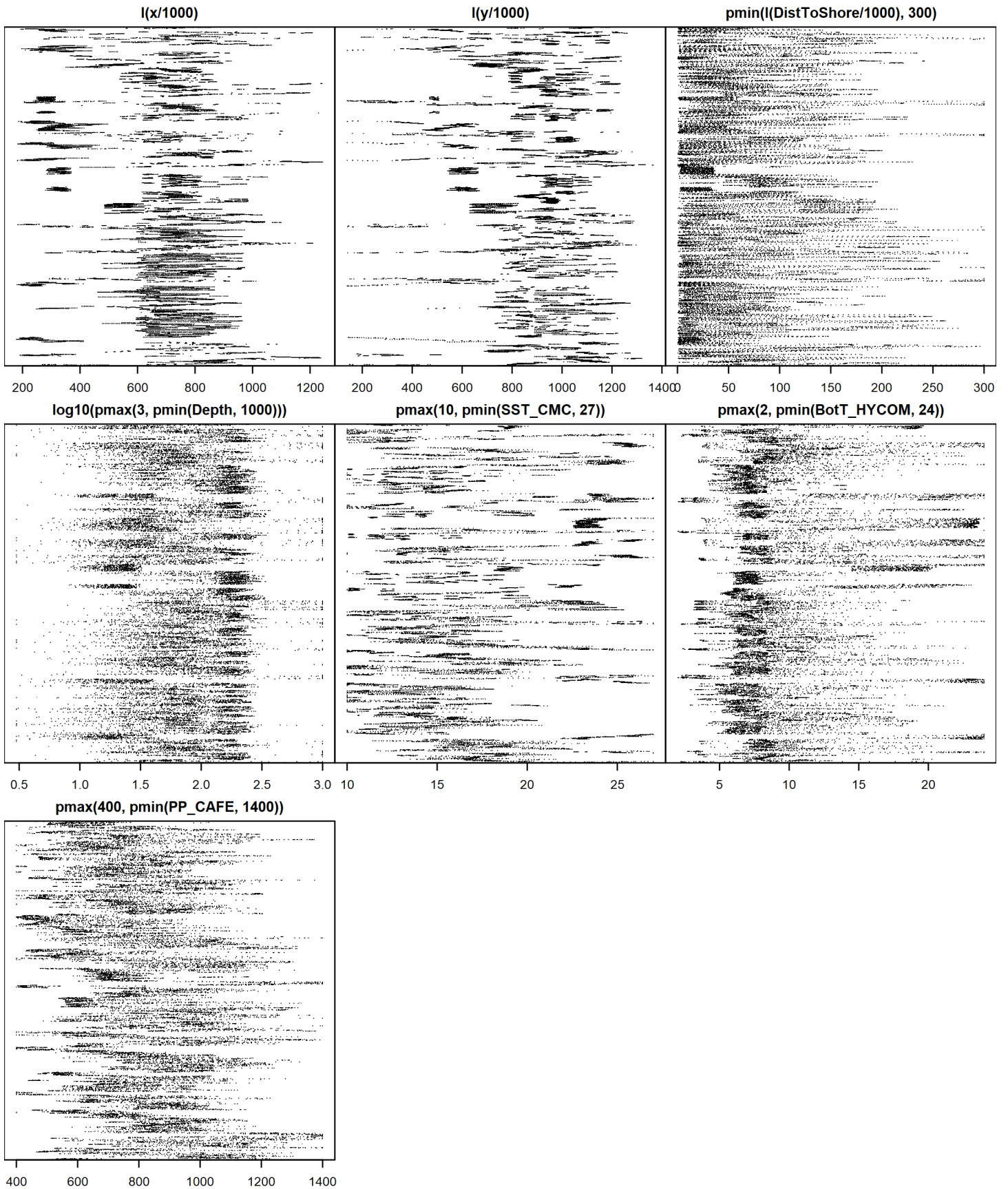Figure 39: Density histograms showing the distributions of the covariates considered during the final model selection step. The final model may have included only a subset of the covariates shown here (see Figure 37), and additional covariates may have been considered in preceding selection steps. Red and blue lines enclose 99% and 95% of the distributions, respectively. Transforms and other treatments are indicated in axis labels. *log10* indicates the covariate was $\log_{10}$ transformed. *pmax* and *pmin* indicate the covariate's minimum and maximum values, respectively, were Winsorized to the values shown. Winsorization was used to prevent runaway extrapolations during prediction when covariates exceeded sampled ranges, or for ecological reasons, depending on the covariate. */1000* indicates meters were transformed to kilometers for interpretation convenience.

Figure 40: Density histograms shown in Figure 39 replotted without Winsorization, to show the full range of sampling represented by survey segments.

Figure 41: Scatterplot matrix of the covariates considered during the final model selection step. The final model may have included only a subset of the covariates shown here (see Figure 37), and additional covariates may have been considered in preceding selection steps. Covariates are transformed and Winsorized as shown in Figure 39. This plot is used to check simple correlations between covariates (via pairwise Pearson coefficients above the diagonal) and visually inspect for concurvity (via scatterplots and red lowess curves below the diagonal).

Figure 42: Dotplot of the covariates considered during the final model selection step. The final model may have included only a subset of the covariates shown here (see Figure 37), and additional covariates may have been considered in preceding selection steps. Covariates are transformed and Winsorized as shown in Figure 39. This plot is used to check for suspicious patterns and outliers in the data. Points are ordered vertically by segment ID, sequentially in time.

4.2.3 Extrapolation Diagnostics

4.2.3.1 Univariate Extrapolation

(a) Depth covariate

(b) DistToShore covariate
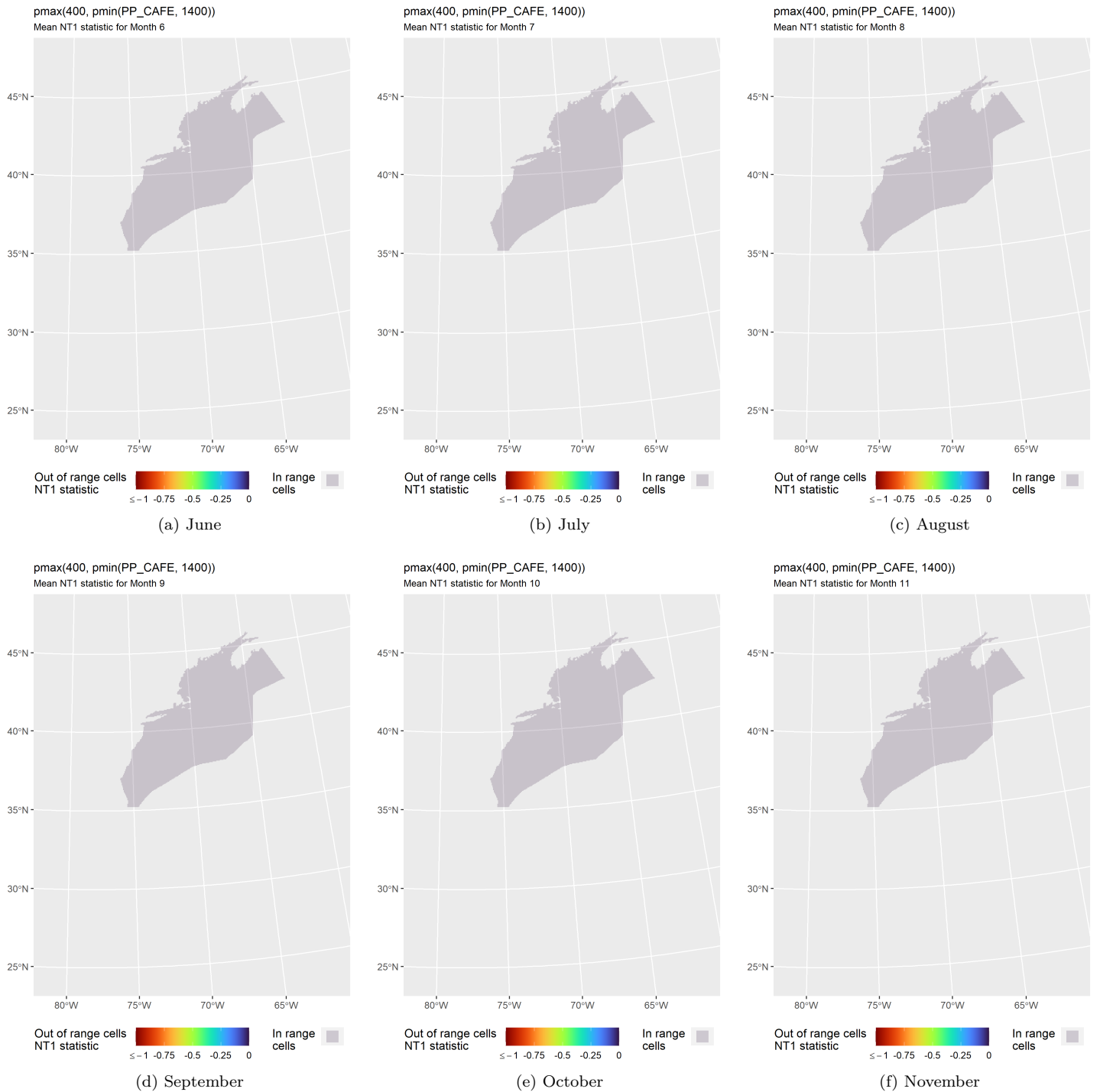
(c) x covariate
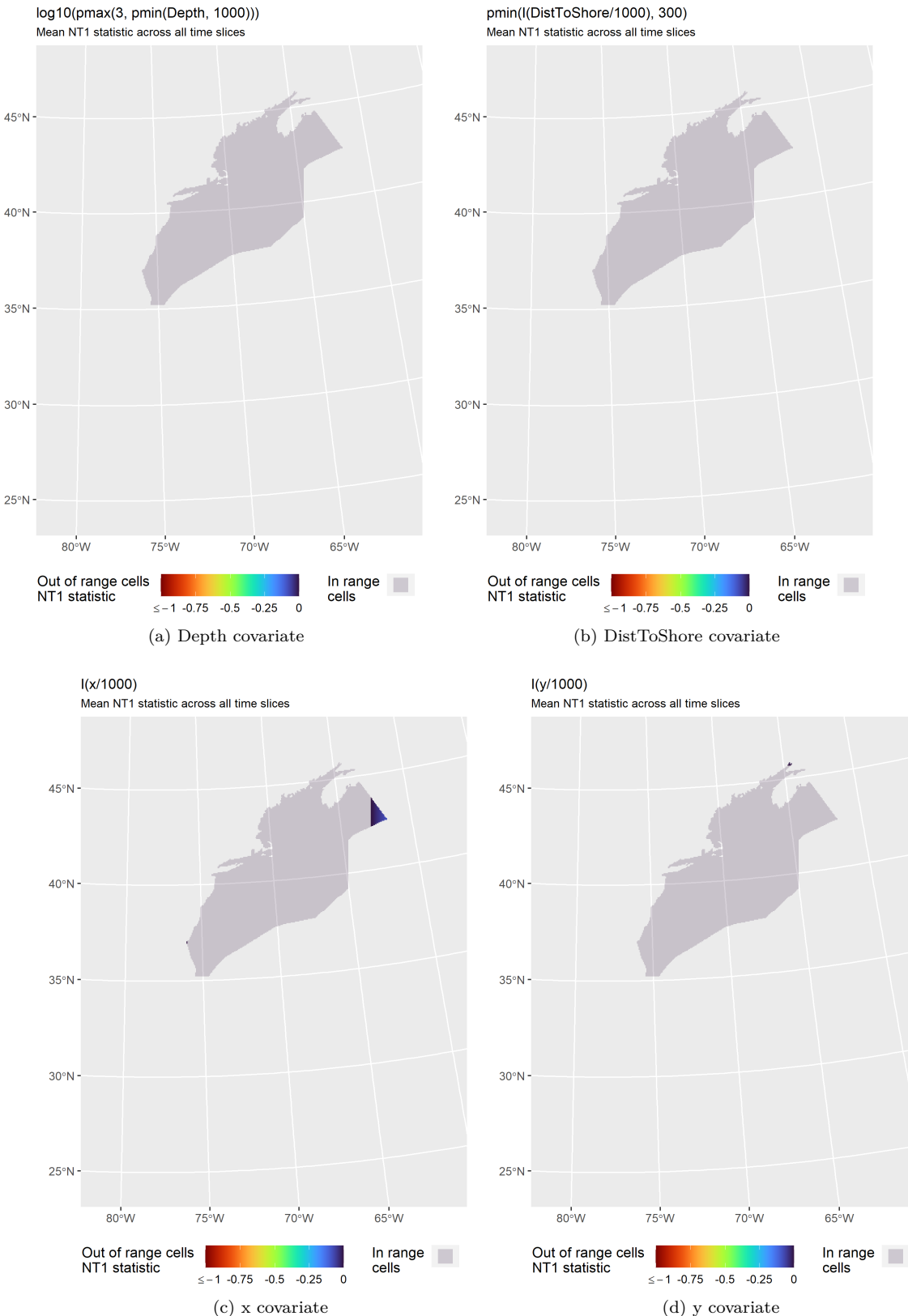
(d) y covariate

Figure 43: NT1 statistic (Mesgaran et al. (2014)) for static covariates used in the model for the region Gulf Stream to Halifax for Summer. Areas outside the sampled range of a covariate appear in color, indicating univariate extrapolation of that covariate occurred there. Areas within the sampled range appear in gray, indicating it did not occur.
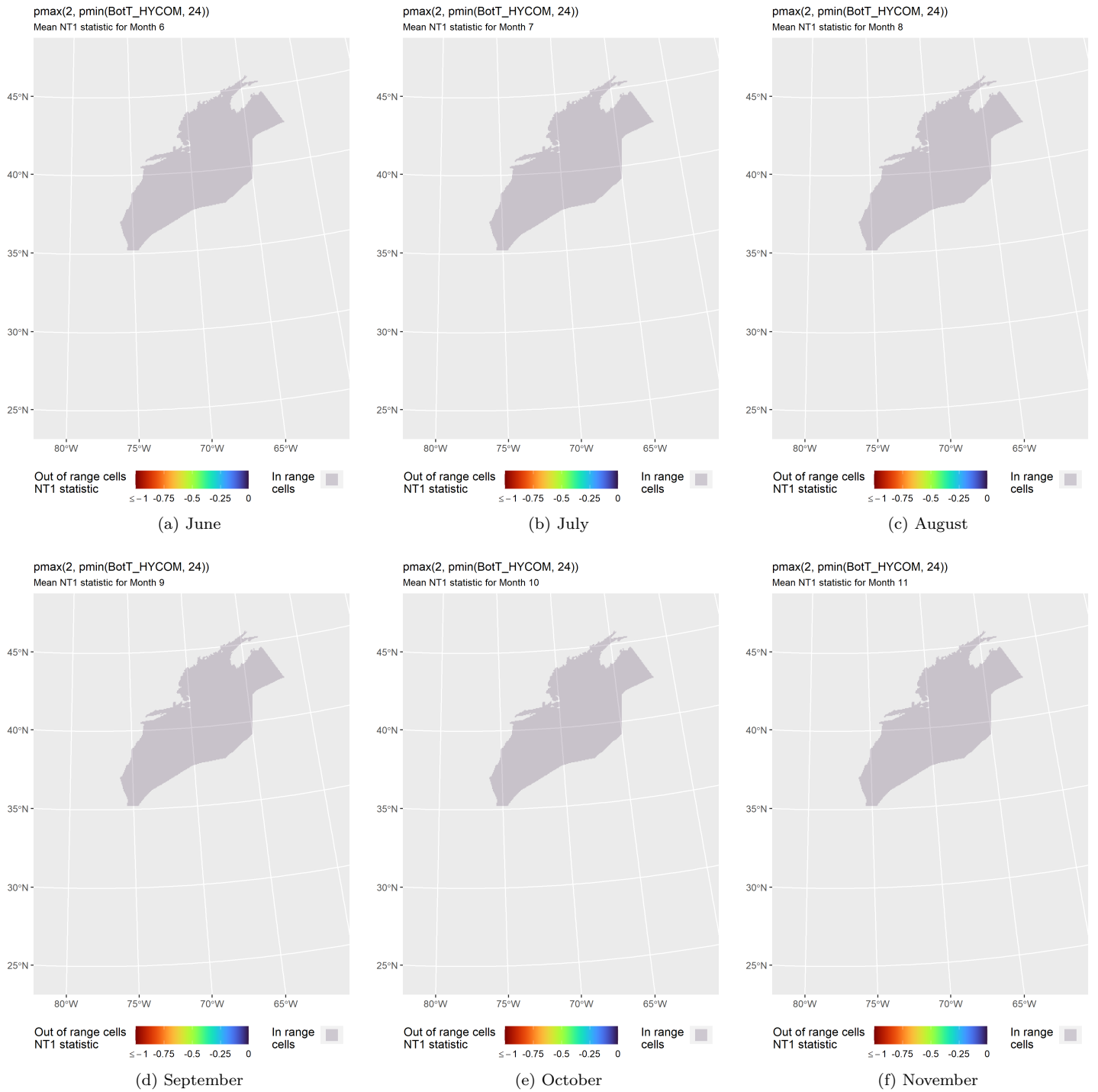
Figure 44: NT1 statistic (Mesgaran et al. (2014)) for the BotT_HYCOM covariate in the model for the region Gulf Stream to Halifax for Summer. Areas outside the sampled range of a covariate appear in color, indicating univariate extrapolation of that covariate occurred there during the month. Areas within the sampled range appear in gray, indicating it did not occur.
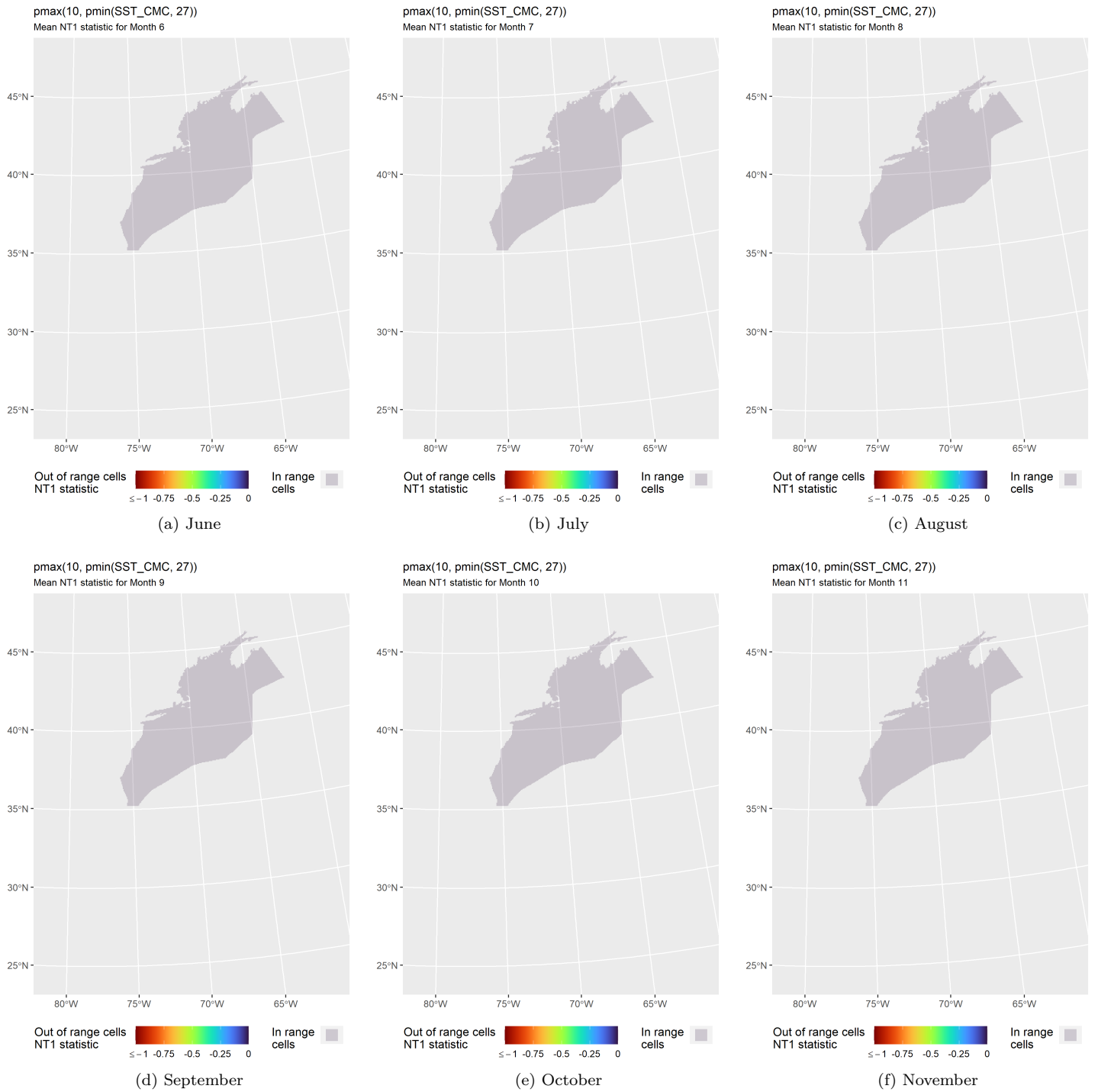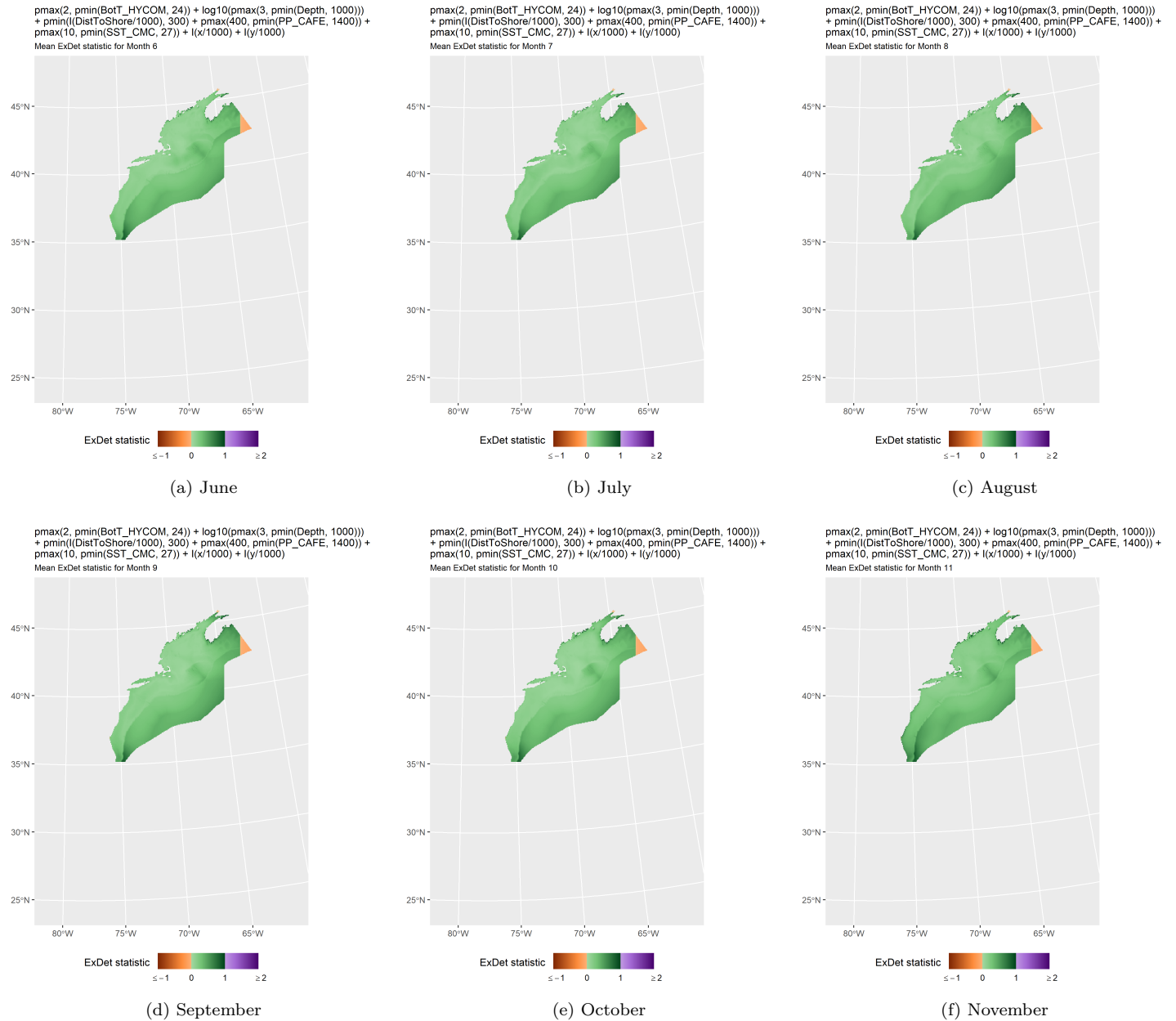
Figure 45: NT1 statistic (Mesgaran et al. (2014)) for the PP_CAFE covariate in the model for the region Gulf Stream to Halifax for Summer. Areas outside the sampled range of a covariate appear in color, indicating univariate extrapolation of that covariate occurred there during the month. Areas within the sampled range appear in gray, indicating it did not occur.

Figure 46: NT1 statistic (Mesgaran et al. (2014)) for the SST_CMC covariate in the model for the region Gulf Stream to Halifax for Summer. Areas outside the sampled range of a covariate appear in color, indicating univariate extrapolation of that covariate occurred there during the month. Areas within the sampled range appear in gray, indicating it did not occur.

4.2.3.2   Multivariate Extrapolation

(a) June   (b) July   (c) August

(d) September   (e) October   (f) November

Figure 47: ExDet statistic (Mesgaran et al. (2014)) for all of the covariates used in the model for the region Gulf Stream to Halifax for Summer. Areas in orange (ExDet < 0) required univariate extrapolation of one or more covariates (see previous section). Areas in purple (ExDet > 1), did not require univariate extrapolation but did require multivariate extrapolation, by virtue of having novel combinations of covariates not represented in the survey data, according to the NT2 statistic (Mesgaran et al. (2014)). Areas in green ($0 \geq$ ExDet ≤ 1) did not require either type of extrapolation.

5 Predictions

Based on our evaluation of this model in the context of what is known of this species (see Section 6), we summarized its predictions into monthly climatological density and uncertainty surfaces, shown in the maps below.
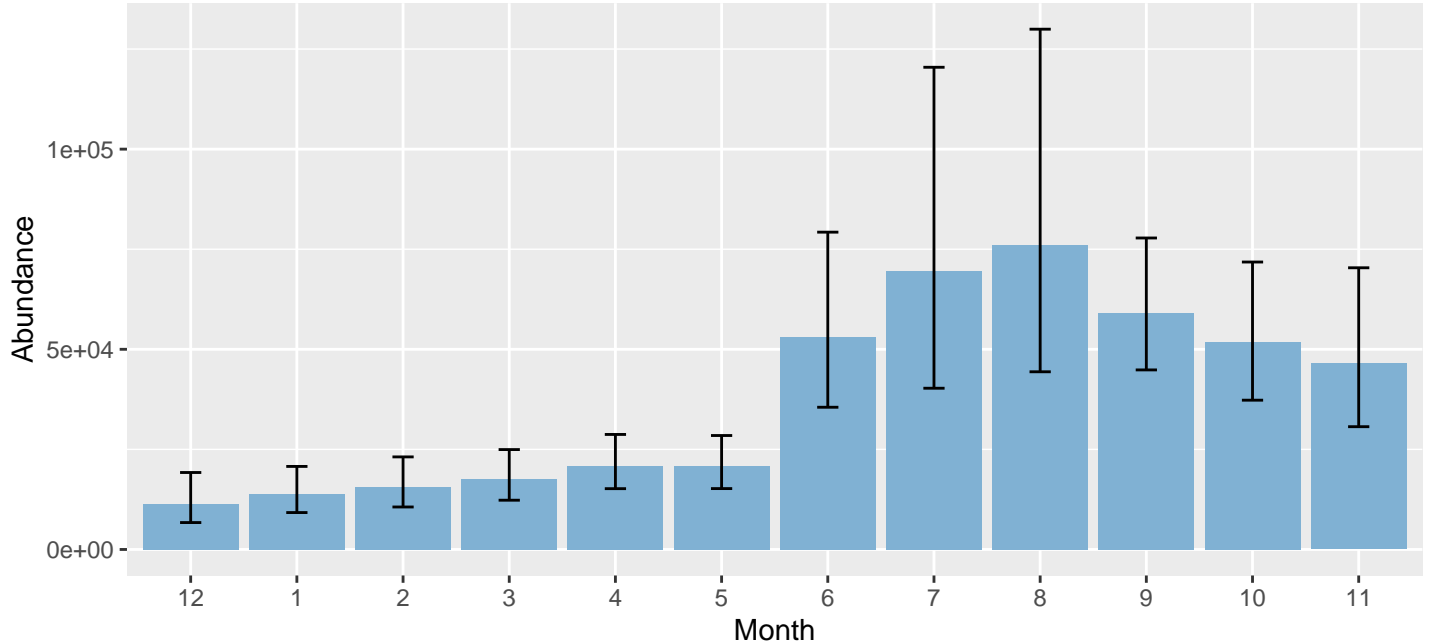
5.1 Summarized Predictions

Figure 48: Mean monthly abundance for the prediction area for December 1998 - November 2020. Note that the prediction area was not the same for all months (see Table 9 below and maps following). Error bars are a 95% interval, made with a log-normal approximation using the prediction's CV. The CV was estimated with the analytic approach given by Miller et al. (2022), Appendix S1, and accounts both for uncertainty in model parameter estimates and for temporal variability in dynamic covariates.

Table 9: Mean monthly abundance and density for the prediction area for December 1998 - November 2020. CV and intervals estimated as described for the previous figure.

| Month	Abundance	CV	95% Interval	Area (km^2)	Density (individuals / 100 km^2)
12	11,369	0.273	6,723 - 19,228	622,000	1.83
1	13,833	0.209	9,223 - 20,746	622,000	2.22
2	15,667	0.201	10,615 - 23,122	622,000	2.52
3	17,523	0.182	12,304 - 24,955	622,000	2.82
4	20,889	0.164	15,188 - 28,730	622,000	3.36
5	20,807	0.161	15,207 - 28,468	622,000	3.35
6	53,064	0.207	35,526 - 79,261	1,154,825	4.60
7	69,650	0.285	40,275 - 120,449	1,154,825	6.03
8	75,951	0.279	44,387 - 129,958	1,154,825	6.58
9	59,071	0.141	44,849 - 77,802	1,154,825	5.12
10	51,748	0.168	37,293 - 71,804	1,154,825	4.48
11	46,458	0.214	30,672 - 70,367	1,154,825	4.02
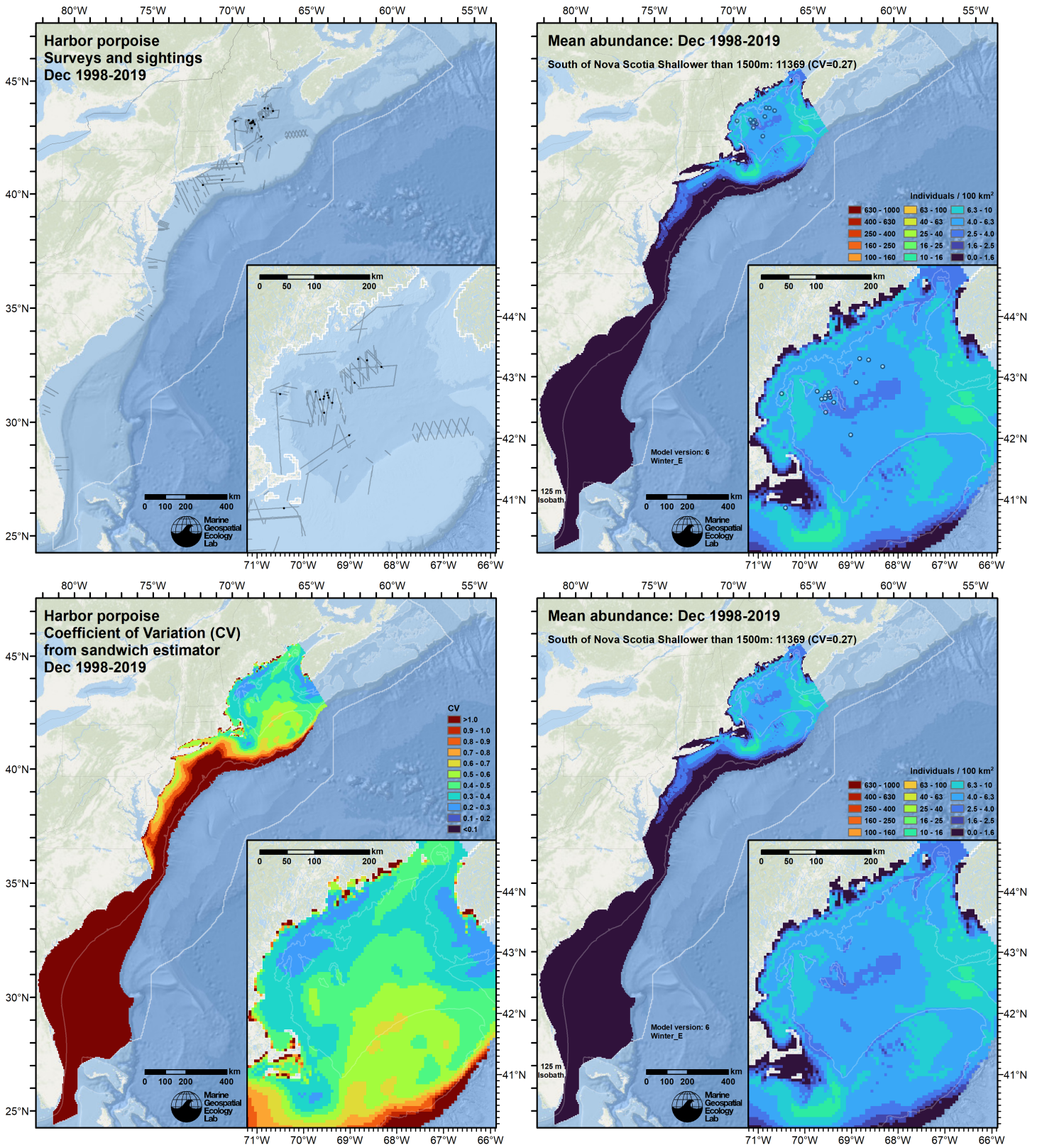
Figure 49: Survey effort and observations (top left), predicted density with observations (top right), predicted density without observations (bottom right), and coefficient of variation of predicted density (bottom left), for the month of December for the given era. Variance was estimated with the analytic approach given by Miller et al. (2022), Appendix S1, and accounts both for uncertainty in model parameter estimates and for temporal variability in dynamic covariates.
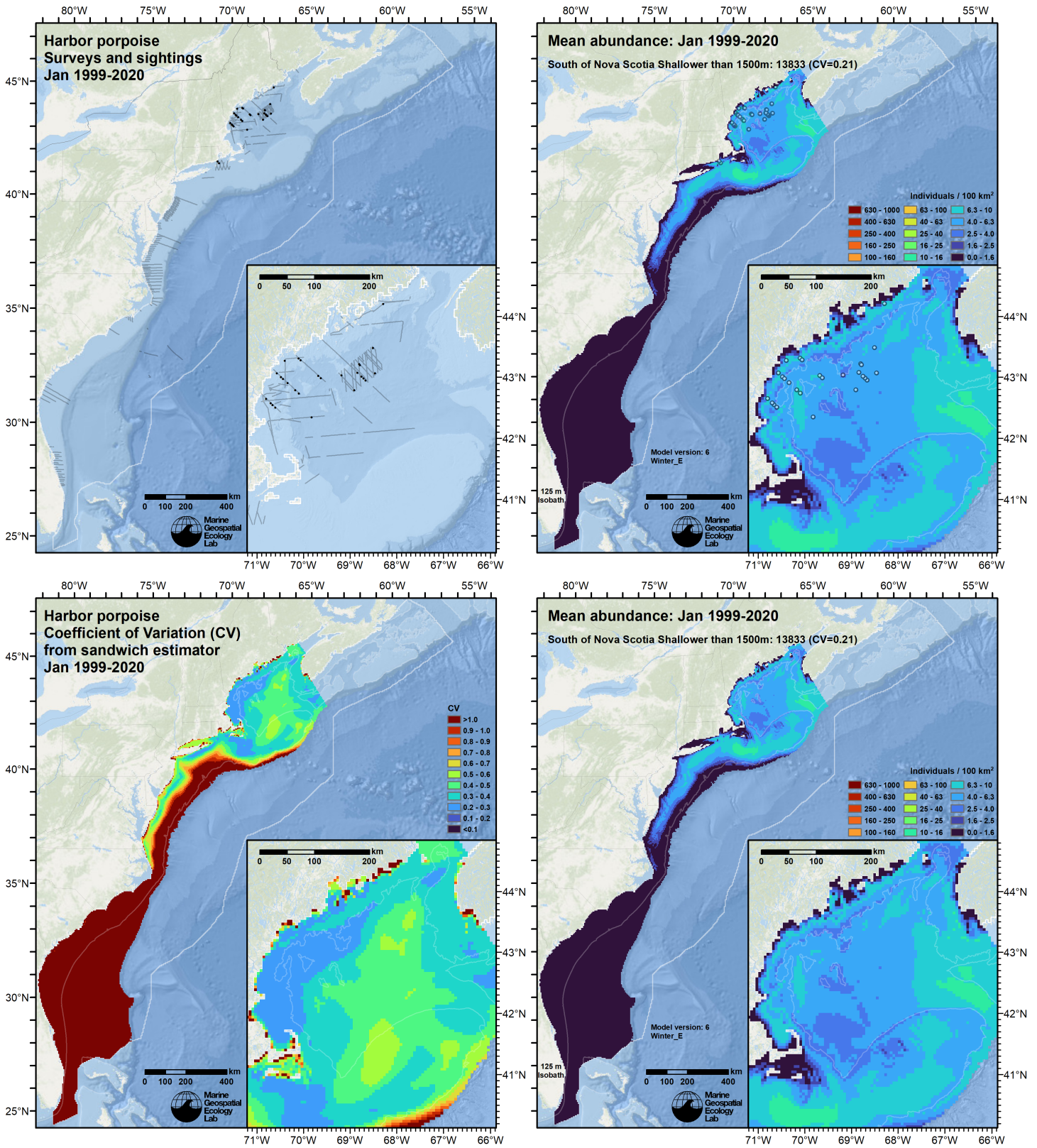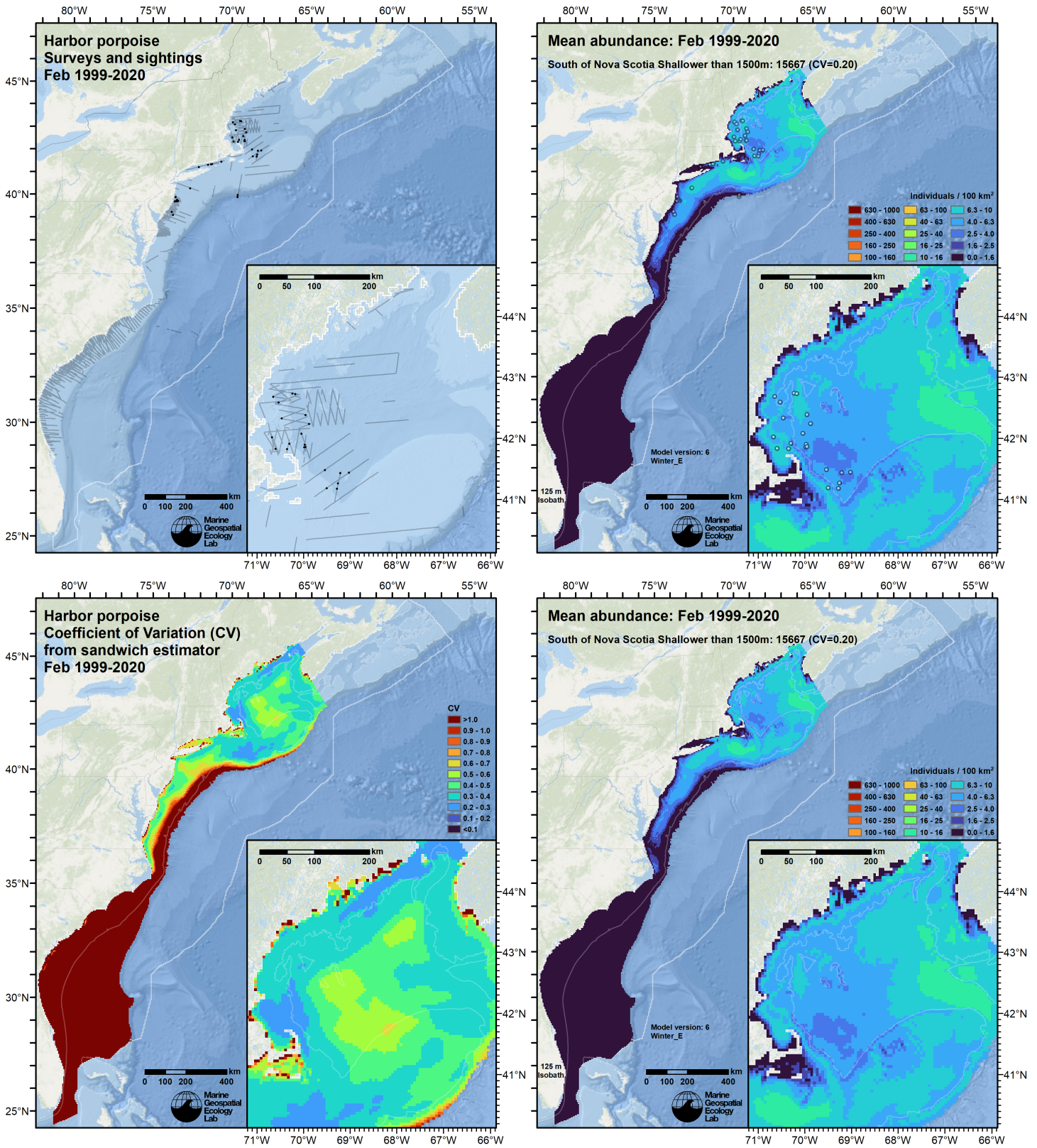
Figure 50: Survey effort and observations (top left), predicted density with observations (top right), predicted density without observations (bottom right), and coefficient of variation of predicted density (bottom left), for the month of January for the given era. Variance was estimated with the analytic approach given by Miller et al. (2022), Appendix S1, and accounts both for uncertainty in model parameter estimates and for temporal variability in dynamic covariates.
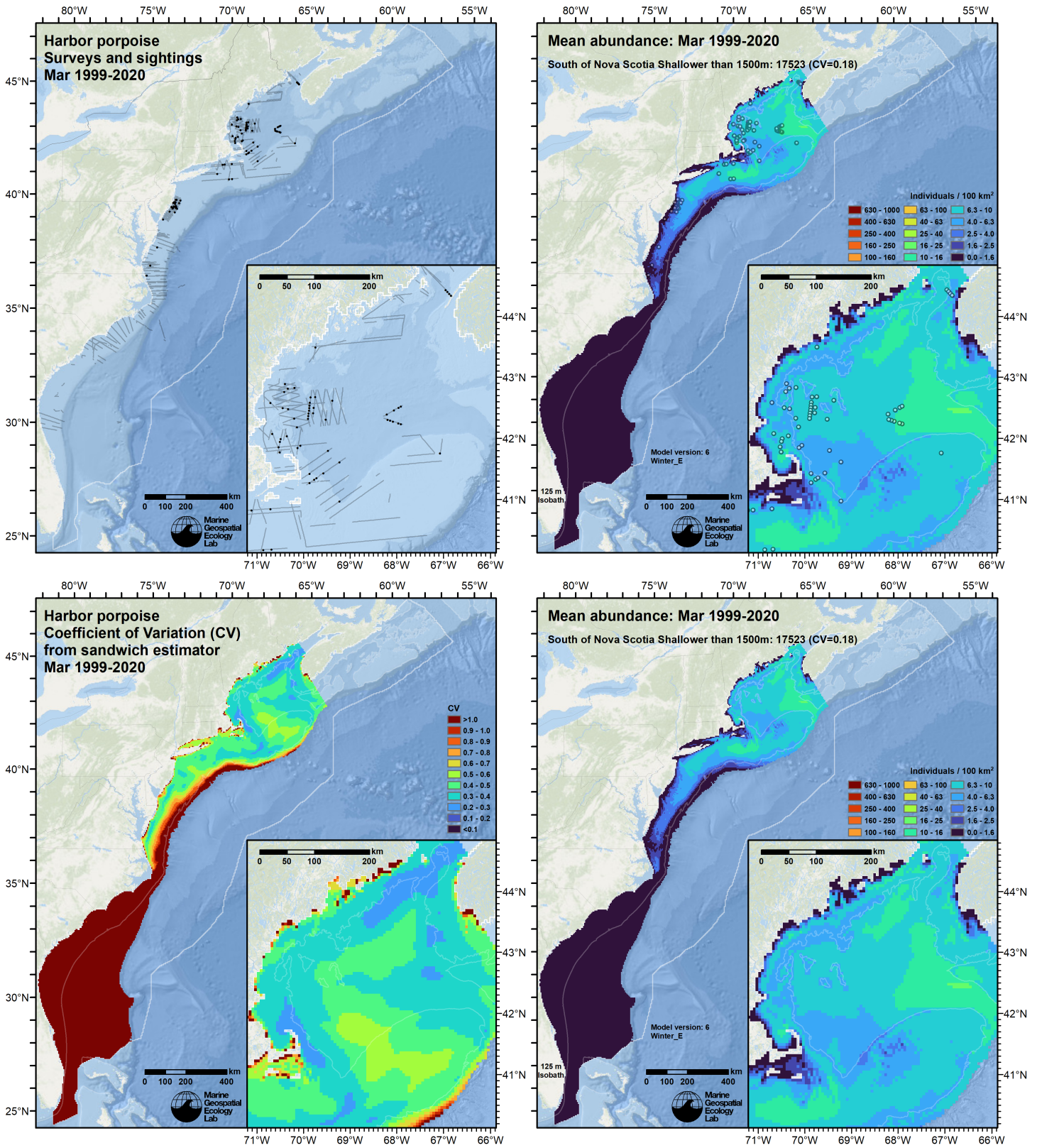
60

Figure 51: Survey effort and observations (top left), predicted density with observations (top right), predicted density without observations (bottom right), and coefficient of variation of predicted density (bottom left), for the month of February for the given era. Variance was estimated with the analytic approach given by Miller et al. (2022), Appendix S1, and accounts both for uncertainty in model parameter estimates and for temporal variability in dynamic covariates.
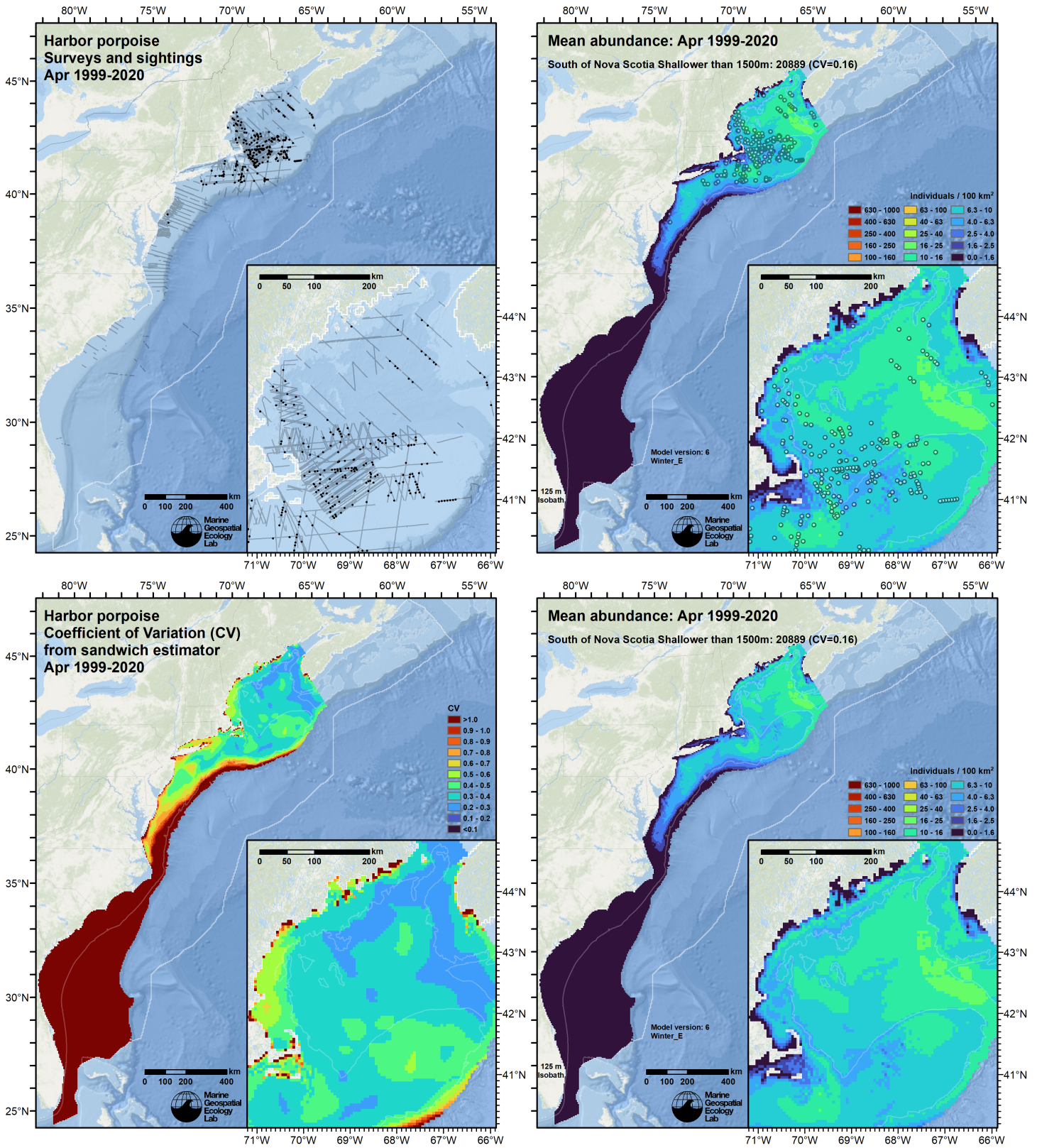
Figure 52: Survey effort and observations (top left), predicted density with observations (top right), predicted density without observations (bottom right), and coefficient of variation of predicted density (bottom left), for the month of March for the given era. Variance was estimated with the analytic approach given by Miller et al. (2022), Appendix S1, and accounts both for uncertainty in model parameter estimates and for temporal variability in dynamic covariates.
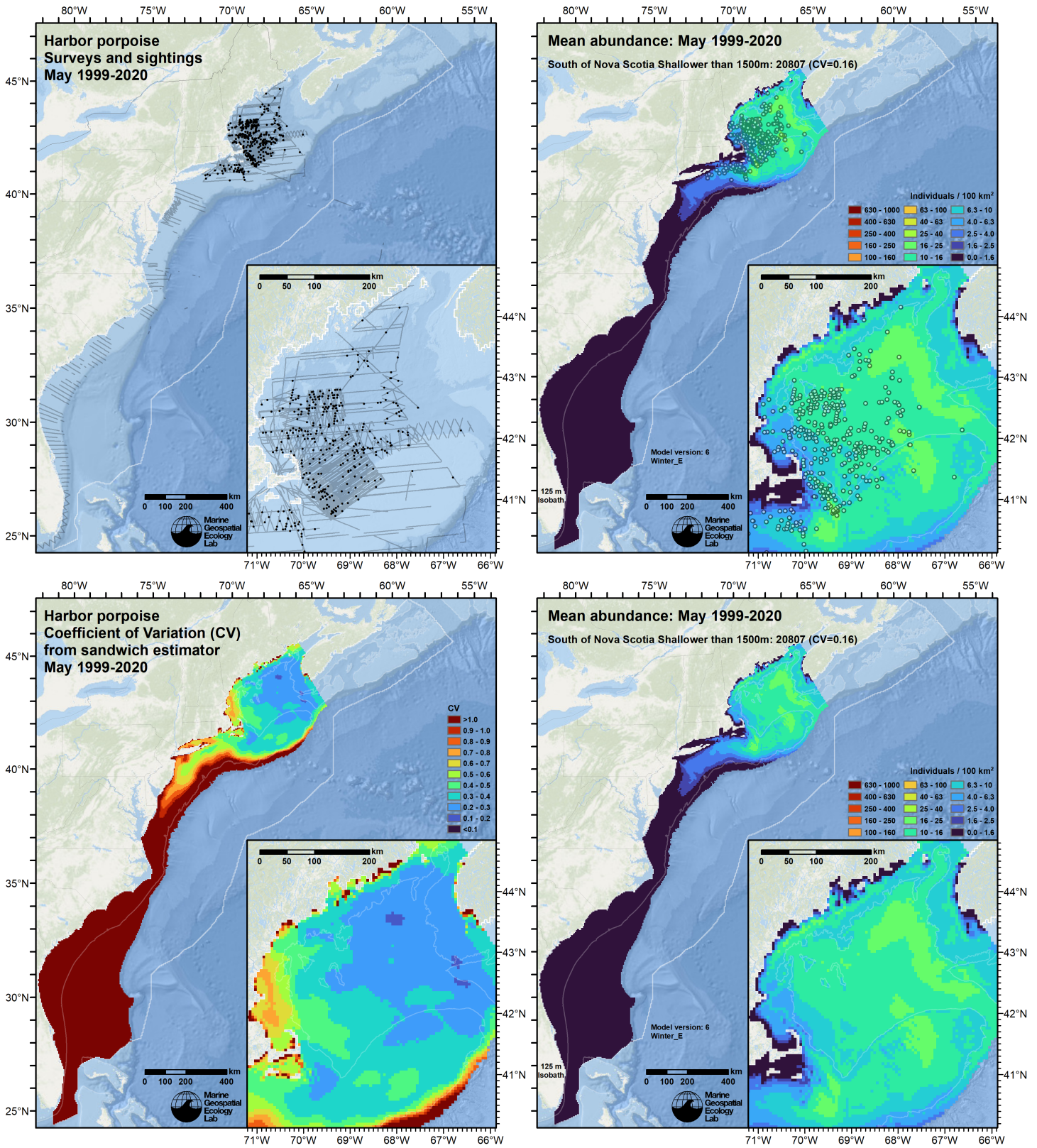
Figure 53: Survey effort and observations (top left), predicted density with observations (top right), predicted density without observations (bottom right), and coefficient of variation of predicted density (bottom left), for the month of April for the given era. Variance was estimated with the analytic approach given by Miller et al. (2022), Appendix S1, and accounts both for uncertainty in model parameter estimates and for temporal variability in dynamic covariates.

Figure 54: Survey effort and observations (top left), predicted density with observations (top right), predicted density without observations (bottom right), and coefficient of variation of predicted density (bottom left), for the month of May for the given era. Variance was estimated with the analytic approach given by Miller et al. (2022), Appendix S1, and accounts both for uncertainty in model parameter estimates and for temporal variability in dynamic covariates.
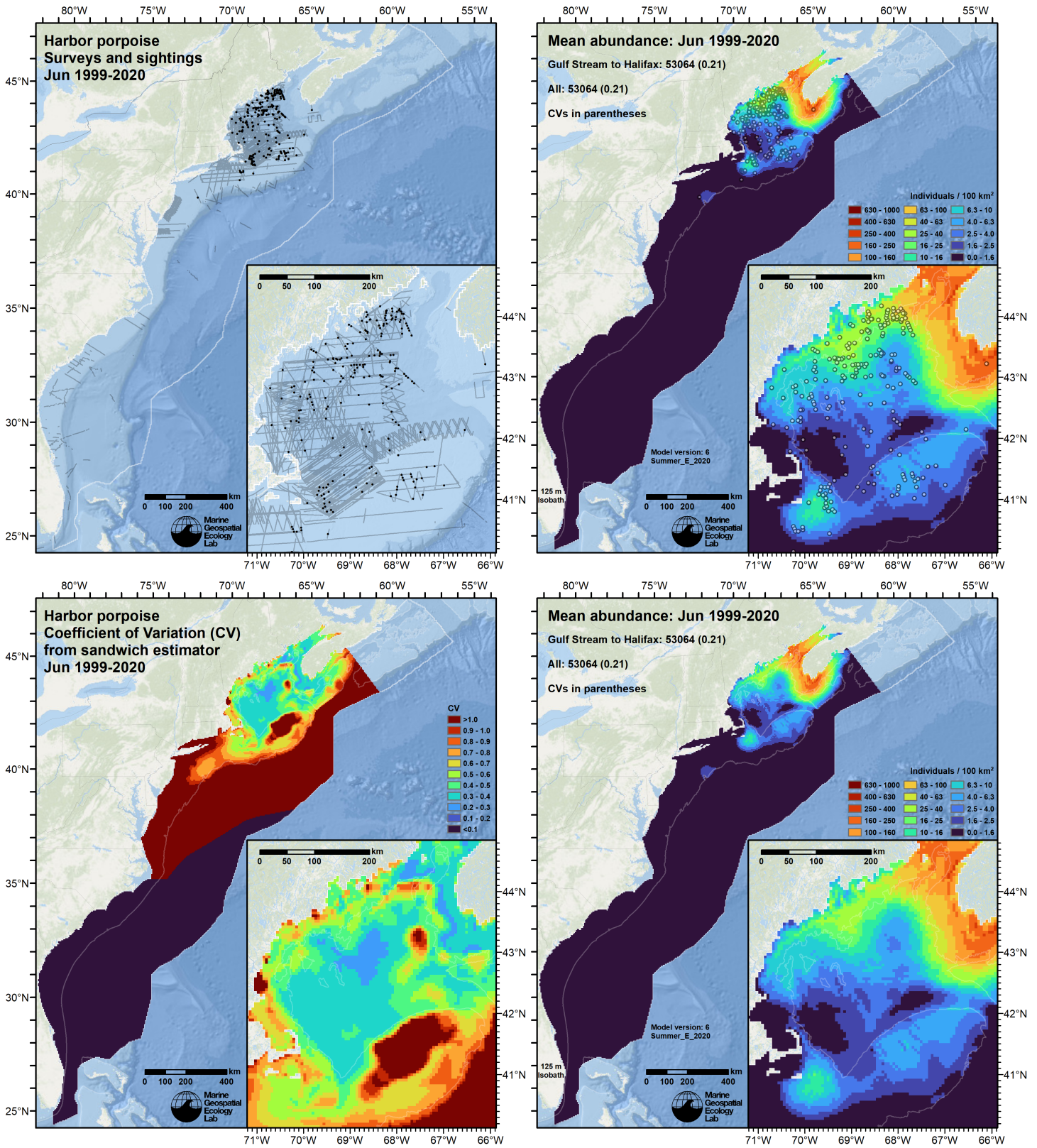
Figure 55: Survey effort and observations (top left), predicted density with observations (top right), predicted density without observations (bottom right), and coefficient of variation of predicted density (bottom left), for the month of June for the given era. Variance was estimated with the analytic approach given by Miller et al. (2022), Appendix S1, and accounts both for uncertainty in model parameter estimates and for temporal variability in dynamic covariates.
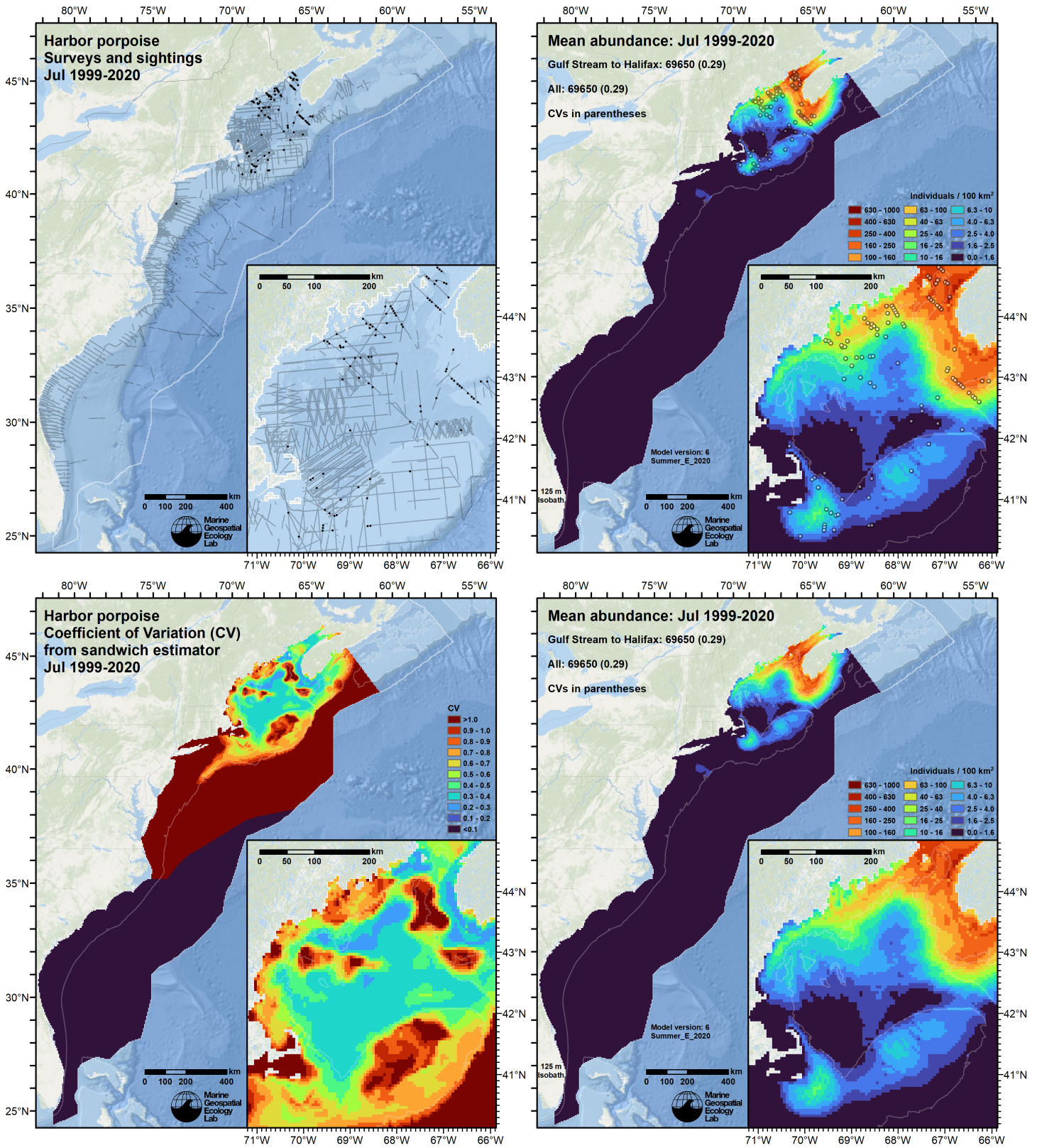
Figure 56: Survey effort and observations (top left), predicted density with observations (top right), predicted density without observations (bottom right), and coefficient of variation of predicted density (bottom left), for the month of July for the given era. Variance was estimated with the analytic approach given by Miller et al. (2022), Appendix S1, and accounts both for uncertainty in model parameter estimates and for temporal variability in dynamic covariates.
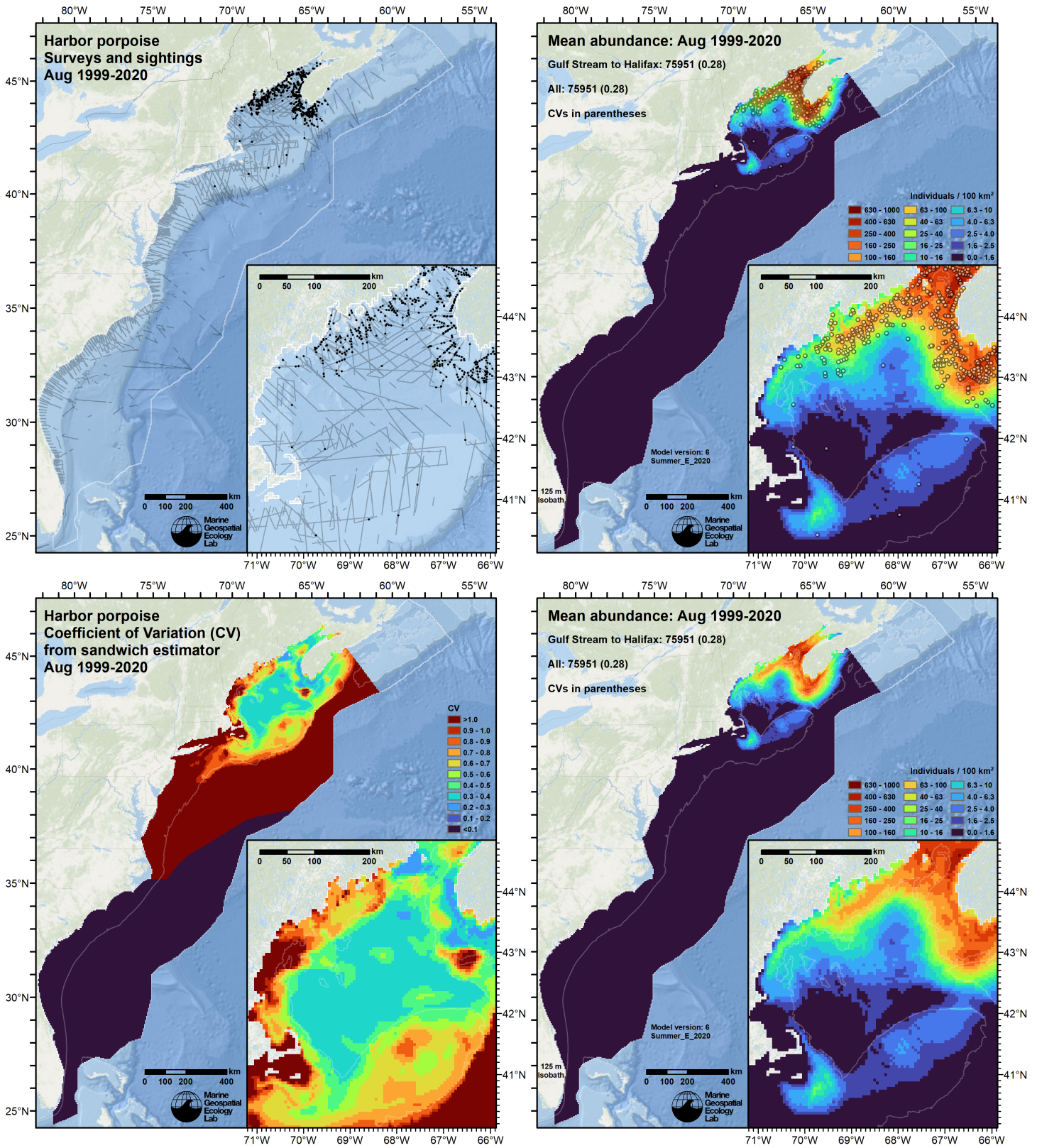
Figure 57: Survey effort and observations (top left), predicted density with observations (top right), predicted density without observations (bottom right), and coefficient of variation of predicted density (bottom left), for the month of August for the given era. Variance was estimated with the analytic approach given by Miller et al. (2022), Appendix S1, and accounts both for uncertainty in model parameter estimates and for temporal variability in dynamic covariates.
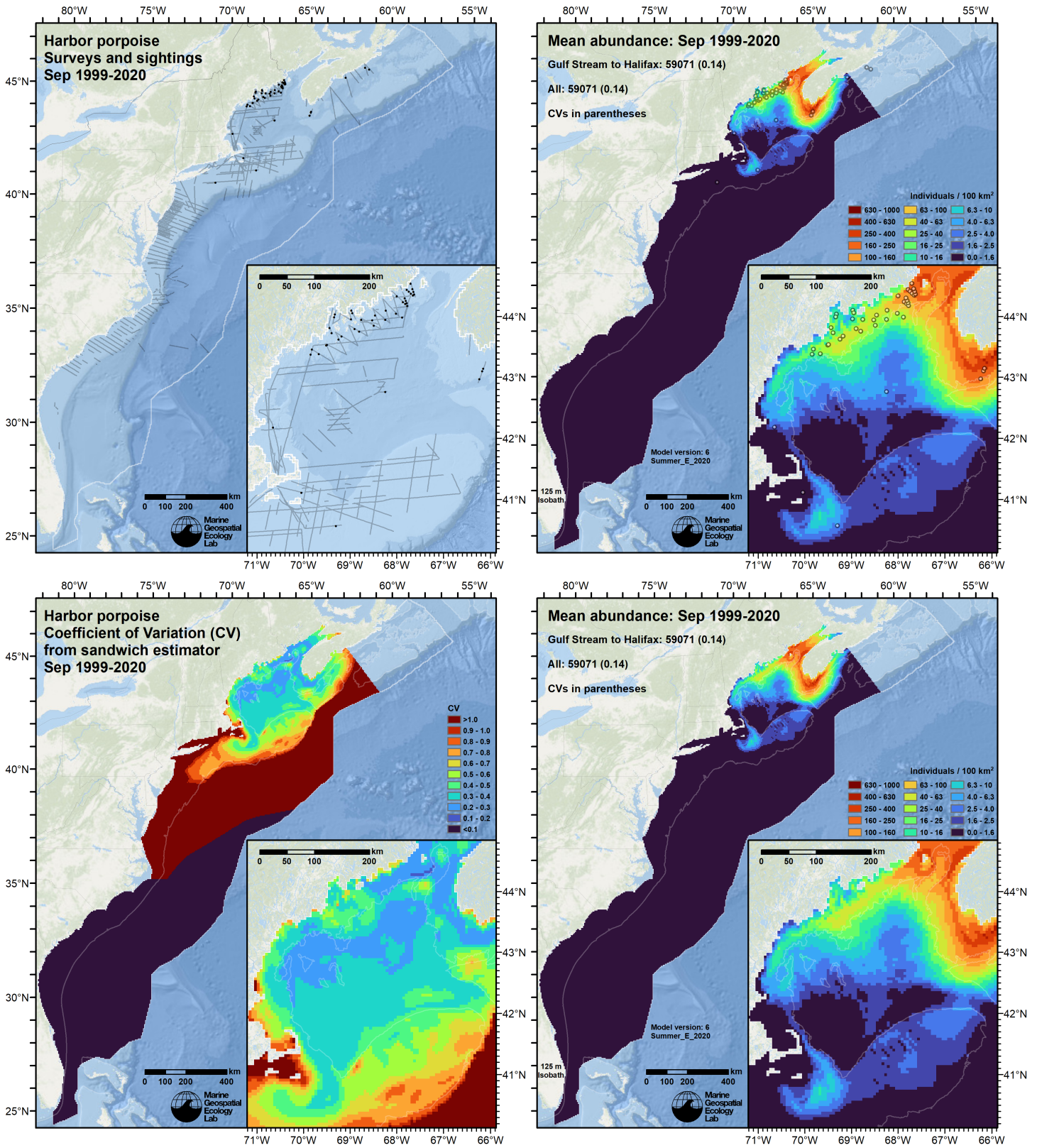
Figure 58: Survey effort and observations (top left), predicted density with observations (top right), predicted density without observations (bottom right), and coefficient of variation of predicted density (bottom left), for the month of September for the given era. Variance was estimated with the analytic approach given by Miller et al. (2022), Appendix S1, and accounts both for uncertainty in model parameter estimates and for temporal variability in dynamic covariates.
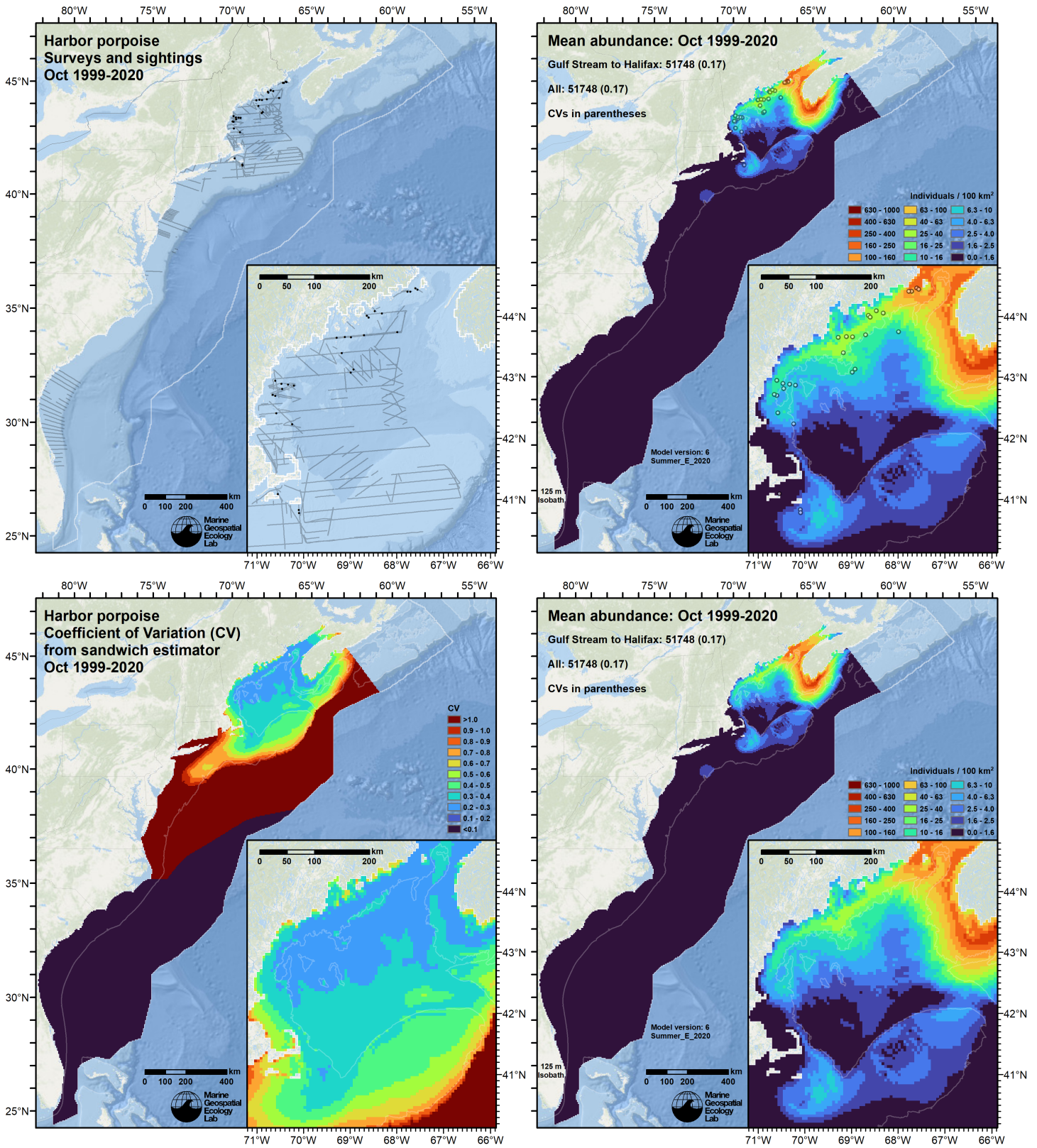
Figure 59: Survey effort and observations (top left), predicted density with observations (top right), predicted density without observations (bottom right), and coefficient of variation of predicted density (bottom left), for the month of October for the given era. Variance was estimated with the analytic approach given by Miller et al. (2022), Appendix S1, and accounts both for uncertainty in model parameter estimates and for temporal variability in dynamic covariates.
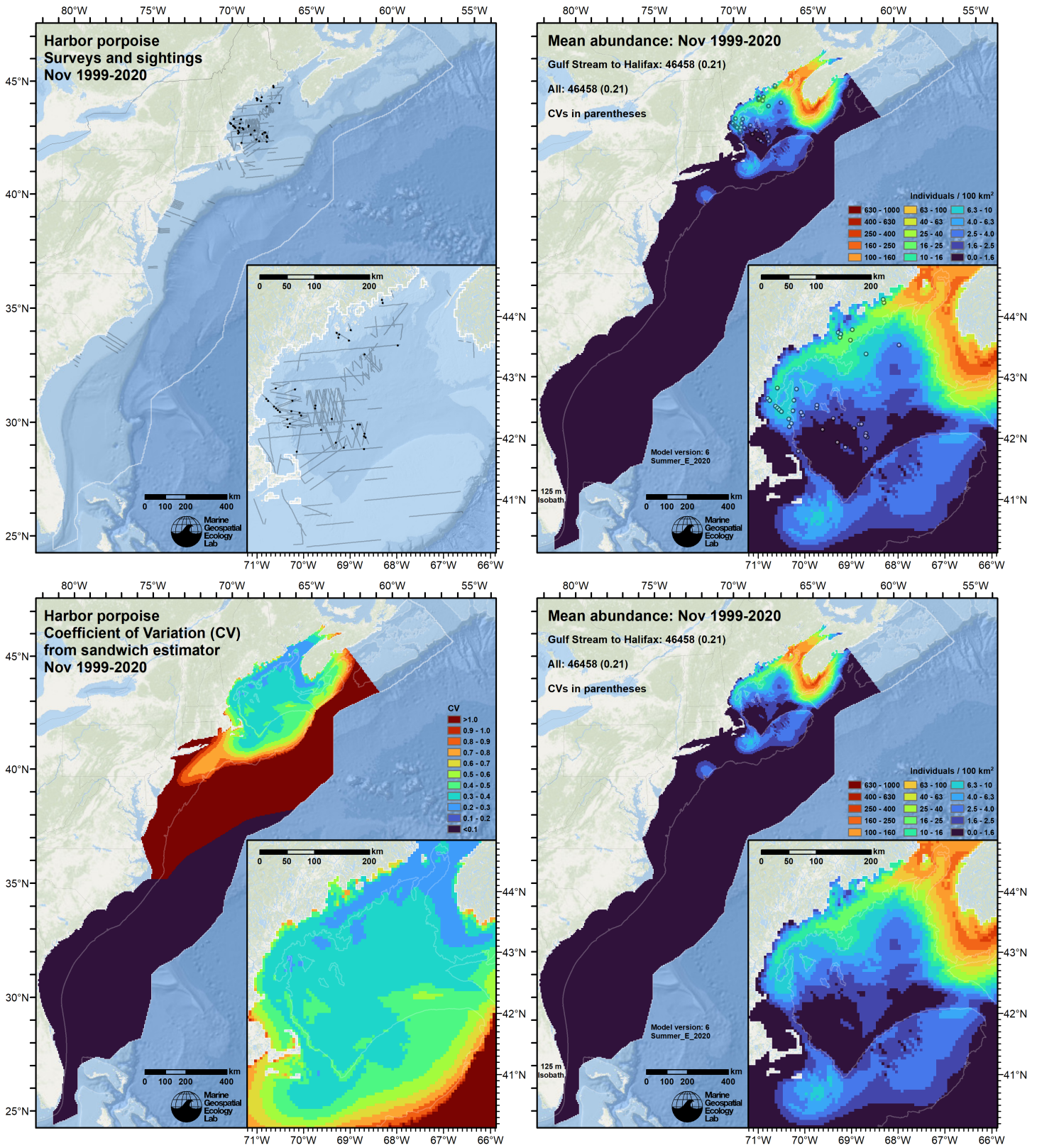
Figure 60: Survey effort and observations (top left), predicted density with observations (top right), predicted density without observations (bottom right), and coefficient of variation of predicted density (bottom left), for the month of November for the given era. Variance was estimated with the analytic approach given by Miller et al. (2022), Appendix S1, and accounts both for uncertainty in model parameter estimates and for temporal variability in dynamic covariates.

5.2 Abundance Comparisons

5.2.1 NOAA Stock Assessment Report

Table 10: Comparison of regional abundance estimates from the 2021 NOAA Stock Assessment Report (SAR) (Hayes et al. (2022)) to estimates from this density model extracted from roughly comparable zones (Figure 61 below). The SAR estimates were based on a single year of surveying, while the model estimates were taken from the multi-year mean density surfaces we provide to model users (Section 5.1).

2021 Stock Assessment Report			Density Model		
Month/Year	Area	N_{est}	Period	Zone	Abundance
Jun-Sep 2016	Central Virginia to Maine[a]	75,079	Jun-Sep 1998-2020	NEFSC	10,804
Aug-Sep 2016	Gulf of St. Lawrence/Bay of Fundy/Scotian Shelf[b]	20,464	Aug-Sep 1998-2020	Canada[c]	56,006
Jun-Sep 2016	Total	95,543	Jun-Sep 1998-2020	Total	66,810

[a] Estimate originally from Palka (2020). Note that this estimate was made from an aerial survey conducted 14 August - 28 September 2016, but because the SAR listed June-September as the months, we extracted our abundance for those months, not August-September. See Section 6 for further discussion.

[b] Estimate derived from Lawson and Gosselin (2018). Although the SAR includes "Gulf of St. Lawrence" in the name of this area, we presume this was in error, and that the estimate was only for the Gulf of Maine/Bay of Fundy stock.

[c] Our Canada zone is roughly comparable to the SAR's "Bay of Fundy/Scotian Shelf" area but does not include the Gulf of St. Lawrence.
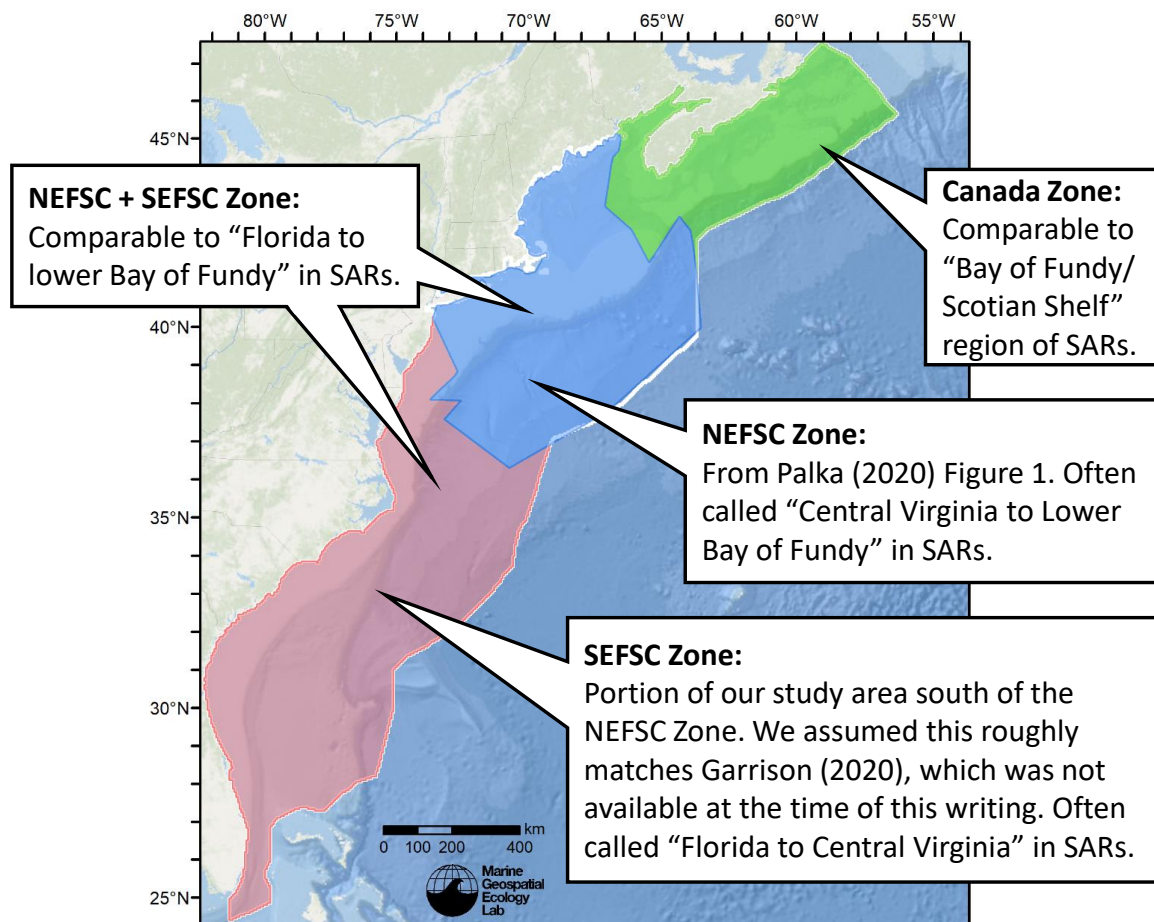

Figure 61: Zones for which we extracted abundance estimates from the density model for comparison to estimates from the NOAA Stock Assessment Report.

5.2.2 Previous Density Model

5.2.2.1 Winter

Figure 62: Comparison of the mean density predictions from the previous model (left) released by Roberts et al. (2017) to those from this model (right) for the Winter season.

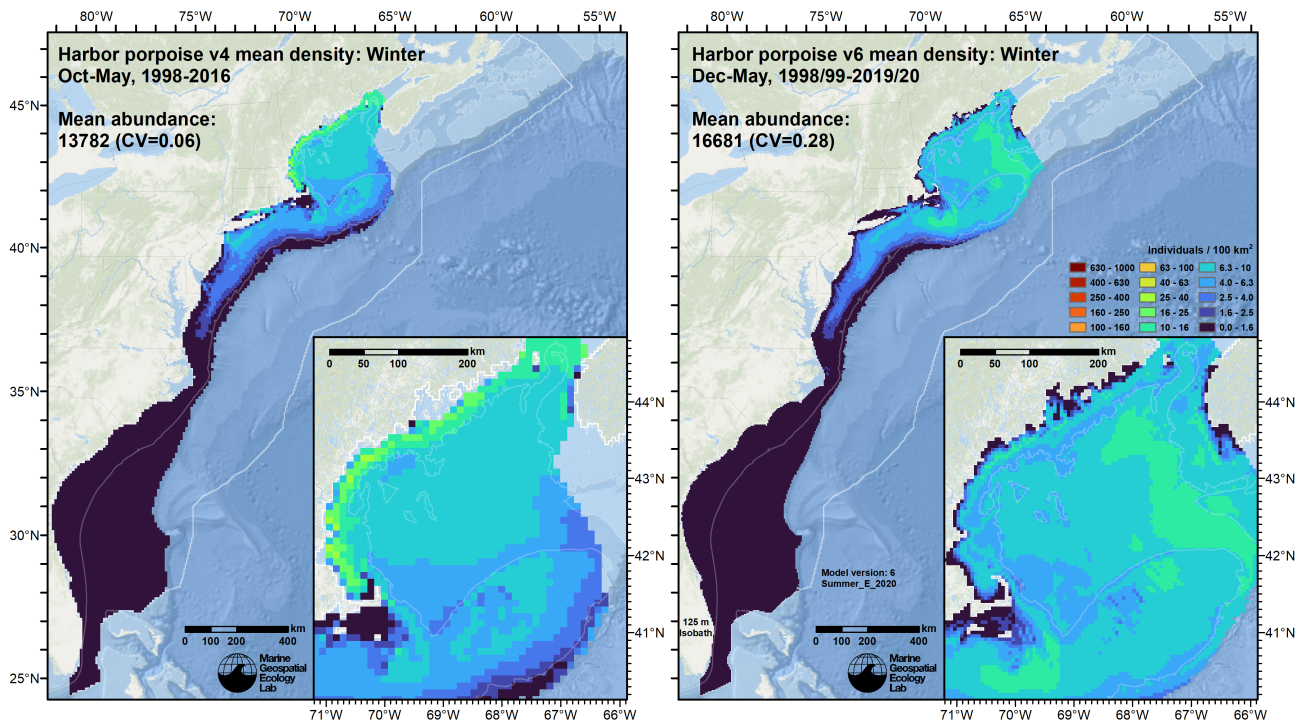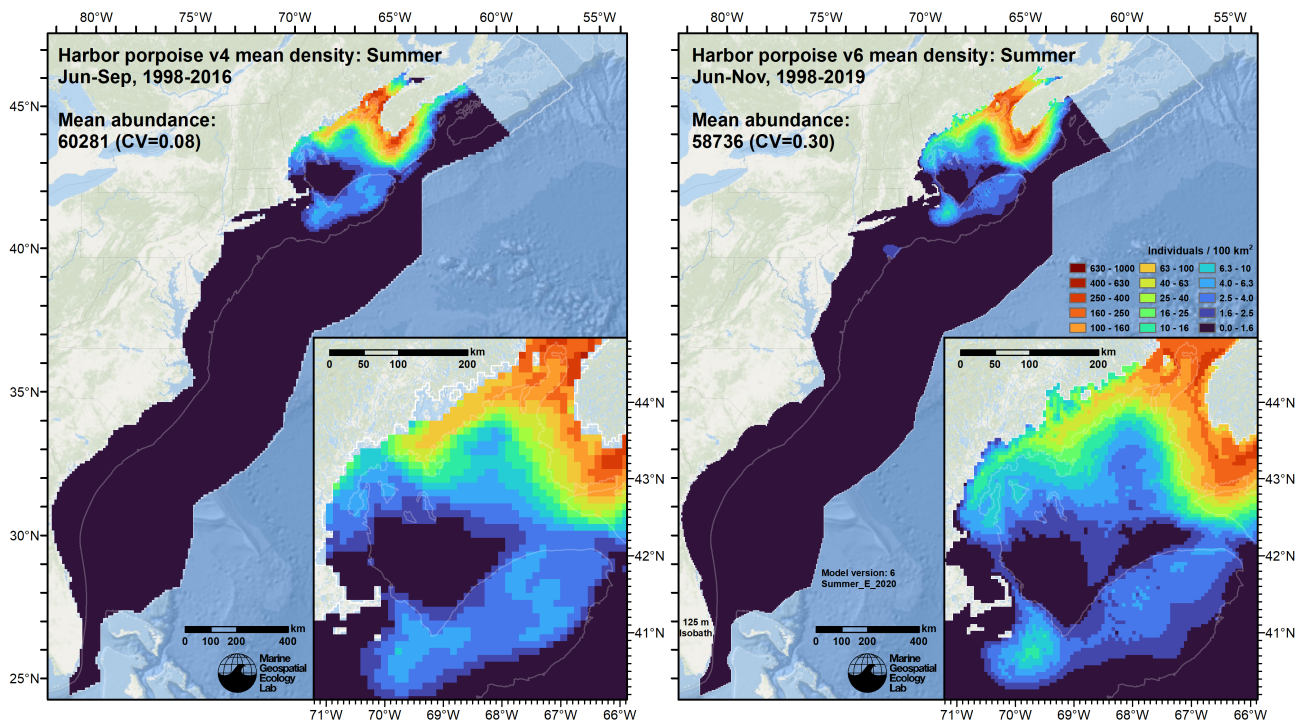### 5.2.2.2 Summer

Figure 63: Comparison of the mean density predictions from the previous model (left) released by Roberts et al. (2017) to those from this model (right) for the Summer season.

6 Discussion

When summarized across the predicted period (December 1998 - November 2020), mean monthly density maps (Figures 49-60) generally agreed with the overall distribution and seasonal pattern described in the literature (see Section 4). In the Winter season (December-May), low to medium density was predicted throughout the Gulf of Maine, rising steadily there and region-wide as the months progressed (Figure 48). Although survey effort was sparse in December through March, due both to a seasonal bias in surveying toward spring and summer months and to rougher seas (Beaufort > 2) in winter months, the continual widespread presence of harbor porpoises across the region was supported by sightings throughout the area, both those used in this model and from sources not usable in this model but available in the OBIS-SEAMAP archive (Halpin et al. 2009).

South of the Gulf of Maine, lower density was predicted extending down the eastern seaboard, reaching Cape Hatteras in February and March, the peak month for strandings reported by Byrd et al. (2014). We caution that survey effort targeting harbor porpoises was quite sparse across the mid-Atlantic during these months, particularly along the mid- and outer shelf, and predictions for large portions of the study area were essentially geographical extrapolations (although not extrapolations in covariate space; see Section 4.2.3). Although uncertainty metrics such as CV remained moderate, additional surveying during these months with porpoise-targeting methods would be helpful. For example, in a future model update, we hope to integrate digital aerial surveys of New York waters conducted by NYSERDA (our current workflow requires an adjustment before it can utilize these surveys).

In the Summer season (June-November), high density was predicted along coastal Maine, the lower Bay of Fundy, and around southwest Nova Scotia. Density rose in June and July to a peak in August, then fell through September-November. Lower densities were predicted across the central Gulf of Maine, Georges Bank, and southeast of Nantucket, where sightings occurred throughout the season in low numbers.

Mean monthly abundance predicted by our model ranged from a low of 11,369 in December to a high of 75,951 in August (Figure 48; Table 9). Our model's mean predicted abundance for the months of June-September of 66,810 was substantially lower than the estimate of 95,543 from the most recent NOAA Stock Assessment Report (SAR) (Hayes et al. 2022) (Table 10). We therefore advise caution when utilizing our model predictions to assess the potential impacts of threats to the species.

Although it is possible this difference is traceable to interannual variability—the SAR was based on one year of surveying while our model incorporated surveys from more than two decades—we suspect a key issue might relate to detection modeling, especially for the NARWSS aerial survey, which accounted for more than half of the aerial sightings used in our model. The NARWSS surveys were flown at a higher altitude (750 ft.) than NOAA's broad-scale abundance surveys (600 ft.). NARWSS did not use a belly observer, and while it did record small cetaceans[2], its protocol called for scanning at farther distances to maximize the chances of spotting large whales, the primary target of NARWSS. As a result, the NARWSS detection function required left truncation (Section 2.1.1.4), presumably because harbor porpoises under the plane had been missed at a higher rate than those further out. Given that, it is likely that a stronger perception bias correction is needed than that of the NOAA AMAPPS program, which was the best correction available (see Section 3.1). Despite this potential bias, NARWSS provided coverage of the Gulf of Maine for non-summer seasons that was essential to modeling porpoise density year-round, so we did not exclude it. But if enough NOAA AMMAPS surveys are eventually conducted in non-summer seasons, we may be able to drop NARWSS from a future update to this model.

Also noteworthy are the regional differences in abundance estimated by our model and by the surveys used for the SAR estimates. Our model, which summarized more than two decades of predictions, estimated that about 80% of the abundance was in Canada, while the SAR, based on one year of surveying (2016), estimated that about 80% of the abundance was in U.S. waters. Our best guess is that this was an interannual effect. For example, Palka (2000) reported large number of sightings in lower Bay of Fundy and along coastal Nova Scotia in summer of 1999, while Lawson and Gosselin (2018) reported relatively few in these regions in 2016. (The 1999 NOAA survey was included in our model but the 2016 DFO survey was not available for our use.)

Given the general match between the model's predictions and what has been reported in the literature, the differences discussed above notwithstanding, we elected to offer density predictions for this species at monthly temporal resolution.

Compared to the previous model (version 4), this model (version 6) predicted 21% higher total abundance in winter (Figure 62) and 3% lower in summer (Figure 63). In winter, this model predicted lower density around the edge of the northern and western Gulf of Maine, in Cape Cod Bay, and in Long Island Sound, but higher density in the eastern Gulf of Maine, across Georges Bank, and southeast of Nantucket. In summer, this model predicted lower density along coastal central Maine and higher density in parts of Canada, as well as southeast of Nantucket. The spatial extent of this model also extended farther inshore, e.g. into Penobscot Bay, which contributed additional abundance not present in the previous model.

---

[2]We only used the NARWSS surveys from 2003-2016 for this model. In 2017, NARWSS changed altitudes to 1000 ft. and stopped recording small cetaceans.

The substantially larger CV in this model compared to the previous version is due to this model using contemporaneous covariates and fully accounting for the temporal variability in predictions as well as the error in model parameter estimates via the method of Miller et al. (2022), while the previous version used climatological covariates and only accounted for the error in model parameter estimates, resulting in an underestimate of variance. The CV estimated for the new model is thus an improvement, by virtue if it accounting for additional important sources of variance.

References

Barco SG, Burt L, DePerte A, Digiovanni R Jr. (2015) Marine Mammal and Sea Turtle Sightings in the Vicinity of the Maryland Wind Energy Area July 2013-June 2015, VAQF Scientific Report #2015-06. Virginia Aquarium & Marine Science Center Foundation, Virginia Beach, VA

Becker JJ, Sandwell DT, Smith WHF, Braud J, Binder B, Depner J, Fabre D, Factor J, Ingalls S, Kim S-H, Ladner R, Marks K, Nelson S, Pharaoh A, Trimmer R, Von Rosenberg J, Wallace G, Weatherall P (2009) Global Bathymetry and Elevation Data at 30 Arc Seconds Resolution: SRTM30_PLUS. Marine Geodesy 32:355–371. doi: 10.1080/01490410903297766

Behrenfeld MJ, Falkowski PG (1997) Photosynthetic rates derived from satellite-based chlorophyll concentration. Limnology and oceanography 42:1–20. doi: 10.4319/lo.1997.42.1.0001

Bjorge A (2003) The harbour porpoise (Phocoena phocoena) in the North Atlantic: Variability in habitat use, trophic ecology and contaminant exposure. NAMMCO Scientific Publications 5:223–228.

Brasnett B (2008) The impact of satellite retrievals in a global sea-surface-temperature analysis. Quarterly Journal of the Royal Meteorological Society 134:1745–1760. doi: 10.1002/qj.319

Buckland ST, Anderson DR, Burnham KP, Laake JL, Borchers DL, Thomas L (2001) Introduction to Distance Sampling: Estimating Abundance of Biological Populations. Oxford University Press, Oxford, UK

Burt ML, Borchers DL, Jenkins KJ, Marques TA (2014) Using mark-recapture distance sampling methods on line transect surveys. Methods in Ecology and Evolution 5:1180–1191. doi: 10.1111/2041-210X.12294

Byrd BL, Harms CA, Hohn AA, McLellan WA, Lovewell GN, Moore KT, Altman KM, Rosel PE, Barco SG, Thayer VG, Friedlaender A (2014) Strandings as indicators of marine mammal biodiversity and human interactions off the coast of North Carolina. Fishery Bulletin 112:1–23. doi: 10.7755/FB.112.1.1

Canada Meteorological Center (2012) GHRSST Level 4 CMC0.2deg Global Foundation Sea Surface Temperature Analysis Version 2.0. PODAAC, CA, USA. doi: 10.5067/GHCMC-4FM02

Canada Meteorological Center (2016) GHRSST Level 4 CMC0.1deg Global Foundation Sea Surface Temperature Analysis Version 3.0. PODAAC, CA, USA. doi: 10.5067/GHCMC-4FM03

Canny JF (1986) A computational approach to edge detection. IEEE Transactions on Pattern Analysis and Machine Intelligence 8:679–698. doi: 10.1016/B978-0-08-051581-6.50024-6

Carretta JV, Lowry MS, Stinchcomb CE, Lynn MS, E. CR (2000) Distribution and abundance of marine mammals at San Clemente Island and surrounding offshore waters: Results from aerial and ground surveys in 1998 and 1999. NOAA Administrative Report LJ-00-02. NOAA National Marine Fisheries Service, Southwest Fisheries Center, La Jolla, CA

Chassignet E, Hurlburt H, Metzger EJ, Smedstad O, Cummings J, Halliwell G, Bleck R, Baraille R, Wallcraft A, Lozano C, Tolman H, Srinivasan A, Hankin S, Cornillon P, Weisberg R, Barth A, He R, Werner F, Wilkin J (2009) US GODAE: Global Ocean Prediction with the HYbrid Coordinate Ocean Model (HYCOM). Oceanog 22:64–75. doi: 10.5670/oceanog.2009.39

Cole T, Gerrior P, Merrick RL (2007) Methodologies of the NOAA National Marine Fisheries Service Aerial Survey Program for Right Whales (Eubalaena glacialis) in the Northeast U.S., 1998-2006. U.S. Department of Commerce, Woods Hole, MA

Eppley RW (1972) Temperature and phytoplankton growth in the sea. Fishery Bulletin 70:1063–1085.

Garrison LP, Martinez A, Maze-Foley K (2010) Habitat and abundance of cetaceans in Atlantic Ocean continental slope waters off the eastern USA. Journal of Cetacean Research and Management 11:267–277.

Geo-Marine, Inc. (2010) New Jersey Department of Environmental Protection Baseline Studies Final Report Volume III: Marine Mammal and Sea Turtle Studies. Geo-Marine, Inc., Plano, TX

Halpin P, Read A, Fujioka E, Best B, Donnelly B, Hazen L, Kot C, Urian K, LaBrecque E, Dimatteo A, Cleary J, Good C, Crowder L, Hyrenbach KD (2009) OBIS-SEAMAP: The World Data Center for Marine Mammal, Sea Bird, and Sea Turtle Distributions. Oceanography 22:104–115. doi: 10.5670/oceanog.2009.42

Hayes SA, Josephson E, Maze-Foley K, Rosel PE, Wallace J, Brossard A, Chavez-Rosales S, Cole TVN, Garrison LP, Hatch J, Henry A, Horstman SC, Litz J, Lyssikatos MC, Mullin KD, Murray K, Orphanides C, Ortega-Ortiz J, Pace RM, Palka DL, Powell J, Rappucci G, Soldevilla M, Wenzel FW (2022) US Atlantic and Gulf of Mexico Marine Mammal Stock Assessments 2021. NOAA National Marine Fisheries Service, Northeast Fisheries Science Center, Woods Hole, MA

Johnston DW, Westgate AJ, Read AJ (2005) Effects of fine-scale oceanographic features on the distribution and movements of harbour porpoises Phocoena phocoena in the Bay of Fundy. Marine Ecology Progress Series 295:279–293.

Laake JL, Calambokidis J, Osmek SD, Rugh DJ (1997) Probability of Detecting Harbor Porpoise From Aerial Surveys: Estimating g(0). Journal of Wildlife Management 61:63–75. doi: 10.2307/3802415

Lawson JW, Gosselin J-F (2018) Estimates of cetacean abundance from the 2016 NAISS aerial surveys of eastern Canadian waters, with a comparison to estimates from the 2007 TNASS. NAMMCO SC/25/AE/09. In: Proceedings of the NAMMCO 25th Scientific Committee (SC). North Atlantic Marine Mammal Commission, Bergen-Tromsø, Norway,

Marsh H, Sinclair DF (1989) Correcting for Visibility Bias in Strip Transect Aerial Surveys of Aquatic Fauna. The Journal of Wildlife Management 53:1017. doi: 10.2307/3809604

McLellan WA, McAlarney RJ, Cummings EW, Read AJ, Paxton CGM, Bell JT, Pabst DA (2018) Distribution and abundance of beaked whales (Family Ziphiidae) Off Cape Hatteras, North Carolina, U.S.A. Marine Mammal Science. doi: 10.1111/mms.12500

Meissner T, Wentz FJ, Scott J, Vazquez-Cuervo J (2016) Sensitivity of Ocean Surface Salinity Measurements From Spaceborne L-Band Radiometers to Ancillary Sea Surface Temperature. IEEE Trans Geosci Remote Sensing 54:7105–7111. doi: 10.1109/TGRS.2016.2596100

Mesgaran MB, Cousens RD, Webber BL (2014) Here be dragons: A tool for quantifying novelty due to covariate range and correlation change when projecting species distribution models. Diversity Distrib 20:1147–1159. doi: 10.1111/ddi.12209

Miller DL, Becker EA, Forney KA, Roberts JJ, Cañadas A, Schick RS (2022) Estimating uncertainty in density surface models. PeerJ 10:e13950. doi: 10.7717/peerj.13950

Morel A (1991) Light and marine photosynthesis: A spectral model with geochemical and climatological implications. Progress in Oceanography 26:263–306. doi: 10.1016/0079-6611(91)90004-6

Mullin KD (1995) Cruise Report: Oregon II Cruise 215 (95-01): 26 January - 11 March 1995. NOAA National Marine Fisheries Service, Southeast Fisheries Science Center, Pascagoula, MS

Mullin KD, Fulling GL (2003) Abundance of cetaceans in the southern U.S. North Atlantic Ocean during summer 1998. Fishery Bulletin 101:603–613.

Palka D (2020) Cetacean Abundance in the US Northwestern Atlantic Ocean Summer 2016. Northeast Fish Sci Cent Ref Doc. 20-05. NOAA National Marine Fisheries Service, Northeast Fisheries Science Center, Woods Hole, MA

Palka D, Aichinger Dias L, Broughton E, Chavez-Rosales S, Cholewiak D, Davis G, DeAngelis A, Garrison L, Haas H, Hatch J, Hyde K, Jech M, Josephson E, Mueller-Brennan L, Orphanides C, Pegg N, Sasso C, Sigourney D, Soldevilla M, Walsh H (2021) Atlantic Marine Assessment Program for Protected Species: FY15 – FY19 (OCS Study BOEM 2021-051). U.S. Deptartment of the Interior, Bureau of Ocean Energy Management, Washington, DC

Palka DL (1996) Update on abundance of Gulf of Maine/Bay of Fundy harbor porpoises. NOAA National Marine Fisheries Service, Northeast Fisheries Science Center, Woods Hole, MA

Palka DL (2000) Abundance of the Gulf of Maine/Bay of Fundy harbor porpoise based on shipboard and aerial surveys during 1999. US Department of Commerce, National Oceanic and Atmospheric Administration, National Marine Fisheries Service, Northeast Region, Northeast Fisheries Science Center

Palka DL (2006) Summer abundance estimates of cetaceans in US North Atlantic navy operating areas (NEFSC Reference Document 06-03). U.S. Department of Commerce, Northeast Fisheries Science Center, Woods Hole, MA

Palka DL, Read AJ, Westgate AJ, Johnston DW (1996) Summary of current knowledge of harbour porpoises in US and Canadian Atlantic waters. Reports of the International Whaling Commission 46:559–565.

Palka DL, Cholewiak D, Broughton E, Jech M, Force M, Guida V, Lowe M, Lawson G (2014) Shipboard habitat survey during March – April 2014: Northeast Fisheries Science Center. NOAA National Marine Fisheries Service, Northeast Fisheries Science Center, Woods Hole, MA

Palka DL, Chavez-Rosales S, Josephson E, Cholewiak D, Haas HL, Garrison L, Jones M, Sigourney D, Waring G, Jech M, Broughton E, Soldevilla M, Davis G, DeAngelis A, Sasso CR, Winton MV, Smolowitz RJ, Fay G, LaBrecque E, Leiness JB, Dettloff K, Warden M, Murray K, Orphanides C (2017) Atlantic Marine Assessment Program for Protected Species:

2010-2014 (OCS Study BOEM 2017-071). U.S. Deptartment of the Interior, Bureau of Ocean Energy Management, Washington, DC

Roberts JJ, Best BD, Dunn DC, Treml EA, Halpin PN (2010) Marine Geospatial Ecology Tools: An integrated framework for ecological geoprocessing with ArcGIS, Python, R, MATLAB, and C++. Environmental Modelling & Software 25:1197–1207. doi: 10.1016/j.envsoft.2010.03.029

Roberts JJ, Best BD, Mannocci L, Fujioka E, Halpin PN, Palka DL, Garrison LP, Mullin KD, Cole TVN, Khan CB, McLellan WA, Pabst DA, Lockhart GG (2016) Habitat-based cetacean density models for the U.S. Atlantic and Gulf of Mexico. Scientific Reports 6:22615. doi: 10.1038/srep22615

Roberts JJ, Mannocci L, Halpin PN (2017) Final Project Report: Marine Species Density Data Gap Assessments and Update for the AFTT Study Area, 2016-2017 (Opt. Year 1), Document Version 1.4. Duke University Marine Geospatial Ecology Lab, Durham, NC

Roberts JJ, Yack TM, Halpin PN (2023) Marine mammal density models for the U.S. Navy Atlantic Fleet Training and Testing (AFTT) study area for the Phase IV Navy Marine Species Density Database (NMSDD), Document Version 1.3. Duke University Marine Geospatial Ecology Lab, Durham, NC

Robertson FC, Koski WR, Brandon JR, Thomas TA, Trites AW (2015) Correction factors account for the availability of bowhead whales exposed to seismic operations in the Beaufort Sea. Journal of Cetacean Research and Management 15:35–44.

Ryan C, Boisseau O, Cucknell A, Romagosa M, Moscrop A, McLanaghan R (2013) Final report for trans-Atlantic research passages between the UK and USA via the Azores and Iceland, conducted from R/V Song of the Whale 26 March to 28 September 2012. Marine Conservation Research International, Essex, UK

Silsbe GM, Behrenfeld MJ, Halsey KH, Milligan AJ, Westberry TK (2016) The CAFE model: A net production model for global ocean phytoplankton. Global Biogeochemical Cycles 30:1756–1777. doi: 10.1002/2016GB005521

Swartz SL, Burks C (2000) Cruise Results: Windwards Humpback (Megaptera novaeangliae) Survey: NOAA Ship Gordon Gunter Cruise GU-00-01: 9 February to 3 April 2000 (NOAA Technical Memorandum NMFS-SEFSC-438). NOAA National Marine Fisheries Service, Southeast Fisheries Science Center, Miami, FL

Westgate AJ, Read AJ, Cox TM, Schofield TD, Whitaker BR, Anderson KE (1998) Monitoring a Rehabilitated Harbor Porpoise Using Satellite Telemetry. Marine Mammal Science 14:599–604. doi: 10.1111/j.1748-7692.1998.tb00746.x

Whitt AD, Powell JA, Richardson AG, Bosyk JR (2015) Abundance and distribution of marine mammals in nearshore waters off New Jersey, USA. Journal of Cetacean Research and Management 15:45–59.

Wingfield JE, O'Brien M, Lyubchich V, Roberts JJ, Halpin PN, Rice AN, Bailey H (2017) Year-round spatiotemporal distribution of harbour porpoises within and around the Maryland wind energy area. PLOS ONE 12:e0176653. doi: 10.1371/journal.pone.0176653

Wood SN (2011) Fast stable restricted maximum likelihood and marginal likelihood estimation of semiparametric generalized linear models. Journal of the Royal Statistical Society: Series B (Statistical Methodology) 73:3–36. doi: 10.1111/j.1467-9868.2010.00749.x